

HU ISSN 1586–2070

JOURNAL OF COMPUTATIONAL AND APPLIED MECHANICS

An Open Access International Journal

Published by the University of Miskolc

VOLUME 10, NUMBER 1 (2015)



MISKOLC UNIVERSITY PRESS

EDITORS

László **BARANYI**, Institute of Energy Engineering and Chemical Machinery, University of Miskolc, H-3515 MISKOLC, Hungary, e-mail: arambl@uni-miskolc.hu

István **PÁCZELT**, Institute of Applied Mechanics, University of Miskolc, H-3515 MISKOLC, Hungary e-mail: mechpacz@uni-miskolc.hu

György **SZEIDL**, Institute of Applied Mechanics, University of Miskolc, H-3515 MISKOLC, Hungary e-mail: Gyorgy.SZEIDL@uni-miskolc.hu

EDITORIAL BOARD

Edgár **BERTÓTI**, Institute of Applied Mechanics, University of Miskolc, H-3515 MISKOLC, Hungary, e-mail: edgar.bertoti@uni-miskolc.hu

Atilla **BAKSA**, Institute of Applied Mechanics, University of Miskolc, H-3515 MISKOLC, Hungary, attila.baksa@uni-miskolc.hu

István **ECSEDI**, Institute of Applied Mechanics, University of Miskolc, H-3515 MISKOLC, Hungary, mechecs@uni-miskolc.hu

Ulrich **GABBERT**, Institut für Mechanik, Otto-von-Guericke-Universität Magdeburg, Universitätsplatz 2, 39106 MAGDEBURG, Germany, ulrich.gabbert@mb.uni-magdeburg.de

Zsolt **GÁSPÁR**, Department of Structural Mechanics, Budapest University of Technology and Economics, Műegyetem rkp. 3, 1111 BUDAPEST, Hungary, gaspar@ep-mech.me.bme.hu

Robert **HABER**, Department of Theoretical and Applied Mechanics, University of Illinois at Urbana-Champaign, 216 Talbot Lab., 104 S. Wright Str., URBANA, IL 61801, USA, r-haber@uiuc.edu

Csaba **HÓS**, Department of Hydraulic Machines, Budapest University of Technology and Economics, Műegyetem rkp. 3, 1111 BUDAPEST, Hungary, HOSCSABA@vizgep.bme.hu

Károly **JÁRMAI**, Institute of Logistics, University of Miskolc, H-3515 MISKOLC, Hungary, altjar@uni-miskolc.hu

László **KOLLÁR**, Department of Strength of Materials and Structures, Budapest University of Technology and Economics, Műegyetem rkp. 3. K.II.42., 1521 BUDAPEST, Hungary, lkollar@eik.bme.hu

József **KÖVECSES**, Mechanical Engineering Department 817 Sherbrooke Street West, MD163 Montreal, Quebec H3A 2K6 jozsef.kovecses@mcgill.ca

Márta **KURUTZ**, Department of Structural Mechanics, Budapest University of Technology and Economics, Műegyetem rkp. 3, 1111 BUDAPEST, Hungary, kurutzm@eik.bme.hu

Herbert **MANG**, Institute for Strength of Materials, University of Technology, Karlsplatz 13, 1040 VIENNA, Austria, Herbert.Mang@tuwien.ac.at

Sanjay **MITTAL**, Department of Aerospace Engineering, Indian Institute of Technology Kanpur, UP 208 016, India, smittal@iitk.ac.in

Zenon **MROZ**, Polish Academy of Sciences, Institute of Fundamental Technological Research, Swietokrzyska 21, WARSAW, Poland zmroz@ippt.gov.pl

Gyula **PATKÓ**, Institute of Machine Tools and Mechatronics, University of Miskolc, H-3515 MISKOLC, Hungary, patko@uni-miskolc.hu

Jan **SLADEK**, Ústav stavbenictva a architektúry, Slovenskej akadémie vied, Dubróvska cesta 9, 842 20 BRATISLAVA, Slovakia, usarslad@savba.sk

Gábor **STÉPÁN**, Department of Applied Mechanics, Budapest University of Technology and Economics, Műegyetem rkp. 3, 1111 BUDAPEST, Hungary, stepan@mm.bme.hu

Barna **SZABÓ**, Center for Computational Mechanics, Washington University, Campus Box 1129, St. LOUIS, MO63130, USA, szabo@me.wustl.edu

Balázs **TÓTH**, Institute of Applied Mechanics, University of Miskolc, 3515 MISKOLC, Hungary, balazs.toth@uni-miskolc.hu

HONORARY EDITORIAL BOARD MEMBERS

Imre **KOZÁK**, Institute of Applied Mechanics, University of Miskolc, H-3515 Miskolc-Egyetemváros, Hungary

Tibor **CZIBERE**, Department of Fluid and Heat Engineering, University of Miskolc, H-3515 Miskolc-Egyetemváros, Hungary

R. Ivan **LEWIS**, Room 2-16 Bruce Building, Newcastle University, NEWCASTLE UPON TYNE, NE1 7RU, UK

Gábor **HALÁSZ**, Department of Hydraulic Machines, Budapest University of Technology and Economics, Műegyetem rkp. 3, 1111 BUDAPEST, Hungary,

BUCKLING OF CIRCULAR PLATES WITH SHELL-STIFFENING ON THE BOUNDARY

DÁNIEL BURMEISTER

Institute of Applied Mechanics, University of Miskolc
H-3515 Miskolc, Miskolc–Egyetemváros, Hungary
daniel.burmeister@uni-miskolc.hu

[Received: January 26, 2015, Accepted: April 15, 2015]

Abstract. The present paper is concerned with the stability problems of a thin solid circular plate and some annular plates, each stiffened by a cylindrical shell on the external boundary. Assuming an axisymmetric dead load and non-axisymmetric deformations we determine the critical load in order to clarify what effect the stiffening shell has on the critical load. Using Kirchhoff's theory of thin shells and plates the paper presents the governing equations both for the circular plate and for the cylindrical shell, where the displacement field of the shell is obtained from a Galerkin function. The deflection of the plate and the Galerkin function are expanded into Fourier series and consequently all physical quantities in the structural elements as well. The boundary- and continuity conditions and last but not least numerical results are also presented.

Mathematical Subject Classification: 74K20, 65L15

Keywords: Buckling, stability problem, shell-stiffened circular plates, cylindrical shell, Galerkin function

1. INTRODUCTION

Stability investigations of engineering structures look back on a long history. As regards the stability problem of circular plates, we mention that the first paper devoted to this issue was published in 1890 [1]. Since then a number of papers have been devoted to this problem. Without aiming at completeness here we cite some important papers [2–11].

There are various methods for increasing the resistance of a circular plate to buckling. For example, one can apply an internal ring support, which can be either rigid or elastic. Thevendran and Wang have examined the buckling problem of annular plates which are simply supported with elastic rotational restraints at the inner or outer boundary [12]. Laura et al. have investigated the buckling of circular, solid and annular plates with an intermediate circular support under the assumption of axisymmetric deformations [13]. By the use of the Kirchhoff-Love plate theory [14, 15] and the Mindlin-Reissner theory [16] Wang and his co-authors studied the same structure under the assumption of non-axisymmetric deformations. Rao and Rao have analysed

the buckling of circular plates which are supported along concentric rings. The supports applied are simple or translational and/or torsional elastic restraints [17–20]. The authors have also investigated a circular plate with elastic foundation [21].

Another method to increase stability of a circular plate is the use of stiffeners. If these are applied densely, their effect can be averaged and smeared out by using orthotropic plates. The theoretical background of this technique can be found in the book written by Troitsky [22]. Buckling of such stiffened plates has been examined among others by Simitsev and Blackmon [23] and Srinivasan and Thiruvengatchari [24].

We can also use discrete stiffeners. The effect on stability of a ring stiffener on the boundary of a circular plate is investigated by Phillips and Carney [25]. A ring stiffened circular plate is investigated in a paper by Turvey and Der Avanessian [26]. The paper cited is concerned among others with experimental results. However, the stability issues are left out of consideration. A further paper by Turvey and Salehi [27] deals with an annular plate stiffened by a single diameter stiffener. The stability problem is, however, again left out of consideration. A further paper by Golmakani and Mehrabian deals with deflection analysis of axisymmetric ring-stiffened circular and annular laminated plates subjected to a transverse uniform load [28].

Rossetto and Miller have investigated symmetric and asymmetric buckling of a circular plate which is stiffened by a ring at an internal radius [29, 30]. The axial rigidity of the stiffening ring has been ignored. Frostig and Simitsev have examined a similar structure but they have not used the simplifications of the aforementioned article [31, 32]. The stiffening ring is modeled as a curved beam.

Szilassy dealt with the stability of circular and annular plates stiffened by a cylindrical shell on its outer boundary in his PhD. thesis [33] and in a further article [34]. It was assumed that (i) the load is an in-plane axisymmetric dead one and (ii) the deformations of the annular plate and the cylindrical shell are also axisymmetric. For solving the corresponding eigenvalue problem, he used the solution of a differential equation set up for the rotation field while the solution for the cylindrical shell is based on the theory of thin shells.

The present paper deals with the non-axisymmetric buckling of circular and annular plates which are stiffened by a cylindrical shell on the outer boundary. The paper outlines the basic assumptions, the governing equations as well as the boundary and continuity conditions. Numerical results are also shown. These represent the influence of shell geometry on buckling load. As regards the cylindrical shell we shall utilize some results from Vlasov [35] and Jezsó [36].

2. PROBLEM FORMULATION

The cross section of the shell-stiffened structure we are concerned with is shown in Figure 1. It consists of either a solid circular plate or an annular one – the latter is shown in Figure 1 – and a cylindrical shell, which stiffens the plate on its external boundary. The inner radius of the plate is denoted by R_i , the radius of the intersection

line of the middle surfaces of the plate and the shell by R_e . If the plate is a circular one then $R_i = 0$. The shell is symmetric with respect to the middle plane of the plate. Its height is $2h$. We shall assume that R_e coincides with the external radius of the plate. The thicknesses of the plate and shell are denoted by b_p and b_s , respectively. The structure is loaded by radial distributed forces with a constant intensity f_o acting in the middle plane of the plate. The load is a dead load.

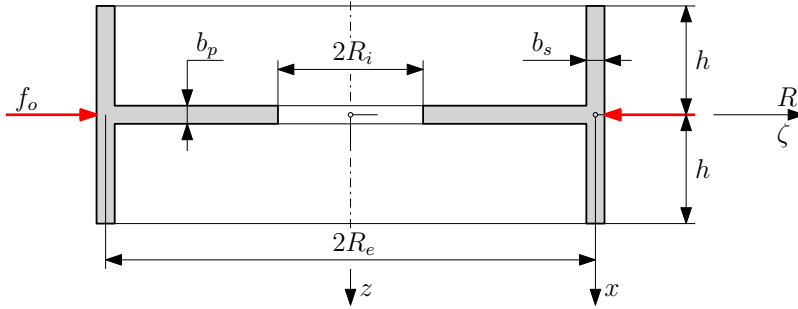


Figure 1. The structure and its load

We shall assume that the plate and the shell are thin, consequently we can use the Kirchhoff theory of plates and shells. It is also assumed that the problem is linear with regard to the kinematic equations and material law. Heat effects are not taken into account. The plate and the shell are made of homogeneous isotropic material for which E_p , E_s and ν_p , ν_s are Young's modulus and Poisson's ratio for the plate and the shell respectively.

Figure 2 shows the various tasks which can be investigated. Figure 2a. is the inner part of a solid circular plate and subfigures b.-d. are supports that can be applied on the inner boundary of an annular plate.

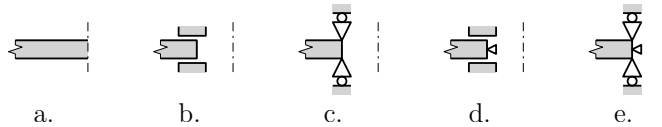


Figure 2. Possible supports

Our main goal is to determine (a) the critical load of the structure and (b) the effect of the stiffening shell on the critical load under the assumption of small, non-axisymmetric and linearly elastic deformations.

The shell and the plate are divided mentally. The cylindrical coordinate system (R, φ, z) is used for the equations of the plate – the plane $z = 0$ coincides with the middle surface of the plate. Figure 3a. shows the corresponding coordinate curves on the circle with radius R_e . The displacements on the middle surface in the directions R , φ and z are denoted by u , v and w respectively.

For the cylindrical shell the coordinate system (ζ, φ, ξ) is applied. The coordinate surface $\xi = z$, $\zeta = 0$ coincides with the middle surface of the shell with radius R_e . The polar angle φ is the same in the two coordinate systems. The coordinate curves on the middle surface of the shell are also shown in Figure 3b. The displacements on the middle surface of the shell in the directions ζ , φ , ξ are denoted by u_ζ , u_φ and u_ξ , respectively.

In the mathematical formulations we use the dimensionless coordinates $\rho = R/R_e$ and $\xi = x/R_e$. The dimensionless coordinates on the boundaries are denoted by $\rho_i = R_i/R_e$ and $\xi_h = h/R_e$.

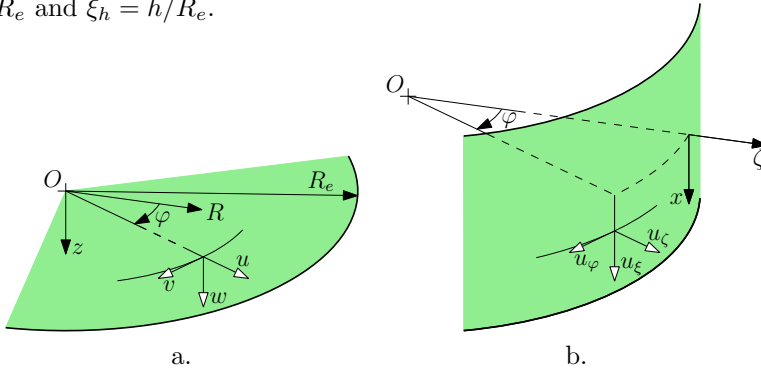


Figure 3. Coordinate curves in the coordinate systems

3. GOVERNING EQUATIONS

3.1. In-plane loads and forces. Figure 4 shows the separated parts of the structure with the inner forces acting in the middle plane of the plate between the two elements. The load is axisymmetric, consequently the equations governing the pre-buckling (membrane) state for each part are axisymmetric as well.

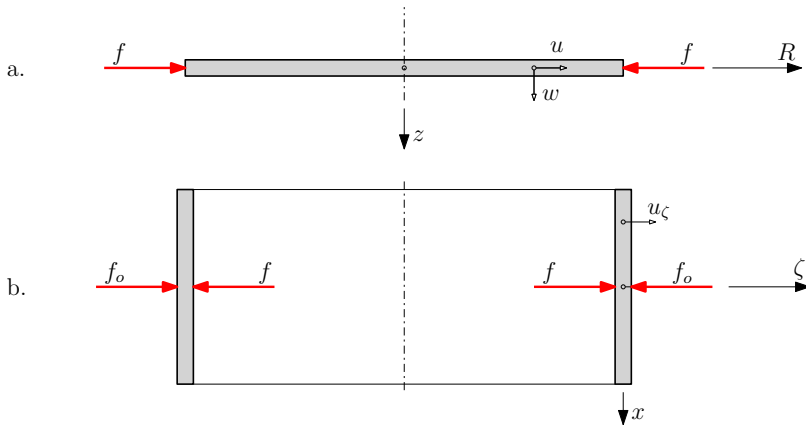


Figure 4. Free body diagram for plate and shell

The distributed load f exerted on the plate by the shell can be obtained from the axisymmetric deformations of the shell and by utilizing the continuity condition between the shell and the plate:

$$u(\rho = 1) = u_\zeta(\xi = 0) = -\underbrace{\frac{\nu_o}{2E_s} \left(\frac{R_e}{b_s}\right)^{\frac{3}{2}} \frac{\cos 2h\beta + \cosh 2h\beta + 2}{\sin 2h\beta + \sinh 2h\beta}}_{\alpha} (f_o - f) = -\alpha (f_o - f). \quad (3.1)$$

where $\nu_o = \sqrt[4]{3(1 - \nu_s^2)}$ and α is defined by the above relation – for details see [37].

Due to the axisymmetry of the in-plane loads, the inner forces in the plate depend only on the radial coordinate ρ . The inner forces due to f take the form

$$N_R = f\mathcal{N}_R = f \left(-A + \frac{B}{\rho^2} \right), \quad (3.2a)$$

$$N_\varphi = f\mathcal{N}_\varphi = f \left(-A - \frac{B}{\rho^2} \right), \quad (3.2b)$$

$$N_{R\varphi} = N_{\varphi R} = f\mathcal{N}_{R\varphi} = 0 \quad (3.2c)$$

where the constants A and B depend on the boundary conditions. It follows from the axisymmetry that $N_{R\varphi}$ vanishes. If the plate is a solid one – see Figure 2a – then

$$A = 1 \quad \text{and} \quad B = 0. \quad (3.3a)$$

If the inner boundary is free and f is the distributed load on the outer boundary – see Figure 2b. and c. – then the constants are as follows:

$$A = \frac{1}{1 - \rho_i^2} \quad \text{and} \quad B = \frac{\rho_i^2}{1 - \rho_i^2}. \quad (3.3b)$$

If the radial displacement vanishes on the inner boundary – see Fig. 2 d. and e. – then

$$A = \frac{1 + \nu_p}{1 + \nu_p + \rho_i^2(1 - \nu_p)} \quad \text{and} \quad B = -\frac{\rho_i^2(1 - \nu_p)}{1 + \nu_p + \rho_i^2(1 - \nu_p)}. \quad (3.3c)$$

The radial displacement on the inner boundary can be calculated by using the relations

$$u(\rho = 1) = -K \frac{R_e}{b_p} \frac{f}{E_p}, \quad (3.4)$$

where the constant K depends on the boundary conditions

$$K = 1 - \nu_p \quad \text{if} \quad \rho_i = 0, \quad (3.5a)$$

$$K = \frac{1 - \nu_p + \rho_i^2(1 + \nu_p)}{1 - \rho_i^2} \quad \text{if} \quad N_R(\rho = \rho_i) = 0, \quad (3.5b)$$

$$K = \frac{(1 - \nu_p^2)(1 - \rho_i^2)}{1 + \nu_p + \rho_i^2(1 - \nu_p)} \quad \text{if} \quad u(\rho = \rho_i) = 0. \quad (3.5c)$$

3.2. Deformation of the annular plate, equations for the displacement field after stability loss. The buckling equation can be given in the form [32]

$$\Delta\Delta w - \mathfrak{F} \left[\mathcal{N}_R \frac{\partial^2 w}{\partial \rho^2} + \mathcal{N}_\varphi \left(\frac{1}{\rho} \frac{\partial w}{\partial \rho} + \frac{1}{\rho^2} \frac{\partial^2 w}{\partial \varphi^2} \right) \right] = 0 \quad (3.6)$$

where

$$\mathfrak{F} = f \frac{R_e^2}{I_{1p} E_{1p}} \quad (3.7)$$

is the dimensionless load parameter wherein

$$I_{1p} = \frac{b_p^3}{12}, \quad E_{1p} = \frac{E_p}{1 - \nu_p^2} \quad (3.8)$$

and

$$\Delta = \frac{\partial^2}{\partial \rho^2} + \frac{1}{\rho} \frac{\partial}{\partial \rho} + \frac{1}{\rho^2} \frac{\partial^2}{\partial \varphi^2} \quad (3.9)$$

is the Laplace operator in the polar coordinate system (ρ, φ) .

The physical quantities which appear in the boundary conditions, such as the rotation, the shear force and the bending moment can all be given in terms of the solution for w as follows

$$\vartheta = -\frac{1}{R_e} \frac{dw}{d\rho}, \quad (3.10a)$$

$$M_R = -\frac{I_{1p} E_{1p}}{R_e^2} \left[\frac{\partial^2 w}{\partial \rho^2} + \frac{\nu_p}{\rho} \left(\frac{\partial w}{\partial \rho} + \frac{1}{\rho} \frac{\partial^2 w}{\partial \varphi^2} \right) \right], \quad (3.10b)$$

$$Q_R = I_{1p} E_{1p} \frac{1}{R_e^3} \frac{\partial}{\partial \rho} (\Delta w) - \frac{N_R}{R_e} \frac{\partial w}{\partial \rho} - \frac{1}{\rho R_e} \frac{\partial M_{R\varphi}}{\partial \varphi}. \quad (3.10c)$$

For non axisymmetric deformations we expand the solution giving the deflection w in a Fourier series of the form

$$w = w_o + \sum_{m=0}^1 \sum_{n=1}^{\infty} w_n^m(\rho) \cos \left(n\varphi - m \frac{\pi}{2} \right) \quad (3.11)$$

and substitute it into (3.9). We obtain that the amplitudes $w_o(\rho)$ and $w_n^m(\rho)$ should fulfill the following differential equations:

$$\Delta_n \Delta_n w_n^m - \mathfrak{F} \left[\mathcal{N}_R \frac{\partial^2 w_n^m}{\partial \rho^2} + \mathcal{N}_\varphi \left(\frac{1}{\rho} \frac{\partial w_n^m}{\partial \rho} - \frac{n^2}{\rho^2} w_n^m \right) \right] = 0 \quad (3.12)$$

$$m = 0, 1; \quad n = 1, 2, \dots$$

where

$$\Delta_n = \frac{d^2}{d\rho^2} + \frac{d}{\rho d\rho} - \frac{n^2}{\rho^2}. \quad (3.13)$$

If the plate is a circular one, than $\mathcal{N}_R = \mathcal{N}_\varphi = 1$, and equations (3.12) have a closed form solution:

$$w_n^m(\rho) = c_1 Z_1 + c_2 Z_2 + c_3 Z_3 + c_4 Z_4, \quad (3.14a)$$

$$Z_1 = \rho^n, \quad Z_2 = \rho^{-n}, \quad Z_3 = J_n(\sqrt{\mathfrak{F}}\rho), \quad Z_4 = Y_n(\sqrt{\mathfrak{F}}\rho), \quad (3.14b)$$

where c_1, c_2, c_3 and c_4 are integration constants. Otherwise, if the plate is an annular one we use a numerical algorithm (for example the Runge-Kutta method) in the solution procedure – see [37] for details.

The physical quantities in the plate can also be expanded into a Fourier series similarly to the deflection. Thus we get

$$\vartheta = \vartheta_o + \sum_{m=0}^1 \sum_{n=1}^{\infty} \vartheta_n^m \cos\left(n\varphi - m\frac{\pi}{2}\right), \quad (3.15a)$$

for the rotation field,

$$M_R = M_{R_o} + \sum_{m=0}^1 \sum_{n=1}^{\infty} M_{Rn}^m \cos\left(n\varphi - m\frac{\pi}{2}\right), \quad (3.15b)$$

for the bending moment, and

$$Q_R = Q_{R_o} + \sum_{m=0}^1 \sum_{n=1}^{\infty} Q_{Rn}^m \cos\left(n\varphi - m\frac{\pi}{2}\right) \quad (3.15c)$$

for the shear force.

It can be shown that the amplitude functions of the rotation ψ_φ , the bending moment M_R and the shear force Q_R can all be given in terms of the amplitudes of w as follows:

$$\vartheta_n^m = -\frac{1}{R_e} \frac{d^m w_n^m}{d\rho}, \quad (3.16a)$$

$$M_{Rn}^m = -\frac{I_1 E_{1p}}{R_e^2} \left[\frac{d^2 w_n^m}{d\rho^2} + \frac{\nu}{\rho} \left(\frac{d w_n^m}{d\rho} - \frac{n^2}{\rho} w_n^m \right) \right] \quad (3.16b)$$

$$Q_{Rn}^m = \frac{I_{1p} E_{1p}}{R_e^3} \left[\frac{d^3 w_n^m}{d\rho^3} + \frac{1}{\rho} \frac{d^2 w_n^m}{d\rho^2} - \left(\frac{1}{\rho^2} (1 + 2n^2(1 - \nu)) + \mathfrak{F} \mathcal{N}_R \right) \frac{d w_n^m}{d\rho} + \frac{3n^2}{\rho^3} w_n^m \right]. \quad (3.16c)$$

3.3. Governing equations for the cylindrical shell.

3.3.1. Field equations for the shell. The kinematic quantities which describe the deformations of the shell can be calculated by the displacements u_φ , u_ξ and u_x . Using the coordinate ξ the rotations can be obtained from the relations

$$\psi_\varphi = \frac{1}{R_e} \frac{\partial u_\xi}{\partial \xi}, \quad (3.17a)$$

$$\psi_x = \frac{1}{R_e} \left(\frac{\partial u_\xi}{\partial \varphi} - u_\varphi \right). \quad (3.17b)$$

The deformations on the middle surface of the shell are also characterized by the axial strains

$$e_{xx} = \frac{1}{R_e} \frac{\partial u_\xi}{\partial \xi}, \quad (3.18a)$$

$$e_{x\varphi} = \frac{1}{2R_e} \left(\frac{\partial u_\xi}{\partial \varphi} + \frac{\partial u_\varphi}{\partial \xi} \right), \quad (3.18b)$$

$$e_{\varphi\varphi} = \frac{1}{R_e} \left(\frac{\partial u_\varphi}{\partial \varphi} + u_\zeta \right) \quad (3.18c)$$

and by the elements of the curvature tensor:

$$\kappa_{xx} = -\frac{1}{R_e^2} \frac{\partial^2 u_\zeta}{\partial \xi^2}, \quad (3.19a)$$

$$\kappa_{\varphi\varphi} = -\frac{1}{R_e^2} \frac{\partial^2 u_\zeta}{\partial \varphi^2}, \quad (3.19b)$$

$$\kappa_{x\varphi} = \kappa_{\varphi x} = -\frac{1}{R_e^2} \frac{\partial^2 u_\zeta}{\partial \xi \partial \varphi}. \quad (3.19c)$$

Using these kinematic quantities the corresponding inner forces are obtained from Hooke's law:

$$N_{xx} = E_{1s} b_s (e_{xx} + \nu e_{\varphi\varphi}), \quad (3.20a)$$

$$N_{\varphi\varphi} = E_{1s} b_s (e_{\varphi\varphi} + \nu e_{xx}), \quad (3.20b)$$

$$N_{\varphi x} = E_{1s} b_s (1 - \nu) e_{x\varphi}. \quad (3.20c)$$

The elements of the internal moments tensor are given by the relations below:

$$M_{xx} = E_{1s} I_{1s} (\kappa_{xx} + \nu \kappa_{\varphi\varphi}), \quad (3.21a)$$

$$M_{\varphi\varphi} = E_{1s} I_{1s} (\kappa_{\varphi\varphi} + \nu \kappa_{xx}), \quad (3.21b)$$

$$M_{x\varphi} = E_{1s} I_{1s} (1 - \nu) \kappa_{x\varphi}. \quad (3.21c)$$

Note that the internal moment tensor is assumed to be symmetric, i.e. $M_{x\varphi} = M_{\varphi x}$.

The shear forces on the middle surface of the shell are denoted by $Q_{x\zeta}$ and $Q_{\varphi\zeta}$. The above equations are associated with the equilibrium equations

$$\frac{1}{R_e} \frac{\partial N_{xx}}{\partial \xi} + \frac{1}{R_e} \frac{\partial N_{\varphi x}}{\partial \varphi} + p_x = 0, \quad (3.22a)$$

$$\frac{1}{R_e} \frac{\partial N_{\varphi x}}{\partial \xi} + \frac{1}{R_e} \frac{\partial N_{\varphi\varphi}}{\partial \varphi} + \frac{1}{R_e} Q_{\varphi\zeta} + p_\varphi = 0, \quad (3.22b)$$

$$-\frac{1}{R_e} \frac{\partial Q_{x\zeta}}{\partial \xi} - \frac{1}{R_e} \frac{Q_{\varphi\zeta}}{\partial \varphi} - \frac{1}{R_e} N_{\varphi\varphi} + p_\zeta = 0, \quad (3.22c)$$

$$\frac{1}{R_e} \frac{\partial M_{xx}}{\partial \xi} + \frac{1}{R_e} \frac{\partial M_{\varphi x}}{\partial \varphi} + Q_{x\zeta} = 0, \quad (3.22d)$$

$$\frac{1}{R_e} \frac{\partial M_{x\varphi}}{\partial \xi} + \frac{1}{R_e} \frac{\partial M_{\varphi\varphi}}{\partial \varphi} + Q_{\varphi\zeta} = 0 \quad (3.22e)$$

in which p_x , p_φ and p_ζ are the intensities of the distributed loads exerted on the middle surface of the shell.

Observe that we have as many equations as there are unknowns (nineteen equations (3.17)-(3.22) in nineteen unknowns).

3.3.2. *The Galerkin function.* For $p_x = p_\varphi = 0$ the fundamental equations (obtained after we have eliminated the intermediate variables) set up for the displacement coordinates u_{xi} , u_φ and u_ζ will be fulfilled identically if we calculate the displacement coordinates in terms of the Galerkin function $\phi(\xi, \varphi)$ using the relations [35, 36]

$$u_\xi = \frac{\partial^3 \phi}{\partial \xi \partial \varphi^2} - \nu_s \frac{\partial^3 \phi}{\partial \xi^3}, \quad (3.23a)$$

$$u_\varphi = -\frac{\partial^3 \phi}{\partial \varphi^3} - (2 + \nu_s) \frac{\partial^3 \phi}{\partial \xi^2 \partial \varphi}, \quad (3.23b)$$

$$u_\zeta = \nabla^2 \nabla^2 \phi \quad (3.23c)$$

in which ϕ should satisfy the differential equation

$$\nabla^2 \nabla^2 \nabla^2 \nabla^2 \phi + 4\hat{\beta}^4 \frac{\partial^4 \phi}{\partial \xi^4} = \frac{4\hat{\beta}^4 R_e^2}{E_s b_s} p_\zeta \quad (3.24)$$

where

$$4\hat{\beta}^4 = 12(1 - \nu_s^2) \frac{R_e^2}{b_s^2} \quad (3.25a)$$

and

$$\nabla^2 = \frac{\partial^2}{\partial \xi^2} + \frac{\partial^2}{\partial \varphi^2}. \quad (3.25b)$$

Every physical quantity appearing in the boundary conditions can be written in terms of the Galerkin function ϕ if we substitute the displacements (3.23) into equations (3.17)-(3.22). Omitting the formal transformations we get:

$$\psi_\varphi = \frac{1}{R_e} \frac{\partial}{\partial \xi} \nabla^2 \nabla^2 \phi, \quad (3.26a)$$

$$N_{xx} = \frac{E_s b_s}{R_e} \frac{\partial^4 \phi}{\partial \xi^2 \partial \varphi^2}, \quad (3.26b)$$

$$N_{\varphi x} = -\frac{E_s b_s}{R_e} \frac{\partial^4 \phi}{\partial \xi^3 \partial \varphi}, \quad (3.26c)$$

$$M_{xx} = -\frac{E_s b_s}{4\hat{\beta}^4} \left[\frac{\partial^2}{\partial \xi^2} + \nu_s \frac{\partial^2}{\partial \varphi^2} \right] \nabla^2 \nabla^2 \phi, \quad (3.26d)$$

$$M_{x\varphi} = -\frac{E_s b_s (1 - \nu_s)}{4\hat{\beta}^4} \frac{\partial^2}{\partial \xi \partial \varphi} \nabla^2 \nabla^2 \phi, \quad (3.26e)$$

$$Q_{x\zeta} = \frac{1}{R_e} \frac{E_s b_s}{4\hat{\beta}^4} \frac{\partial}{\partial \xi} \nabla^2 \nabla^2 \nabla^2 \phi. \quad (3.26f)$$

3.3.3. *Solution for the Galerkin function.* Let us expand the function $\phi(\xi, \varphi)$ into a Fourier series similarly to the deflection w . We can write

$$\phi = \phi(\xi, \varphi) = \phi_o(\xi) + \sum_{n=1}^{\infty} \sum_{m=0}^1 \phi_n^m(\xi) \cos\left(n\varphi - m\frac{\pi}{2}\right). \quad (3.27)$$

Substituting the series (3.27) into differential equation (3.24) we obtain that the coefficients ϕ_n^m of the series should satisfy the ordinary differential equations

$$\frac{d^8 \phi_n^m}{d\xi^8} - 4n^2 \frac{d^6 \phi_n^m}{d\xi^6} + 6n^4 \frac{d^4 \phi_n^m}{d\xi^4} - 4n^6 \frac{d^2 \phi_n^m}{d\xi^2} + n^8 \phi_n^m + 4\hat{\beta}^4 \frac{d^4 \phi_n^m}{d\xi^4} = \frac{4\hat{\beta}^4 R_e^2}{Eb_s} p_{\zeta n}^m \quad (3.28)$$

$$m = 0, 1; \quad n = 0, 1, 2, \dots$$

where the coefficients $p_{\zeta n}^m$ on the right side are those of the Fourier series that belongs to the load exerted on the middle surface of the shell:

$$p_{\zeta}(\xi, \varphi) = p_{\zeta o}(\xi) + \sum_{n=1}^{\infty} \sum_{m=0}^1 p_{\zeta n}^m(\xi) \cos\left(n\varphi - m\frac{\pi}{2}\right) \quad (3.29)$$

In the investigated problem this load is zero, consequently the solutions of differential equations (3.28) have only a homogeneous part.

The solution of equation (3.28) is sought in the form

$$\phi_n^m = e^{\lambda_n \xi}. \quad (3.30)$$

After substituting it into equation (3.28) we get the characteristic polynomial for the (m, n) -th differential equation:

$$(\lambda_n^2 - n^2)^4 = -4\hat{\beta}^4 \lambda_n^4 \quad (3.31)$$

By introducing the notations

$$b_n = \frac{\hat{\beta}}{2} \sqrt{\sqrt{1 + 4\left(\frac{n}{\hat{\beta}}\right)^4} + 2\left(\frac{n}{\hat{\beta}}\right)^2}, \quad (3.32a)$$

$$a_n = \frac{\hat{\beta}}{2} \sqrt{\sqrt{1 + 4\left(\frac{n}{\hat{\beta}}\right)^4} - 2\left(\frac{n}{\hat{\beta}}\right)^2}, \quad (3.32b)$$

and

$$\beta_{n1} = b_n + \frac{\hat{\beta}}{2}, \quad (3.33a)$$

$$\beta_{n2} = b_n - \frac{\hat{\beta}}{2}, \quad (3.33b)$$

$$\alpha_{n1} = \frac{\hat{\beta}}{2} + a_n, \quad (3.33c)$$

$$\alpha_{n2} = \frac{\hat{\beta}}{2} - a_n \quad (3.33d)$$

it can be shown that the roots of equation (3.31) are as follows:

$$\lambda_{n1} = -\beta_{n2} + i\alpha_{n2}, \quad (3.34a)$$

$$\lambda_{n2} = -\beta_{n1} + i\alpha_{n1}, \quad (3.34b)$$

$$\lambda_{n3} = -\beta_{n2} - i\alpha_{n2}, \quad (3.34c)$$

$$\lambda_{n4} = -\beta_{n1} - i\alpha_{n1}, \quad (3.34d)$$

$$\lambda_{n5} = -\lambda_{n1}, \quad (3.34e)$$

$$\lambda_{n6} = -\lambda_{n2}, \quad (3.34f)$$

$$\lambda_{n7} = -\lambda_{n3}, \quad (3.34g)$$

$$\lambda_{n8} = -\lambda_{n4}. \quad (3.34h)$$

Substituting solution (3.34) into (3.30) and making some manipulations we get the real part of the solution for the Galerkin function:

$$\begin{aligned} \phi_n^m = \sum_{j=1}^2 \left\{ \begin{aligned} & \overset{m}{K}_{nj} \sinh(\beta_{nj}\xi) \sin(\alpha_{nj}\xi) + \overset{m}{M}_{nj} \sinh(\beta_{nj}\xi) \cos(\alpha_{nj}\xi) + \\ & + \overset{m}{P}_{nj} \cosh(\beta_{nj}\xi) \sin(\alpha_{nj}\xi) + \overset{m}{S}_{nj} \cosh(\beta_{nj}\xi) \cos(\alpha_{nj}\xi) \end{aligned} \right\} \quad (3.35) \end{aligned}$$

where $\overset{m}{K}_{nj}$, $\overset{m}{M}_{nj}$, $\overset{m}{P}_{nj}$ and $\overset{m}{S}_{nj}$ constitute eight undetermined integration constants.

The Fourier series of the physical quantities in the shell can be written in a form similar to the series (3.11):

$$u_\xi = u_{\xi o} + \sum_{n=1}^{\infty} \sum_{m=0}^1 \overset{m}{u}_{\xi n} \cos\left(n\varphi - m\frac{\pi}{2}\right), \quad (3.36a)$$

$$u_\varphi = u_{\varphi o} + \sum_{n=1}^{\infty} \sum_{m=0}^1 \overset{m}{u}_{\varphi n} \sin\left(n\varphi - m\frac{\pi}{2}\right), \quad (3.36b)$$

$$u_\zeta = u_{\zeta o} + \sum_{n=1}^{\infty} \sum_{m=0}^1 \overset{m}{u}_{\zeta n} \cos\left(n\varphi - m\frac{\pi}{2}\right), \quad (3.36c)$$

$$\psi_\varphi = \psi_{\varphi o} + \sum_{n=1}^{\infty} \sum_{m=0}^1 \overset{m}{\psi}_{\varphi n} \cos\left(n\varphi - m\frac{\pi}{2}\right), \quad (3.36d)$$

$$N_{xx} = N_{xx o} + \sum_{n=1}^{\infty} \sum_{m=0}^1 \overset{m}{N}_{xx n} \cos\left(n\varphi - m\frac{\pi}{2}\right), \quad (3.36e)$$

$$N_{\varphi x} = N_{\varphi x o} + \sum_{n=1}^{\infty} \sum_{m=0}^1 \overset{m}{N}_{\varphi x n} \sin\left(n\varphi - m\frac{\pi}{2}\right), \quad (3.36f)$$

$$M_{xx} = M_{xxo} + \sum_{n=1}^{\infty} \sum_{m=0}^1 M_{xxn}^m \cos\left(n\varphi - m\frac{\pi}{2}\right), \quad (3.36g)$$

$$M_{x\varphi} = M_{x\varphi o} + \sum_{n=1}^{\infty} \sum_{m=0}^1 M_{x\varphi n}^m \sin\left(n\varphi - m\frac{\pi}{2}\right), \quad (3.36h)$$

$$Q_{x\zeta} = Q_{x\zeta o} + \sum_{n=1}^{\infty} \sum_{m=0}^1 Q_{x\zeta n}^m \cos\left(n\varphi - m\frac{\pi}{2}\right). \quad (3.36i)$$

Utilizing relations (3.23) and (3.26), which provide the physical quantities on the middle surface of the shell in terms of the Galerkin function, the coefficients in the series (3.36) can also be given in terms of the coefficients ϕ_n^m of the Galerkin functions

$$u_{\xi n}^m = - \left(n^2 \frac{d\phi_n^m}{d\xi} + \nu \frac{d^3\phi_n^m}{d\xi^3} \right), \quad (3.37a)$$

$$u_{\varphi n}^m = \left(-n^3 \phi_n^m + n(2 + \nu) \frac{d^2\phi_n^m}{d\xi^2} \right), \quad (3.37b)$$

$$u_{\zeta n}^m = \left(n^4 \phi_n^m - 2n^2 \frac{d^2\phi_n^m}{d\xi^2} + \frac{d^4\phi_n^m}{d\xi^4} \right), \quad (3.37c)$$

$$\psi_{\phi n}^m = -\frac{1}{R_e} \left(n^4 \frac{d\phi_n^m}{d\xi} - 2n^2 \frac{d^3\phi_n^m}{d\xi^3} + \frac{d^5\phi_n^m}{d\xi^5} \right), \quad (3.37d)$$

$$N_{xxn}^m = -\frac{E_s b_s}{R_e} n^2 \frac{d^2\phi_n^m}{d\xi^2}, \quad (3.37e)$$

$$N_{\varphi xn}^m = -\frac{E_s b_s}{R_e} n \frac{d^3\phi_n^m}{d\xi^3}, \quad (3.37f)$$

$$M_{xxn}^m = -\frac{E_s b_s}{4\hat{\beta}^4} \left(n^4 \frac{d^2\phi_n^m}{d\xi^2} - 2n^2 \frac{d^4\phi_n^m}{d\xi^4} + \frac{d^6\phi_n^m}{d\xi^6} - \nu n^2 \left[n^4 \phi_n^m - 2n^2 \frac{d^2\phi_n^m}{d\xi^2} + \frac{d^4\phi_n^m}{d\xi^4} \right] \right), \quad (3.37g)$$

$$M_{x\varphi n}^m = \frac{(1 - \nu) E_s b_s}{4\hat{\beta}^4} \left(n^5 \frac{d\phi_n^m}{d\xi} - 2n^3 \frac{d^3\phi_n^m}{d\xi^3} + n \frac{d^5\phi_n^m}{d\xi^5} \right), \quad (3.37h)$$

$$Q_{x\zeta n}^m = \frac{1}{R_e} \frac{E_s b_s}{4\hat{\beta}^4} \left(-n^6 \frac{d\phi_n^m}{d\xi} + 3n^4 \frac{d^3\phi_n^m}{d\xi^3} - 3n^2 \frac{d^5\phi_n^m}{d\xi^5} + \frac{d^7\phi_n^m}{d\xi^7} \right). \quad (3.37i)$$

Substituting equation (3.35) into the above relations we obtain the Fourier coefficients of the physical quantities appearing in the boundary conditions in terms of the coordinate ξ . For the sake of brevity these are omitted here.

3.4. Boundary- and continuity conditions. A solution for the amplitude of the displacement field on the middle surface of the plate contains four, while a solution for ϕ_n^m involves eight integration constants. The stiffening shell is mentally divided in two separate shells at the intersection line of the middle surfaces of the plate and the shell. Therefore we need two solutions for each of the two parts of the shell, consequently we have to determine altogether twenty integration constants.

In what follows we shall present the boundary- and continuity conditions which provide the integration constants. We begin with the free boundaries of the shell, where the following conditions should be satisfied:

$$N_{xxn}^m(\xi = \pm\xi_h) = 0, \quad (3.38a)$$

$$N_{x\varphi n}^m(\xi = \pm\xi_h) + nM_{x\varphi n}^m(\xi = \pm\xi_h)/R_e = 0, \quad (3.38b)$$

$$M_{xxn}^m(\xi = \pm\xi_h) = 0, \quad (3.38c)$$

$$Q_{x\zeta n}^m(\xi = \pm\xi_h) - nM_{x\varphi n}^m(\xi = \pm\xi_h)/R_e = 0. \quad (3.38d)$$

These are altogether eight equations.

The shell and plate deform together on the intersection line of the middle surfaces of the shell and the plate, which results in the following kinematic continuity conditions:

$$u_{\xi n}^m(\xi = \pm 0) = w_n^m(\rho = 1), \quad (3.39a)$$

$$\psi_{\varphi n}^m(\xi = \pm 0) = \vartheta_n^m(\rho = 1), \quad (3.39b)$$

$$u_{\zeta n}^m(\xi = \pm 0) = u_n^m(\rho = 1) = 0, \quad (3.39c)$$

$$u_{\varphi n}^m(\xi = \pm 0) = v_n^m(\rho = 1) = 0, \quad (3.39d)$$

$$n \neq 0$$

Here the two sides of the plate at $\xi = 0$ are designated by $\xi = +0$ and $\xi = -0$. Observe that conditions (3.39c,d) reflect the fact that the plane stress problem is axisymmetric, i.e. condition (3.1) together with (3.4), furthermore $v_o^m(\rho = 1) = u_{\varphi o}^m(\xi = 0)$ holds if $n = 0$. The kinematic continuity conditions provide eight independent equations.

For the shear force $Q_{x\zeta n}^m$ we can not prescribe any condition, since $u_{\zeta n}^m(\xi = 0) = 0$. Since $u_{\varphi n}^m(\rho = 1) = 0$ we can not prescribe continuity conditions for the inner forces $N_{R\varphi n}^m$ and $N_{x\varphi n}^m$. However the axisymmetric parts of these quantities are also equal to zero.

It follows from the global equilibrium of the structure that the axisymmetric part of the shear force should meet the condition $Q_{Ro} = 0$. Otherwise the continuity

condition

$$\overset{m}{Q}_{Rn}(\rho = 1) + \overset{m}{N}_{xxn}(\xi = +0) - \overset{m}{N}_{xxn}(\xi = -0) = 0 \quad (3.40)$$

should be fulfilled – see Figure 5 a.

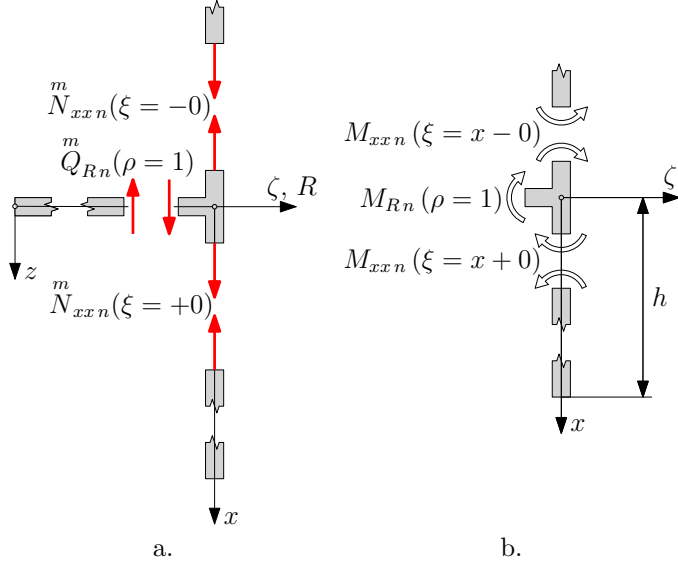


Figure 5. Forces and moments between the two elements

As regards the bending moments, equation

$$\overset{m}{M}_{Rn}(\rho = 1) + \overset{m}{M}_{xxn}(\xi = +0) - \overset{m}{M}_{xxn}(\xi = -0) = 0 \quad (3.41)$$

is the continuity condition for the coefficients of the Fourier series – see Figure 5b.

The boundary conditions on the inner boundary of the plate depend on the supports applied. It is clear that two boundary conditions can be prescribed on the inner boundary. Consequently the boundary- and continuity conditions provide altogether twenty homogenous equations for the twenty integration constants. These equations involve \mathfrak{F} as a parameter. Therefore the critical value of \mathfrak{F} can be determined from the condition that the system determinant should vanish.

4. NUMERICAL RESULTS

4.1. **Circular plate.** If the plate has no hole in it then the displacement $\overset{m}{w}_n$ and its derivatives (i.e. the rotation $\overset{m}{\psi}_{\varphi n}$) have to be finite:

$$\overset{m}{w}_n = \text{finite} , \quad (4.1a)$$

$$\overset{m}{\psi}_{\varphi n} = \text{finite} . \quad (4.1b)$$

A code has been written in Fortran 90 to solve the non-linear equation for \mathfrak{F}_{cr} and compute \mathfrak{F}_{ocr} . The calculations were made with the material and thickness properties taken as the same ($E = E_p = E_s = 200$ GPa, $\nu = \nu_p = \nu_s = 0.3$, $b = b_p = b_s$) and the thickness to radius ratio had a fixed value ($b/R_e = 0.01$). The computational results are presented in Figure 6 for the first 4 members of the Fourier-series and for axisymmetric deformations ($n = 0$). It is clear from the graphs that the height of the plate does not affect the critical load if the height is larger than a certain value. One can see that the lowest value of the critical load belongs to the case of the axisymmetric deformation; the only exception is the critical load if $n = 2$ and the shell height (i.e. the $\frac{h}{R_e}$ ratio) is small.

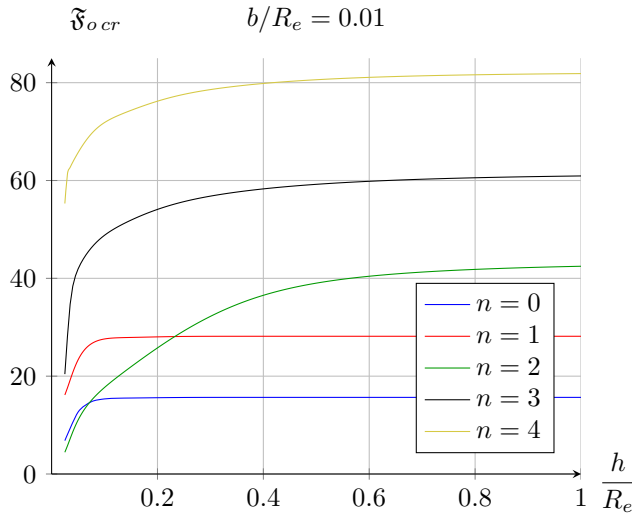


Figure 6. Critical load for a circular plate

4.2. Annular plate with simple support. Consider a stiffened annular plate with simple support on its inner boundary –see Figure 2 c. The boundary conditions at the inner edge are as follows:

$$w_n^m(\rho = \rho_i) = 0, \quad (4.2a)$$

$$M_{Rn}^m(\rho = \rho_i) = 0. \quad (4.2b)$$

Figure 7 shows the buckling load parameter \mathfrak{F} versus the $\frac{h}{R_e}$ height of the shell in three diagrams if the inner radii are $\rho_i = 0.25$, $\rho_i = 0.5$ and $\rho_i = 0.75$. The other data were the same as in the previous problem. The curves are all asymptotic in a different measure. The smallest critical load belongs to axisymmetric deformations, but if the height is relatively small the curve belonging to $n = 2$ has smaller values. This curve has also the slowest convergence. The range where asymmetric mode gives the buckling load increases if the inner radius becomes greater.

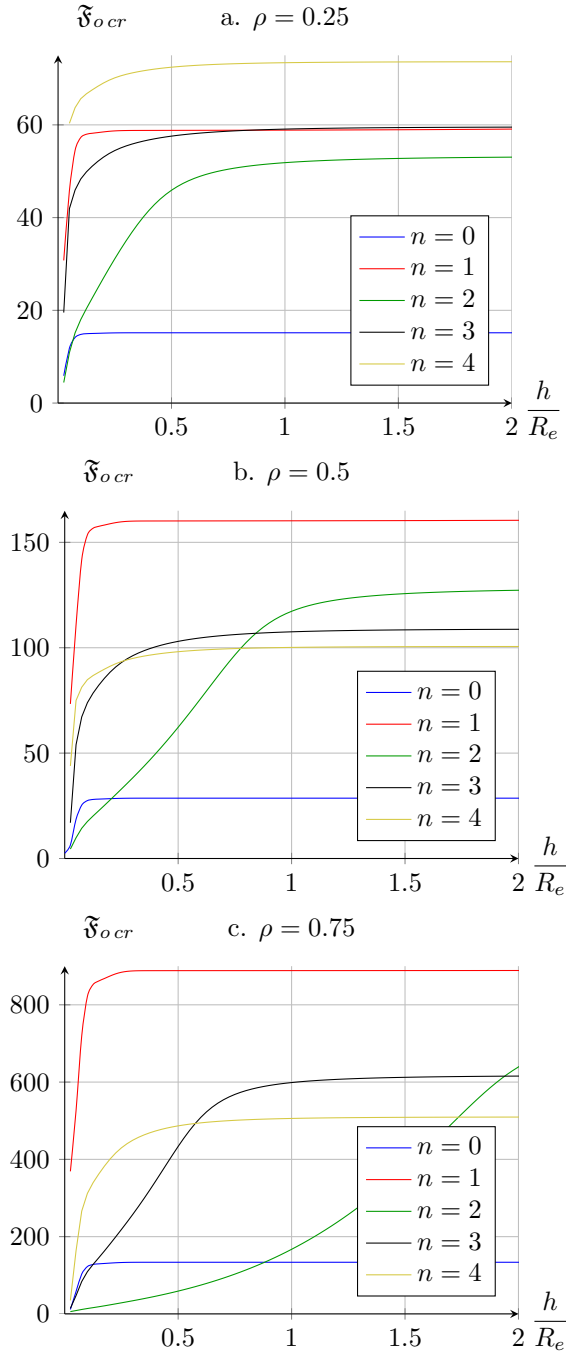


Figure 7. Critical load of simply supported annular plates

Figure 8 shows the critical load against ρ_i and $\frac{h}{R_e}$ for the modes $n = 1, \dots, 4$. The axis $\mathfrak{F}_{o\ cr}$ is a logarithmic one.

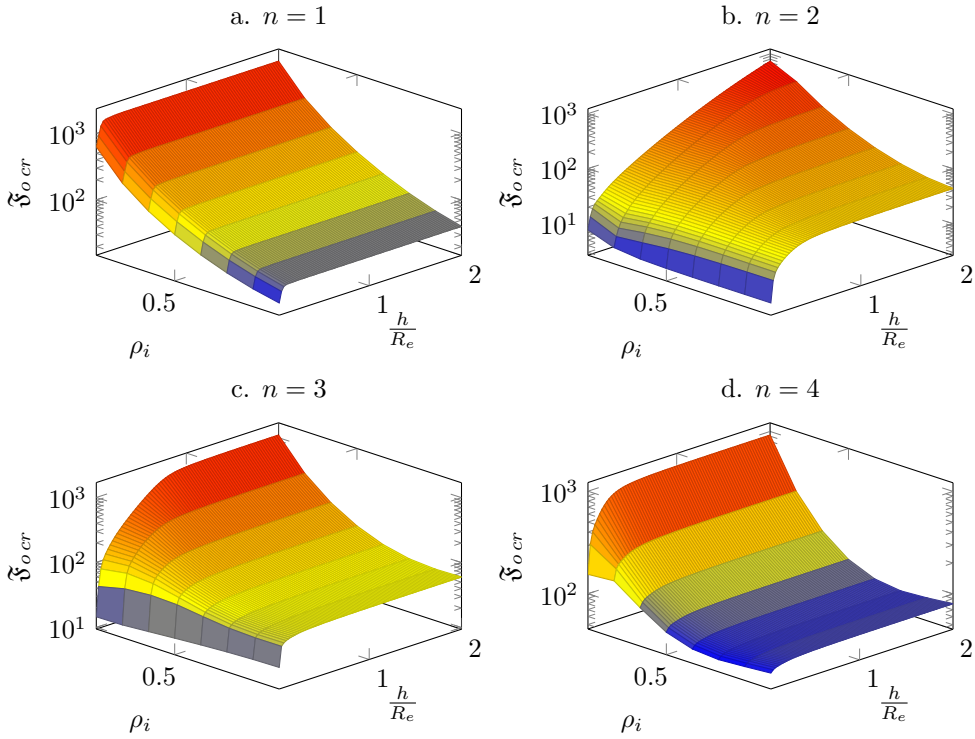


Figure 8. Critical load against ρ_i and h/R_e

4.3. Annular plate with clamped inner boundary. If (a) the radial displacement is not prescribed on the inner boundary but (b) the rotation is zero (in contrast to the previous problem) – see Fig. 2b. for further details – then the equation

$$\vartheta_n^m(\rho = \rho_i) = 0 \quad (4.3)$$

together with equation (4.2a) are the boundary conditions on the inner boundary.

Figure 9 shows the critical load $\mathfrak{F}_{o\ cr}$ against the height of the shell (i.e. $\frac{h}{R_e}$). The curves in the diagrams have a similar progress to the ones presented in the previous problem. AS the inner radius is getting greater, the interval where asymmetric deformations give the lowest critical load increases. Doing the calculations for higher numbers of n also the asymptotic values of the critical load approach values belonging to axisymmetric deformations. In some cases its even smaller – see Figure 10, where the critical load is shown against the inner radius ρ_i . The height of the stiffening shell is kept constant ($\frac{h}{R_e} = 2$).

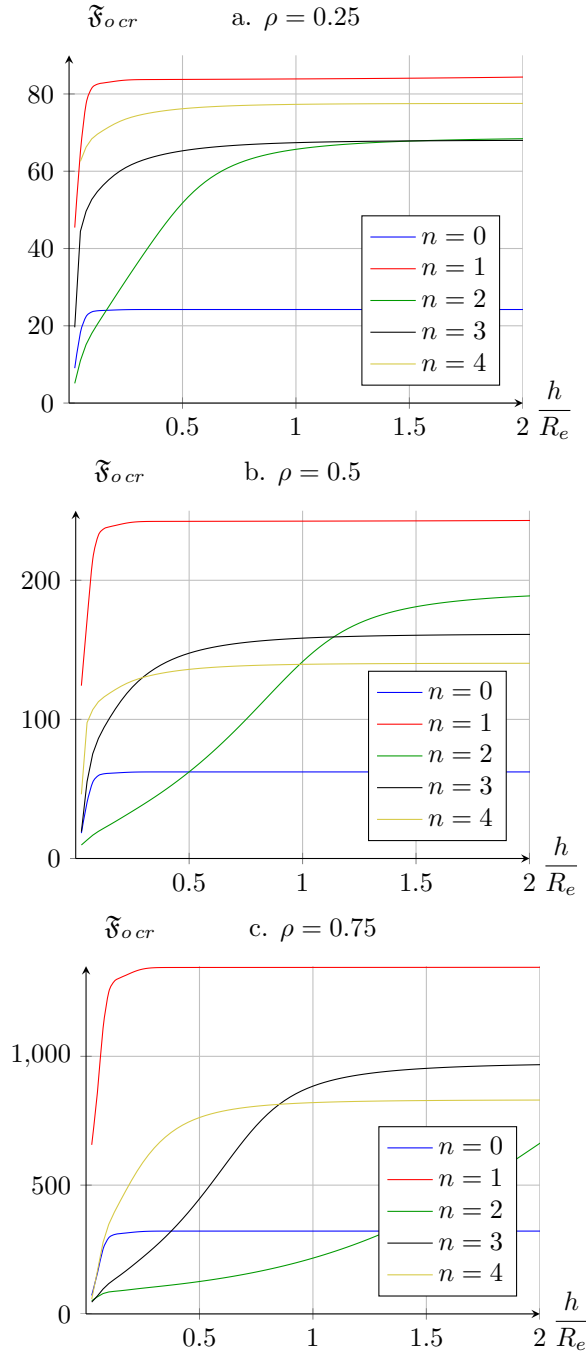


Figure 9. Critical load of plates with clamped inner boundary

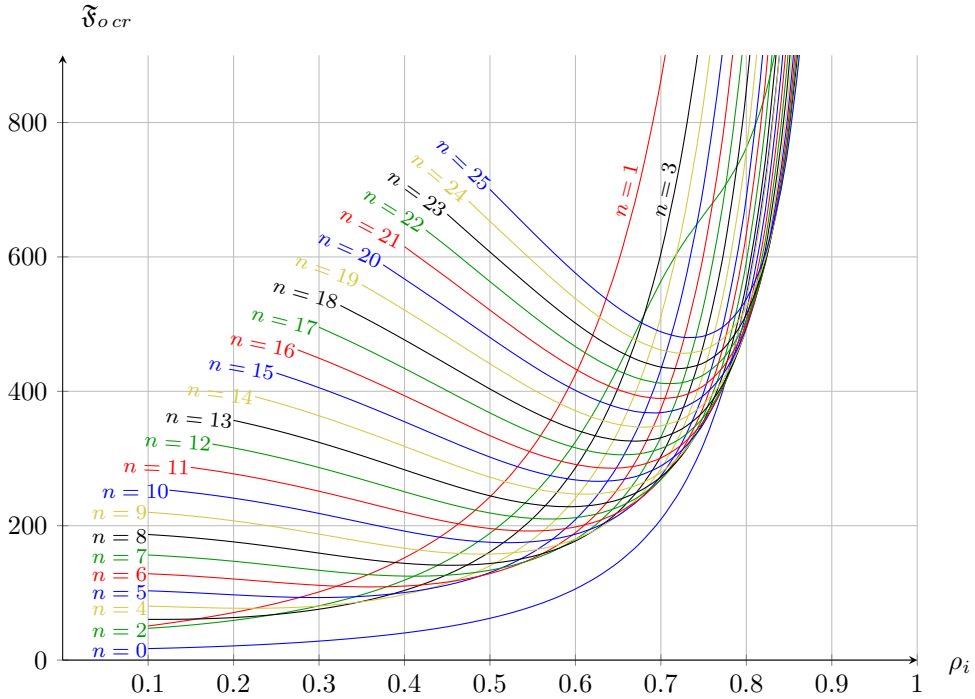


Figure 10. Critical load versus inner radius

5. CONCLUDING REMARKS

The present paper has established the equations that can be used to determine the critical load of circular and annular plates stiffened on the outer edge by a cylindrical shell under the assumption of non-axisymmetric deformations. We have clarified what the continuity conditions are between the two separate elements of the structure. We have also presented the solutions for the critical load of circular and annular plates with two different types of support assuming axisymmetric and non-axisymmetric deformations. It is obvious from the results that the stiffening significantly increases the critical load. It has been observed that buckling load belongs to axisymmetric buckling mode if the plate is circular. Non-axisymmetric buckling modes can be observed if the geometric properties (inner radius, shell height) are in a certain range.

Acknowledgements. This research was (partially) carried out in the framework of the Center of Excellence of Innovative Engineering Design and Technologies at the University of Miskolc.

REFERENCES

1. BRYAN, G. H.: On the stability of a plate under thrust in its own plane with applications to the buckling of the sides of a ship. *Proceedings of the London Mathematical Society*, (1890), 54–67.

2. NÁDAI, A.: Über das Ausbeulen von Kreisförmigen Platten. *Zeitschrift des Vereines deutscher Ingenieure*, **59**(11), (1915), 221–224.
3. BICKLEY, W.: Deflexions and vibrations of a circular elastic plate under tension. *Phil. Mag.*, **59**, (1933), 777–797.
4. FISCHER, U.: Untersuchung der elastischen Beulung von Kreisringplatten unter der Wirkung rotationssymmetrischer Randkräfte. Ph.D. thesis, TH Magdeburg, 1965.
5. MAJUMDAR, S.: Buckling of a thin annular plate under uniform compression. *AIAA Journal*, **9**, (1971), 1701–1707.
6. PARDOEN, G.: Vibration and buckling analysis of axisymmetric polar orthotropic circular plates. *Computers & Structures*, **4**, (1974), 951–960.
7. RAMAIAH, G. and VIJAYAKUMAR, K.: Elastic stability of annular plates under uniform compressive forces along the outer edge. *AIAA Journal*, **13**, (1975), 832–834.
8. CHEN, L.-W. and DONG, J.-L.: Vibrations of an initially stressed transversely isotropic circular thick plate. *International Journal of Mechanical Sciences*, **26**(4), (1984), 253–263.
9. WANG, C. M. and AUNG, T. M.: Buckling of circular plates under intermediate and edge radial loads. *Thin-Walled Structures*, **43**, (2005), 1926–1933.
10. ZHANG, Y., CHEN, L., SWADDIWUDHIPONG, S., LIU, Z., ET AL.: Buckling Deformation of Annular Plates Describing Natural Forms. *International Journal of Structural Stability and Dynamics*, **14**(1), (2014), 1350054[15 pages].
11. JILLELLA, N. and PEDDIESON, J.: Elastic Stability of Annular Thin Plates with One Free Edge. *Journal of Structures*, **2013**.
12. THEVENDRAN, V. and WANG, C. M.: Buckling of Annular Plates Elastically Restrained against Rotation along Edges. *Thin-Walled Structures*, **25**(3), (1996), 231–246.
13. LAURA, P. A. A., GUTIÉRREZ, R. H., SANZI, H. C., and ELVIRA, G.: Buckling of circular, solid and annular plates with an intermediate circular support. *Ocean Engineering*, **27**, (2000), 749–755.
14. WANG, C. Y. and WANG, C. M.: Buckling of circular plates with an internal ring support and elastically restrained edges. *Thin-Walled Structures*, **39**, (2001), 821–825.
15. REDDY, J. N., WANG, C. M., and WANG, C. Y.: *Exact Solutions for Buckling of Structural Members*. CRC Press, 2005.
16. WANG, C. M. and AUNG, T. M.: Buckling of Circular Mindlin Plates with an Internal Ring Support and Elastically Restrained Edge. *Journal of Engineering Mechanics*, **131**(4), (2005), 359–366.
17. RAO, L. B. and RAO, C. K.: Buckling of Circular Plates with an Internal Elastic Ring Support and Elastically Restrained Guided Edge Against Translation. *Mechanics Based Design of Structures and Machines: An International Journal*, **37**(1), (2009), 60–72.
18. RAO, L. B. and RAO, C. K.: Buckling Analysis of Circular Plates with Elastically Restrained Edges and Resting on Internal Elastic Ring Support. *Mechanics Based Design of Structures and Machines: An International Journal*, **38**(4), (2010), 440–452.
19. RAO, L. B. and RAO, C. K.: Buckling of circular plates with an internal elastic ring support and outer edge restrained against translation. *Journal of Engineering Science and Technology*, **7**(3), (2012), 393–401.

20. RAO, L. B. and RAO, C. K.: Fundamental buckling of circular plates with elastically restrained edges and resting on concentric rigid ring support. *Frontiers of Mechanical Engineering*, **8**(3), (2013), 291–297.
21. RAO, L. B. and RAO, C. K.: Buckling of circular plate with foundation and elastic edge. *International Journal of Mechanics and Materials in Design*.
22. TROITSKY, M.: *Stiffened Plates*. Elsevier, 1971.
23. SIMITSES, G. J. and BLACKMON, C. M.: Buckling of eccentrically stiffened, thin circular plates. *AIAA Journal*, **7**(6), (1969), 1200–1202.
24. SRINIVASAN, R. S. and THIRUVENKATACHARI, V.: Static and Dynamic Analysis of Stiffened Plates. *Computers & Structures*, **21**(3), (1985), 395–403.
25. PHILLIPS, J. S. and CARNEY, J. F.: Stability of an Annular Plate Reinforced With a Surrounding Edge Beam. *Journal of Applied Mechanics, ASME*, **41**(2), (1974), 497–501.
26. TURVEY, G. J. and DER AVANESSIEN, N. G. V.: Axisymmetric elasto-plastic large deflection response of ring stiffened circular plates. *International Journal of Mechanical Sciences*, **31**(11–12), (1989), 905–924.
27. TURVEY, G. J. and SALEHI, M.: Elasto-plastic large deflection response of pressure loaded circular plates stiffened by a single diameter stiffener. *Thin-Walled Structures*, **46**, (2008), 996–1002.
28. GOLMAKANI, M. E. and MEHRABIAN, M.: Nonlinear bending analysis of ring-stiffened circular and annular general angle-ply laminated plates with various boundary conditions. *Mechanics Research Communications*, **59**, (2014), 42–50.
29. ROSSETTOS, J. N. and MILLER, W. H.: On the Buckling of Ring-Stiffened Circular Plates. *Journal of Applied Mechanics, ASME*, **51**(3), (1984), 689–691.
30. ROSSETTOS, J. N. and YANG, G.: Asymmetric Buckling of Ring Stiffened Circular Plates. *Journal of Applied Mechanics, ASME*, **53**(2), (1986), 475–476.
31. FROSTIG, Y. and SIMITSES, G. J.: Effect of boundary conditions and rigidities on the buckling of annular plates. *Thin-Walled Structures*, **5**(4), (1987), 229–246.
32. FROSTIG, Y. and SIMITSES, G. J.: Buckling of ring-stiffened multi-annular plates. *Computers & Structures*, **29**(3), (1988), 519–526.
33. SZILASSY, I.: Stability of circular plates with a hole loaded on their outer boundary. Ph.D. thesis, University of Miskolc, 1971. (in Hungarian).
34. SZILASSY, I.: Stability of an annular disc loaded on its external flange by an arbitrary force system. *Publ. Techn. Univ. Heavy Industry. Ser. D. Natural Sciences*, **33**, (1976), 31–55.
35. VLASOV, V. Z.: General theory of shells and its applications in engineering, in: *Selected Papers* [in Russian]. Vol. 1, Izd. Akad. Nauk SSSR, Moscow, 1962.
36. JEZSÓ, K.: *Cylindrical shells subjected to non-axisymmetrical loading – a solution procedure*. Ph.D. thesis, University of Miskolc, 1980. (in Hungarian).
37. BURMEISTER, D.: Stability of shell-stiffened and axisymmetrically loaded annular plates. *Technische Mechanik*, **33**(1), (2013), 1–18.

STATIC AND DYNAMIC ANALYSES OF COMPOSITE BEAMS WITH INTERLAYER SLIP

ÁKOS JÓZSEF LENGYEL AND ISTVÁN ECSEDI
Institute of Applied Mechanics, University of Miskolc
H-3515 Miskolc, Miskolc–Egyetemváros, Hungary
mehlen@uni-miskolc.hu, mechecs@uni-miskolc.hu

[Received: November 17, 2014, Accepted: January 16, 2015]

Abstract. The present paper gives analytical solutions for shear deformable two-layer beams with weak shear connections. Timoshenko's kinematic assumptions are applied to both layers with different cross-sectional rotations. A linear constitutive equation is used between the horizontal shear force and the interlayer slip. The applied loads act in the plane of symmetry of a two-layered beam and the material-geometrical properties do not depend on the axial coordinate. For simply supported beam closed form solutions are derived for the deflection, slip and cross-sectional rotations. The eigenfrequencies of a simply supported beam are determined and compared with the solutions obtained by the applications of Euler-Bernoulli and Euler-Bernoulli-Rayleigh beam models.

Mathematical Subject Classification: 74G05, 34B05

Keywords: interlayer slip, shear connection, composite beam, free vibration

1. INTRODUCTION

Layered beams made of different elastic materials are frequently used in construction and they have created a growing interest in the different engineering sectors where both high strength-to-weight and stiffness-to-weight ratio are desired. There are many ways to form a connection between layers made of different materials. In some cases it occurs that the connection is weak in shear permitting only a relative slip, but preserving the contact in normal direction. The problem of layered beams with deformable shear connections has been studied for a long time. The first theories for these composite beams were developed by Granholm [1], Pleskov [2], Stüssi [3] and Newmark et al. [4]. The static analysis done by Newmark et al. [4] is based on the Euler-Bernoulli beam theory and has become a basis for investigating layered beam systems with interlayer slip [5–22]. Today the analytical and numerical FEM solution are refined [5–26]. Several studies [5–8, 13] present FEM solutions for multilayer beams with weak shear connections using the Euler-Bernoulli beam theory. Exact first and second order static analyses for composite beam-columns with partial shear interaction subjected to transverse and axial loads are given by Girhammar and Gopu [9]. By using variational methods Girhammar and Pan [10] derive ordinary differential

equations for the deflections and set up the corresponding boundary conditions for partially composite Euler-Bernoulli beams and beam-columns. A simplified analysis and design method for composite members with partial shear interaction that predicts the deflections and stresses has been proposed by Girhammar [11]. In [16,17,20] researchers developed FEM formulations for composite beams with deformable shear connection. The derived stiffness matrix takes the effects of interface slip and shear deformations into account. In [20] it is assumed that the cross-sectional rotations are not the same for the different beam components and the effect of shear connectors on a composite beam element is described by two springs which are separately placed at the two ends of the considered element.

Dynamic analysis of a composite beam with deformable shear connections based on the Euler-Bernoulli beam theory is presented by Girhammar and Gopu [23]. They consider free and forced vibrations. The governing differential equations and corresponding boundary conditions are derived for partial-interaction composite members and exact analytical solution for simply supported boundary conditions is presented in [25]. In paper [24] an analytical solution for free vibrations of shear-deformable two-layer beams with interlayer slip and axial load is developed. The effect of transverse shear flexibility of two layers is taken into account in a general way. Each layer behaves as a Timoshenko beam.

The present paper deals with two-layer beams with interlayer slip and gives analytical solutions for deflection, slip and cross-sectional rotations in the case of a static equilibrium problem. By introducing the inertia forces into the equilibrium equations we derive the equations of free vibrations as well. Applications of the equations we have established are illustrated via numerical examples.

2. GOVERNING EQUATIONS

In the reference configuration a composite beam with two components occupies the cylindrical region $B = A \times [0, L]$ generated by translating its cross-section A with a regular boundary ∂A along a rectilinear axis, normal to the cross-section. The cross-section A is divided into two parts A_1 and A_2 by the curve ∂A_{12} describing the positions of continuous connection such that (see Figure 1)

$$B_i = A_i \times (0, L), \quad (i = 1, 2), \quad A = A_1 \cup A_2, \quad B = B_1 \cup B_2, \quad (2.1)$$

$$\partial A_i = \partial A_{i0} \cup \partial A_{12}, \quad (i = 1, 2), \quad \partial A = \partial A_{10} \cup \partial A_{12}. \quad (2.2)$$

Here L is the length of the beam. A point P in $\bar{B} = B \cup \partial B$ (∂B is the boundary surface of B) is indicated by the position vector $\mathbf{r} = x\mathbf{e}_x + y\mathbf{e}_y + z\mathbf{e}_z$, where x, y, z and \mathbf{e}_m ($|\mathbf{e}_m| = 1, m = x, y, z$) refer to a rectangular coordinate system $Oxyz$. The equation of the common boundary surface of the beam components B_1 and B_2 is $y = 0, 0 \leq z \leq L$ (see Figure 1). The center of A_i is denoted by C_i ($i = 1, 2$). The plane yz is the plane of symmetry for the geometrical and material properties and loading conditions. According to Timoshenko's beam theory, which is valid for each homogeneous layer, the deformation of the beam is described by the following displacement field (see Figure 2)

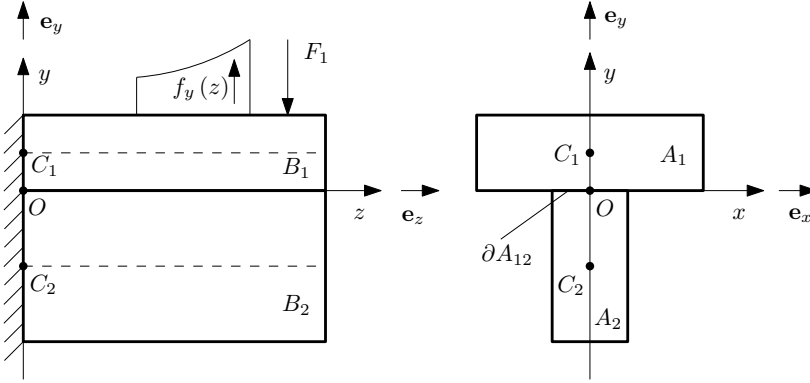


Figure 1. A composite beam with weak shear connection

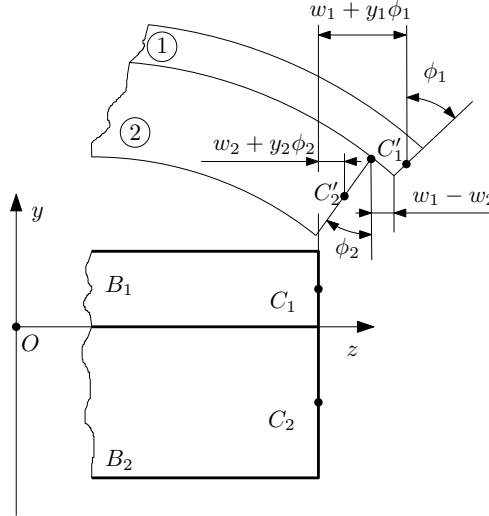


Figure 2. Kinematical model for a composite beam with interlayer slip

$$\mathbf{u} = u(x, y, z) \mathbf{e}_x + v(x, y, z) \mathbf{e}_y + w(x, y, z) \mathbf{e}_z, \quad (2.3)$$

where

$$u = 0, \quad v = v(z), \quad w(y, z) = w_i(z) + y\phi_i(z), \quad (x, y, z) \in B_i, \quad (i = 1, 2). \quad (2.4)$$

In Figure 2 C'_i ($i = 1, 2$) denotes the center of A_i in the deformed configuration of the considered cross-section. On the common boundary of the beam component the axial displacement w has a jump which is called an interlayer slip. From equation (2.4) and the definition of interlayer slip s it follows that

$$s(x, y, z) = w_1(z) - w_2(z), \quad y = 0, \quad 0 \leq z \leq L. \quad (2.5)$$

Application of the strain displacement relationships of the linearized theory of elasticity yields [27, 28]

$$\varepsilon_x = \varepsilon_y = \gamma_{xy} = \gamma_{xz} = 0, \quad (2.6)$$

$$\varepsilon_z = \frac{dw_i}{dz} + y \frac{d\phi_i}{dz}, \quad (x, y, z) \in B_i, \quad (i = 1, 2), \quad (2.7)$$

$$\gamma_{yz} = \frac{dv}{dz} + \phi_i, \quad (x, y, z) \in B_i, \quad (i = 1, 2), \quad (2.8)$$

where $\varepsilon_x, \varepsilon_y, \varepsilon_z$ and $\gamma_{xy}, \gamma_{xz}, \gamma_{yz}$ are the axial and shearing strains. From Hooke's law we get the normal stress σ_z and the shearing stress τ_{yz} in terms of strains as

$$\sigma_z = E_i \left(\frac{dw_i}{dz} + y \frac{d\phi_i}{dz} \right), \quad (x, y, z) \in B_i, \quad (i = 1, 2), \quad (2.9)$$

$$\tau_{yz} = G_i \left(\frac{dv}{dz} + \phi_i \right), \quad (x, y, z) \in B_i, \quad (i = 1, 2). \quad (2.10)$$

In equations (2.9), (2.10) E_i is the Young modulus and G_i is the shear modulus. We introduce the following section forces and section moment

$$N_i = \int_{A_i} \sigma_z dA = A_i E_i \left(\frac{dw_i}{dz} + y_i \frac{d\phi_i}{dz} \right), \quad y_i = \frac{1}{A_i} \int_{A_i} y dA, \quad (i = 1, 2), \quad (2.11)$$

$$M_i = \int_{A_i} y \sigma_z dA = A_i E_i \left(y_i \frac{dw_i}{dz} + g_i^2 \frac{d\phi_i}{dz} \right), \quad g_i^2 = \frac{1}{A_i} \int_{A_i} y^2 dA, \quad (i = 1, 2), \quad (2.12)$$

$$V_i = \kappa_i A_i G_i \left(\frac{dv}{dz} + \phi_i \right), \quad (i = 1, 2), \quad (2.13)$$

where κ_i is the shear factor of the cross-section A_i ($i = 1, 2$) [29]. The analysis of the composite beam with interlayer slip is restricted to the case of absent axial force N , that is, we have

$$N = N_1 + N_2 = A_1 E_1 \left(\frac{dw_1}{dz} + y_1 \frac{d\phi_1}{dz} \right) + A_2 E_2 \left(\frac{dw_2}{dz} + y_2 \frac{d\phi_2}{dz} \right) = 0. \quad (2.14)$$

From equations (2.5), (2.14) it follows that

$$\frac{dw_1}{dz} = \frac{A_2 E_2}{\langle AE \rangle} \frac{ds}{dz} - y_1 \frac{A_1 E_1}{\langle AE \rangle} \frac{d\phi_1}{dz} - y_2 \frac{A_2 E_2}{\langle AE \rangle} \frac{d\phi_2}{dz}, \quad (2.15)$$

$$\frac{dw_2}{dz} = -\frac{A_1 E_1}{\langle AE \rangle} \frac{ds}{dz} - y_1 \frac{A_1 E_1}{\langle AE \rangle} \frac{d\phi_1}{dz} - y_2 \frac{A_2 E_2}{\langle AE \rangle} \frac{d\phi_2}{dz}. \quad (2.16)$$

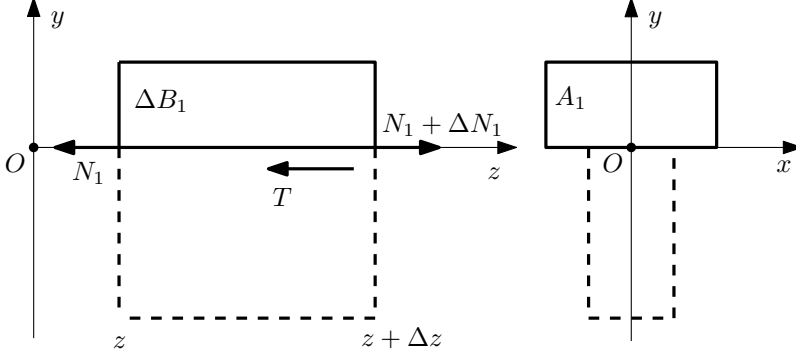


Figure 3. Equilibrium condition in the direction z for a small beam element

Here

$$\langle AE \rangle = A_1 E_1 + A_2 E_2. \quad (2.17)$$

It is obvious that

$$N_1 = \langle AE \rangle_{-1} \left[\frac{ds}{dz} + y_1 \frac{d\phi_1}{dz} - y_2 \frac{d\phi_2}{dz} \right], \quad (2.18)$$

$$N_2 = \langle AE \rangle_{-1} \left[-\frac{ds}{dz} - y_1 \frac{d\phi_1}{dz} + y_2 \frac{d\phi_2}{dz} \right], \quad (2.19)$$

$$M_1 = \langle AE \rangle_{-1} \left[y_1 \frac{ds}{dz} + c_1 \frac{d\phi_1}{dz} - y_1 y_2 \frac{d\phi_2}{dz} \right], \quad (2.20)$$

$$M_2 = \langle AE \rangle_{-1} \left[-y_2 \frac{ds}{dz} - y_1 y_2 \frac{d\phi_1}{dz} + c_2 \frac{d\phi_2}{dz} \right], \quad (2.21)$$

where

$$\frac{1}{\langle AE \rangle_{-1}} = \frac{1}{A_1 E_1} + \frac{1}{A_2 E_2}, \quad (2.22)$$

$$c_1 = \frac{A_1 E_1}{\langle AE \rangle_{-1}} g_1^2 - y_1^2 \frac{A_1 E_1}{A_2 E_2}, \quad (2.23)$$

$$c_2 = \frac{A_2 E_2}{\langle AE \rangle_{-1}} g_2^2 - y_2^2 \frac{A_2 E_2}{A_1 E_1}. \quad (2.24)$$

Application of the equilibrium condition for the axial forces in the beam component B_1 yields (see Figure 3)

$$\frac{dN_1}{dz} - T = 0. \quad (2.25)$$

In equation (2.25) T is the interlayer shear force. It is assumed that T is a linear function of the interlayer slip, that is

$$T = ks, \quad (2.26)$$

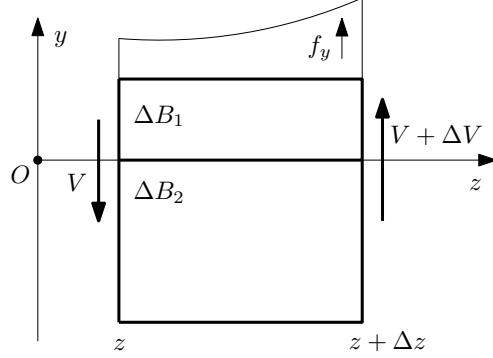


Figure 4. Shear force and vertical load on a small beam element $\Delta B = \Delta B_1 \cup \Delta B_2$

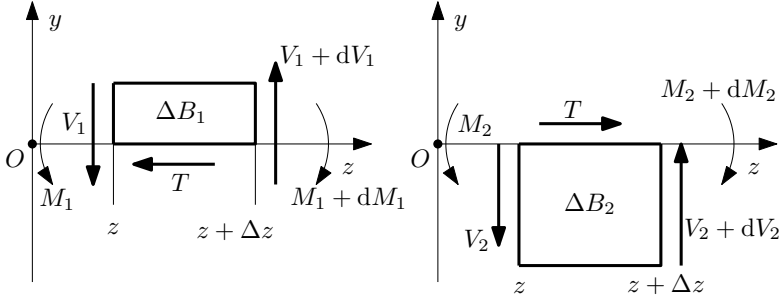


Figure 5. Shear forces and bending moments on beam elements ΔB_1 and ΔB_2

where k is the slip modulus. From Figures 4 and Figure 5 we have the following equilibrium equations:

$$\frac{dV}{dz} + f_y = 0, \quad V = V_1 + V_2, \quad (2.27)$$

$$\frac{dM_1}{dz} - V_1 = 0, \quad (2.28)$$

$$\frac{dM_2}{dz} - V_2 = 0. \quad (2.29)$$

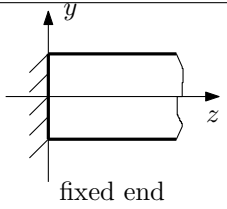
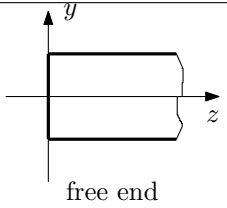
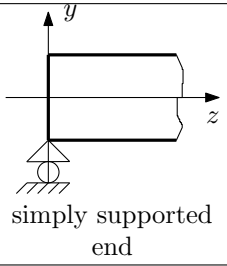
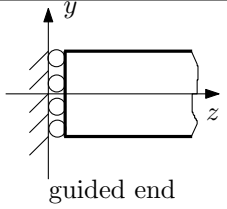
In order to formulate the possible boundary conditions we shall consider the virtual work of the section forces and section moments on a kinematically admissible displacement field

$$\tilde{\mathbf{u}}_i = \tilde{v}(z) \mathbf{e}_y + \left(\tilde{w}_i(z) + y \tilde{\phi}_i(z) \right) \mathbf{e}_z, \quad (x, y, z) \in B_i, \quad (i = 1, 2). \quad (2.30)$$

A detailed computation results in

$$W = \int_{A_1} \sigma_z \tilde{w}_1(z) dA + \int_{A_2} \sigma_z \tilde{w}_2(z) dA + \int_{A_1} y \sigma_z \tilde{\phi}_1(z) dA + \int_{A_2} y \sigma_z \tilde{\phi}_2(z) dA +$$

Table 1. Classical boundary conditions

| Type | Boundary condition |
|---|--|
|  <p>fixed end</p> | $v = 0, s = 0, \phi_1 = 0, \phi_2 = 0$ (kinematical boundary conditions) |
|  <p>free end</p> | $N_1 = 0, V = 0, M_1 = 0, M_2 = 0$ (forced boundary conditions) |
|  <p>simply supported end</p> | $v = 0, N_1 = 0, M_1 = 0, M_2 = 0$ (mixed boundary conditions) |
|  <p>guided end</p> | $s = 0, \phi_1 = 0, \phi_2 = 0, V = 0$ (mixed boundary conditions) |

$$+ \int_A \tau_{yz} \tilde{v}(z) dA = N_1 \tilde{w}_1 + N_2 \tilde{w}_2 + M_1 \tilde{\phi}_1 + M_2 \tilde{\phi}_2 + V \tilde{v} = N_1 \tilde{s} + M_1 \tilde{\phi}_1 + M_2 \tilde{\phi}_2 + V \tilde{v} \quad (2.31)$$

where

$$\tilde{s} = \tilde{w}_1(z) - \tilde{w}_2(z). \quad (2.32)$$

From equation (2.31) we obtain the possible combinations of the boundary conditions at the end cross-section

$$V \text{ or } v \text{ may be prescribed,} \quad (2.33)$$

$$N_1 \text{ or } s \text{ may be prescribed,} \quad (2.34)$$

$$M_1 \text{ or } \phi_1 \text{ may be prescribed,} \quad (2.35)$$

$$M_2 \text{ or } \phi_2 \text{ may be prescribed.} \quad (2.36)$$

We remark that some classical boundary conditions are listed on the basis of equations (2.33–2.36) in Table 1. It can be checked by utilizing equations (2.18) and (2.20) that the boundary conditions for a simply supported end and a free end are

$$\frac{ds}{dz} = 0, \quad \frac{d\phi_1}{dz} = 0, \quad \frac{d\phi_2}{dz} = 0. \quad (2.37)$$

The combination of equations (2.13), (2.18), (2.20), (2.21), (2.26) with equations (2.25), (2.27), (2.28), (2.29) yields a system of linear differential equations for the functions $v = v(z)$, $s = s(z)$, $\phi_1 = \phi_1(z)$ and $\phi_2 = \phi_2(z)$

$$\frac{d^2s}{dz^2} + y_1 \frac{d^2\phi_1}{dz^2} - y_2 \frac{d^2\phi_2}{dz^2} - \frac{k}{\langle AE \rangle_{-1}} s = 0, \quad (2.38)$$

$$y_1 \frac{d^2s}{dz^2} + c_1 \frac{d^2\phi_1}{dz^2} - y_1 y_2 \frac{d^2\phi_2}{dz^2} - \kappa_1 \frac{G_1 A_1}{\langle AE \rangle_{-1}} \left(\frac{dv}{dz} + \phi_1 \right) = 0, \quad (2.39)$$

$$-y_2 \frac{d^2s}{dz^2} - y_1 y_2 \frac{d^2\phi_1}{dz^2} + c_2 \frac{d^2\phi_2}{dz^2} - \kappa_2 \frac{G_2 A_2}{\langle AE \rangle_{-1}} \left(\frac{dv}{dz} + \phi_2 \right) = 0, \quad (2.40)$$

$$\kappa_1 G_1 A_1 \left(\frac{d^2v}{dz^2} + \frac{d\phi_1}{dz} \right) + \kappa_2 G_2 A_2 \left(\frac{d^2v}{dz^2} + \frac{d\phi_2}{dz} \right) = -f_y(z). \quad (2.41)$$

3. SOLUTION FOR A SIMPLY SUPPORTED BEAM

For a simply supported beam we look for the solution of the ordinary differential equation system (2.38–2.41) in the following form:

$$v(z) = \sum_{j=1}^{\infty} v_j \sin j \frac{\pi}{L} z, \quad s(z) = \sum_{j=1}^{\infty} s_j \cos j \frac{\pi}{L} z, \quad (3.1a)$$

$$\phi_1(z) = \sum_{j=1}^{\infty} \phi_{1j} \cos j \frac{\pi}{L} z, \quad \phi_2(z) = \sum_{j=1}^{\infty} \phi_{2j} \cos j \frac{\pi}{L} z. \quad (3.1b)$$

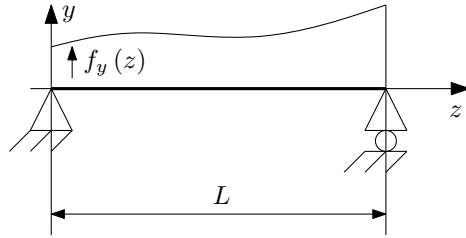


Figure 6. Simply supported beam

These functions satisfy the boundary conditions

$$v = 0, \quad N_1 = 0, \quad M_1 = 0, \quad M_2 = 0 \quad (3.2)$$

for arbitrary values of $v_j, s_j, \phi_{1j}, \phi_{2j}, (j = 1, 2, \dots)$ at both ends of the beam. Substitution of $v = v(z), s = s(z), \phi_1 = \phi_1(z)$ and $\phi_2 = \phi_2(z)$ into the ODE system (2.38–2.41) results in a system of linear equations for $v_j, s_j, \phi_{1j}, \phi_{2j}, (j = 1, 2, \dots)$. This can be written as

$$\mathbf{C}_j \mathbf{x}_j = \mathbf{f}_j, \quad (j = 1, 2, \dots) \quad (3.3)$$

where

$$\mathbf{C}_j = [c_{jpq}], \quad (p, q = 1, 2, 3, 4), \quad (3.4)$$

$$c_{j11} = -\left(j\frac{\pi}{L}\right)^2 - \frac{k}{\langle AE \rangle_{-1}}, \quad c_{j12} = -y_1 \left(j\frac{\pi}{L}\right)^2, \quad c_{j13} = y_2 \left(j\frac{\pi}{L}\right)^2, \quad c_{j14} = 0, \quad (3.5)$$

$$c_{j21} = -y_1 \left(j\frac{\pi}{L}\right)^2, \quad c_{j22} = -c_1 \left(j\frac{\pi}{L}\right)^2 + \frac{\kappa_1 G_1 A_1}{\langle AE \rangle_{-1}},$$

$$c_{j23} = y_1 y_2 \left(j\frac{\pi}{L}\right)^2, \quad c_{j24} = -\frac{\kappa_1 G_1 A_1}{\langle AE \rangle_{-1}} j \frac{\pi}{L}, \quad (3.6)$$

$$c_{j31} = y_2 \left(j\frac{\pi}{L}\right)^2, \quad c_{j32} = y_1 y_2 \left(j\frac{\pi}{L}\right)^2,$$

$$c_{j33} = -c_2 \left(j\frac{\pi}{L}\right)^2 + \frac{\kappa_2 G_2 A_2}{\langle AE \rangle_{-1}}, \quad c_{j34} = -\frac{\kappa_2 G_2 A_2}{\langle AE \rangle_{-1}} j \frac{\pi}{L}, \quad (3.7)$$

$$c_{j41} = 0, \quad c_{j42} = -\kappa_1 G_1 A_1 j \frac{\pi}{L}, \quad c_{j43} = -\kappa_2 G_2 A_2 j \frac{\pi}{L},$$

$$c_{j44} = -(\kappa_1 G_1 A_1 + \kappa_2 G_2 A_2) \left(j\frac{\pi}{L}\right)^2, \quad (3.8)$$

$$\mathbf{x}_j^T = [s_j, \phi_{1j}, \phi_{2j}, v_j], \quad (3.9)$$

$$\mathbf{f}_j^T = [0, 0, 0, f_j]. \quad (3.10)$$

In formula (3.10) f_j is defined as

$$f_j = \frac{2}{L} \int_0^L f_y(z) \sin j \frac{\pi}{L} z dz, \quad (j = 1, 2, \dots). \quad (3.11)$$

Assume that the beam is subjected to the load

$$f_y(z) = -f \left[H\left(z - \frac{L}{2} + \frac{l}{2}\right) - H\left(z - \frac{L}{2} - \frac{l}{2}\right) \right] \quad (3.12)$$

where $H = H(z)$ is the Heaviside function. The type of applied load given by equation (3.12) and the meanings of f and l ($0 \leq l \leq L$) are shown in Figure 7. For this load the Fourier coefficients f_j are given by the following equation:

$$f_j = -\frac{4f}{j\pi} \sin\left(\frac{j\pi}{2}\right) \sin\left(\frac{j\pi l}{2L}\right), \quad (j = 1, 2, \dots). \quad (3.13)$$

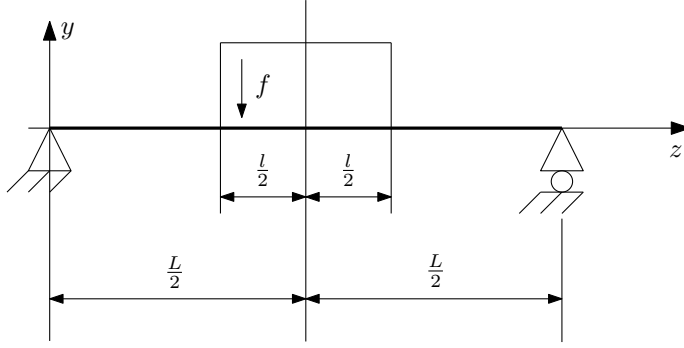


Figure 7. Illustration of applied load

4. FREE VIBRATIONS OF A SIMPLY SUPPORTED BEAM

To formulate the governing equations of the free vibrations we introduce the inertia forces into equations (2.27), (2.28) and (2.29). It is obvious that all physical quantities depend on time t too, that is $v = v(z, t)$, $s = s(z, t)$, $\phi_1 = \phi_1(z, t)$, $\phi_2 = \phi_2(z, t)$, etc. Assuming free vibrations we obtain

$$v = \bar{v}(z) \sin \omega t, \quad s = \bar{s}(z) \sin \omega t, \quad \phi_1 = \bar{\phi}_1(z) \sin \omega t, \quad \phi_2 = \bar{\phi}_2(z) \sin \omega t, \quad (4.1)$$

where ω is a natural frequency and $\bar{v}(z), \dots, \bar{\phi}_2(z)$ are the unknown amplitude functions. The inertia force from the vertical motion is of the form

$$f_y(z, t) = -(\rho_1 A_1 + \rho_2 A_2) \frac{\partial^2 v}{\partial t^2} = \omega^2 (\rho_1 A_1 + \rho_2 A_2) \bar{v}(z) \sin \omega t. \quad (4.2)$$

The inertia couples from the cross-sectional rotations are

$$m_1(z, t) = -\rho_1 I_1 \frac{\partial^2 \phi_1}{\partial t^2} = \omega^2 \rho_1 I_1 \bar{\phi}_1(z) \sin \omega t, \quad (4.3)$$

$$m_2(z, t) = -\rho_2 I_2 \frac{\partial^2 \phi_2}{\partial t^2} = \omega^2 \rho_2 I_2 \bar{\phi}_2(z) \sin \omega t. \quad (4.4)$$

In equations (4.2–4.4) ρ_i ($i = 1, 2$) is the mass density and

$$I_i = \int_{A_i} y^2 dA, \quad (i = 1, 2). \quad (4.5)$$

Upon substitution of equation (4.2) into equation (2.27) we obtain

$$\kappa_1 G_1 A_1 \left(\frac{d\bar{v}}{dz} + \bar{\phi}_1 \right) + \kappa_2 G_2 A_2 \left(\frac{d\bar{v}}{dz} + \bar{\phi}_2 \right) + \omega^2 (\rho_1 A_1 + \rho_2 A_2) \bar{v} = 0. \quad (4.6)$$

Combination of equations (2.28) and (2.29) with equations (4.3) and (4.4) yields the following two equations:

$$y_1 \frac{d^2 \bar{s}}{dz^2} + c_1 \frac{d^2 \bar{\phi}_1}{dz^2} - y_1 y_2 \frac{d^2 \bar{\phi}_2}{dz^2} - \frac{\kappa_1 G_1 A_1}{\langle AE \rangle_{-1}} \left(\frac{d\bar{v}}{dz} + \bar{\phi}_1 \right) + \omega^2 \frac{\rho_1 I_1}{\langle AE \rangle_{-1}} \bar{\phi}_1(z) = 0, \quad (4.7)$$

$$-y_2 \frac{d^2 \bar{s}}{dz^2} - y_1 y_2 \frac{d^2 \bar{\phi}_1}{dz^2} + c_2 \frac{d^2 \bar{\phi}_2}{dz^2} - \frac{\kappa_2 G_2 A_2}{\langle AE \rangle_{-1}} \left(\frac{d\bar{v}}{dz} + \bar{\phi}_2 \right) + \omega^2 \frac{\rho_2 I_2}{\langle AE \rangle_{-1}} \bar{\phi}_2(z) = 0. \quad (4.8)$$

We introduce the mass matrix \mathbf{M} by the following definition

$$\mathbf{M}_j = [m_{jpp}], \quad (p, q = 1, 2, 3, 4), \quad i = 1, 2, \dots, \quad (4.9)$$

$$m_{j11} = m_{j12} = m_{j13} = m_{j14} = 0, \quad (4.10)$$

$$m_{j21} = m_{j23} = m_{j24} = 0, \quad m_{j22} = -\frac{\rho_1 I_1}{\langle AE \rangle_{-1}}, \quad (4.11)$$

$$m_{j31} = m_{j32} = m_{j34} = 0, \quad m_{j33} = -\frac{\rho_2 I_2}{\langle AE \rangle_{-1}}, \quad (4.12)$$

$$m_{j41} = m_{j42} = m_{j43} = 0, \quad m_{j44} = (\rho_1 A_1 + \rho_2 A_2). \quad (4.13)$$

Further let

$$\mathbf{X}_j^T = [\bar{s}_j, \bar{\phi}_{1j}, \bar{\phi}_{2j}, \bar{v}_j]. \quad (4.14)$$

For the free vibrations of simply supported composite beams with weak shear connection we assume that

$$\bar{v}(z) = \sum_{j=1}^{\infty} \tilde{v}_j \sin j \frac{\pi}{L} z, \quad \bar{s}(z) = \sum_{j=1}^{\infty} \tilde{s}_j \cos j \frac{\pi}{L} z, \quad (4.15)$$

$$\bar{\phi}_1(z) = \sum_{j=1}^{\infty} \tilde{\phi}_{1j} \cos j \frac{\pi}{L} z, \quad \bar{\phi}_2(z) = \sum_{j=1}^{\infty} \tilde{\phi}_{2j} \cos j \frac{\pi}{L} z. \quad (4.16)$$

A comparison with equations (3.1) shows that the boundary conditions (3.2) are again satisfied. By repeating the line of thought resulting in equation (3.3) the eigenvalue problem for the free vibrations of simply supported two-layer beams with flexible shear connection can be formulated as

$$(\mathbf{C}_j + \omega^2 \mathbf{M}_j) \mathbf{X}_j = \mathbf{0}, \quad (j = 1, 2, \dots). \quad (4.17)$$

For each j we have three different natural frequencies. The smaller value of ω_j^2 corresponds to the bending deformation mode and the other two values of ω_j^2 correspond to the shear deformation modes. For the Euler-Bernoulli and Euler-Bernoulli-Rayleigh beams we have only bending deformation mode and the natural frequencies can be obtained – see [26] – from the following equation

$$\Omega_j^2 = \frac{\langle IE \rangle \left[\left(\frac{j\pi}{L} \right)^4 + \left(\frac{j\Gamma}{L} \right)^2 \right] \left(\frac{j\pi}{L} \right)^2}{\left[m + I_m \left(\frac{j\pi}{L} \right)^2 \right] \left[\frac{k}{\langle AE \rangle_{-1}} + \left(\frac{j\pi}{L} \right)^2 \right]}, \quad (4.18)$$

where

$$\langle IE \rangle = E_i \int_{A_i} (y - y_i)^2 dA, \quad (i = 1, 2), \quad m = \rho_1 A_1 + \rho_2 A_2, \quad (4.19)$$

$$\Gamma^2 = \frac{k \{IE\}}{\langle AE \rangle_{-1} \langle IE \rangle}, \quad \{IE\} = \langle IE \rangle + (y_1 - y_2)^2 \langle AE \rangle_{-1}, \quad (4.20)$$

$$I_m = 0 \quad (\text{Euler-Bernoulli beam}), \quad (4.21)$$

$$I_m = \sum_{i=1}^2 \left[\rho_i \int_{A_i} (y - y_i)^2 dA + y_i^2 \rho_i A_i \right] \quad (\text{Euler-Bernoulli-Rayleigh beam}) . \quad (4.22)$$

5. NUMERICAL EXAMPLES

5.1. Simply supported beam loaded by uniform distributed force. This example is taken from paper [18] by Schnabl et al. The simply supported beam, its cross-section and the applied load are shown in Figure 8. The following data are used $h_1 = 0.2$ [m], $h_2 = 0.3$ [m], $b = 0.3$ [m], $E_1 = 1.2 \times 10^{10}$ [Pa], $E_2 = 1.2 \times 10^{10}$ [Pa], $G_1 = 8 \times 10^8$ [Pa], $G_2 = 1.2 \times 10^9$ [Pa], $f = 5 \times 10^4$ [N/m], $k = 2.43 \times 10^6$ [Pa], $L = 2.5$ [m], $\kappa_1 = \kappa_2 = 5/6$. The functions $v = v(z)$ and $s = s(z)$ are shown in Figures 9 and 10. The functions $\phi_1 = \phi_1(z)$ and $\phi_2 = \phi_2(z)$ are also presented in graphical format – see Figure 11. A comparison of the deflection $v(\frac{L}{2})$ and the slip $s(0)$ with the results obtained by Schnabl et al. [18] is given in Table 2.

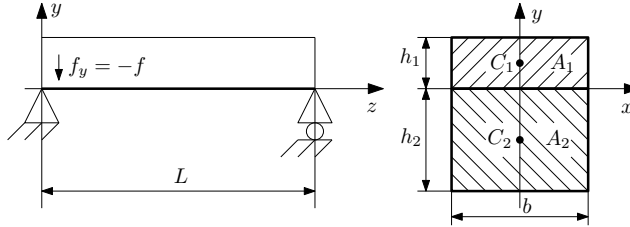


Figure 8. Simply supported composite beam with uniform load

Table 2. Comparison of deflection and slip

| | paper [18] (FEM) | present paper |
|--------------|------------------|---------------|
| $v(L/2)$ [m] | -0.00271026 | -0.0027082964 |
| $s(0)$ [m] | -0.00077293 | -0.0007713293 |

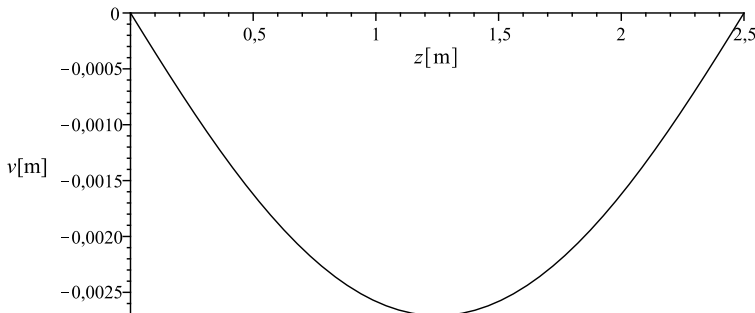


Figure 9. The plot of $v(z)$

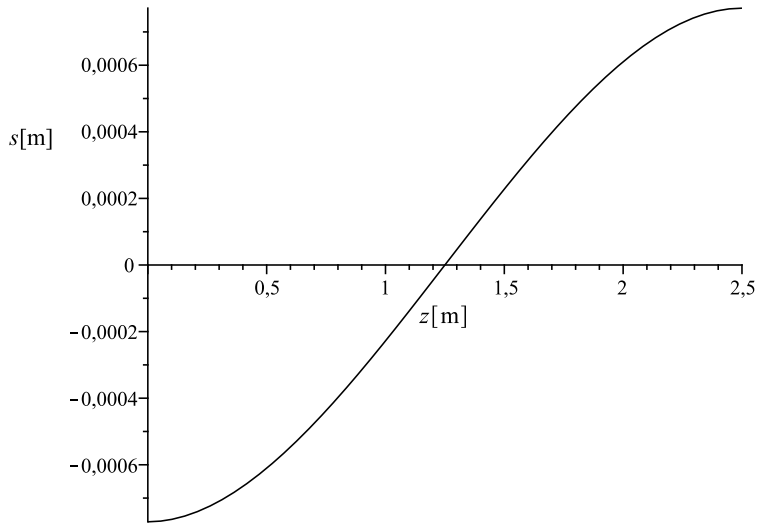


Figure 10. The plot of $s(z)$

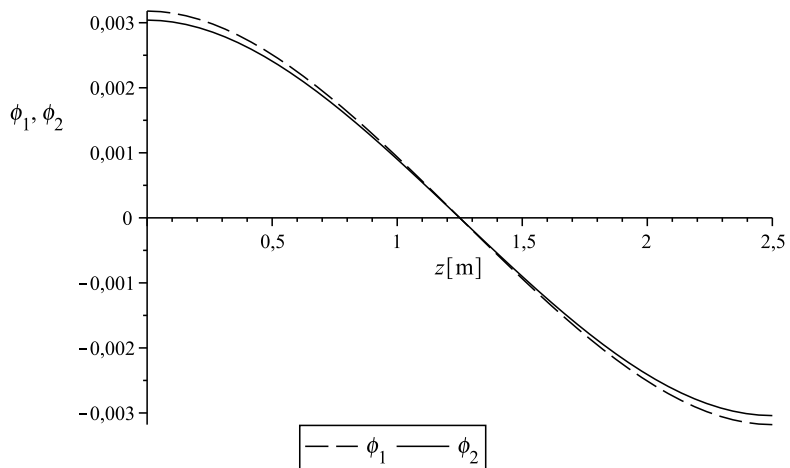


Figure 11. The plots of $\phi_1(z)$ and $\phi_2(z)$

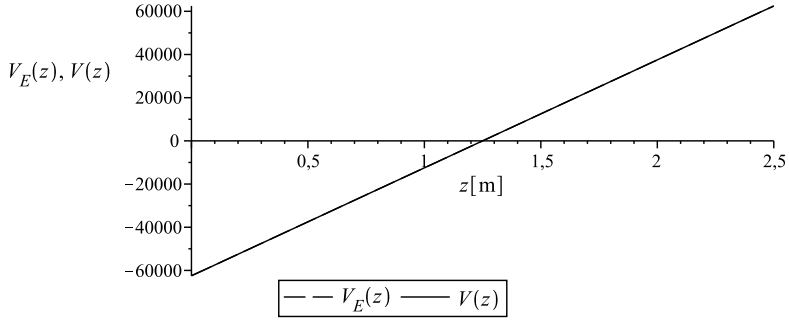


Figure 12. The shear force functions

For completeness Figure 12 shows the shear force

$$V_E(z) = f \left(z - \frac{L}{2} \right). \quad (5.1)$$

The shear force function $V = V(z)$ is computed from the deflection and the cross-sectional rotation by utilizing equations (2.13), (2.27)₁

$$V(z) = \kappa_1 G_1 A_1 \left(\frac{dv}{dz} + \phi_1 \right) + \kappa_2 G_2 A_2 \left(\frac{dv}{dz} + \phi_2 \right). \quad (5.2)$$

This function is also shown in Figure 12. The curves $V_E(z)$ and $V(z)$ coincide and this fact is evidence for the accuracy of the presented solutions.

5.2. Natural frequencies of the free vibrations. The data for this example are the same as those in Example 5.1. The densities should also be given: $\rho_1 = 5000 \text{ [kg/m}^3\text{]}$, $\rho_2 = 7000 \text{ [kg/m}^3\text{]}$. The results we have obtained for the natural frequencies are listed in Table 3.

Table 3. Natural frequencies

| j | Euler-Bernoulli | Euler-Bernoulli-Rayleigh | Timoshenko | | |
|---|-----------------|--------------------------|-------------|-------------|-------------|
| | | | Bending | Shear | Shear |
| 1 | 155.290664 | 152.6194487 | 151.4225922 | 2338.54532 | 8394.253453 |
| 2 | 622.4043575 | 582.6170364 | 504.1041551 | 2901.662787 | 3724.202344 |
| 3 | 1400.929022 | 1220.369015 | 941.8521016 | 3635.127974 | 4202.393801 |
| 4 | 2490.863793 | 1991.111501 | 1414.604281 | 4451.987908 | 4779.655958 |
| 5 | 3892.20856 | 2836.587389 | 1902.205348 | 5291.520318 | 5444.286196 |

6. CONCLUSIONS

In this paper an analytical model has been developed to analyse the deformation of composite beams with weak shear connections. Timoshenko beam theory is used, assuming that the layers have different cross-sectional rotations. Analytical solutions

for deflection, slip and cross-sectional rotations are derived. The eigenfrequencies of free vibrations of a simply supported beam are also computed. The presented solutions are based on the representations of applied load, deflection, slip and cross-sectional rotations by Fourier series. The numerical results we have obtained are compared with a FEM solution and good agreement has been found.

Acknowledgements. This research was carried out as a part of TÁMOP-4.2.1.B-10/2KONV-2010-0001 project with support by European Union and co-financed by European Social Found.

REFERENCES

1. GRANHOLM, H.: *On composite beams and columns with special regard to nailed structures*. Trans. No. 88. Chalmers University of Technology, Göteborg, Sweden, 1949. (in Swedish).
2. PLESKOV, F. P.: *Theoretical Studies of Composite Wood Structures*. Soviet Union, 1952. (in Russian).
3. STÜSSI, F.: Zusammengesetzte Vollwandträger. *IABSE Publications*, **8**, (1947), 249–269.
4. NEWMARK, N. M., SIESS, C. P., and VIEST, I. M.: Test and analysis of composite beam with incomplete interaction. *Proc. Soc. Exp. Stress Anal.*, **9**, (1951), 75–92.
5. GOODMAN, I.: *Layered wood system with interlayer slip*. Ph. D. thesis, University of California, Berkeley, CA, 1967.
6. GOODMAN, I. and POPOV, E.: Layered beam system with inter-layer slip. *Journal of the Structural Engineering, Division ASCE*, **94**(11), (1968), 2537–2547.
7. GOODMAN, I. and POPOV, E.: Layered wood system with inter-layer slip. *Wood Science*, **1**(3), (1969), 148–158.
8. THOMSON, F., GOODMAN, I., and VANDERBILT, M.: Finite element analysis of layered wood systems. *Journ. of Struct., Division ASCE*, **101**(12), (1975), 2659–2672.
9. GIRHAMMAR, U. A. and GOPU, V.: Composite beam-columns with interlayer slip – exact analysis. *Journ. Struct. Eng.*, **119**(4), (1993), 1265–1282.
10. GIRHAMMAR, U. A. and PAN, D. H.: Exact static analysis of partially composite beams and beam-columns. *Int. Journ. Mech. Sci.*, **49**(2), (2007), 239–255.
11. GIRHAMMAR, U. A.: A simplified analysis method for composite beams with interlayer slip. *Int. Journ. Mech. Sci.*, **51**(7), (2009), 515–530.
12. ECSEDI, I. and BAKSA, A.: Static analysis of composite beams with weak shear connection. *Appl. Math. Mod.*, (35), (2011), 1739–1750.
13. RANZI, G., BRADFORD, M., and UY, B.: A direct stiffness analysis of composite beam with partial interaction. *Int. Journ. Num. Methods Eng.*, **61**(5), (2004), 657–672.
14. WANG, C.: Deflection of steel-concrete composite beams with partial shear interaction. *Journ. Struct. Eng.*, **124**(10), (1998), 1159–1165.
15. XU, R. and WU, Y.: Static, dynamic and buckling analysis of partial interaction composite members using Timoshenko beam theory. *Int. Journ. Mech. Sci.*, **49**(10), (2007), 1139–1155.
16. NGUYEN, Q., MARTINELLI, E., and HJIAJ, M.: Derivation of the exact stiffness matrix for a two-layer Timoshenko beam element with partial interaction. *Eng. Struct.*, **33**(2), (2011), 298–307.

17. NGUYEN, Q., HJIAJ, M., and GUEZOULI, S.: Exact finite element model for shear-deformable two-layer beams with discrete shear connection. *Finite Element in Analysis and Design*, **47**(7), (2011), 718–727.
18. SCHNABL, S., SAJE, M., TURK, G., and PLANINC, I.: Locking free two-layer Timoshenko beam element with interlayer slip. *Finite Elements in Analysis and Design*, **43**(9), (2007), 705–714.
19. LIN, X. and ZHANG, Y.: A novel one-dimensional two-node shear-flexible layered composite beam element. *Finite Elements in Analysis and Design*, **47**(7), (2011), 676–682.
20. JIANG, S., ZENG, X., and ZHOU, D.: Novel two-node linear composite beam element with both interface slip and shear deformation into consideration: Formulation and validation. *Int. Journ. Mech. Sci.*, **85**, (2014), 110–119.
21. SCHNABL, S., SAJE, M., TURK, G., and PLANINC, I.: Analytical solution of two-layer beam taking into account interlayer slip and shear deformation. *Journ. Struct. Eng. ASCE*, **133**(6), (2007), 886–894.
22. SAJE, M., CAS, B., and PLANINC, I.: Non-linear finite element analysis of composite planar frames with an interlayer slip. *Comp. Struc.*, **82**(23-26), (2004), 1901–1912.
23. GIRHAMMAR, U. A. and PAN, D.: Dynamic analysis of composite members with interlayer slip. *Int. Journ. Solids and Struct.*, **30**(6), (1993), 797–823.
24. WU, Y. F., XU, R., and CHEN, W.: Free vibrations of the partial-interaction composite members with axial force. *Journ. Sound and Vib.*, **299**(4-5), (2007), 1074–1093.
25. NGUYEN, Q. H., HJIAJ, M., and GRONEC, P. L.: Analytical approach for free vibration analysis of two-layer Timoshenko beams with interlayer slip. *Journ. Sound and Vib.*, **331**(3), (2012), 2949–2961.
26. ECSEDI, I. and DLUHI, K.: Linear analysis of composite beam-columns with weak shear connection. In *MicroCAD 2005 International Scientific Conference*, 2005, pp. 37–42. Section G: Applied Mechanics, Modern Numerical Methods.
27. SOKOLNIKOFF, I. S.: *Mathematical Theory of Elasticity*. McGraw-Hill, New York, 2nd edn., 1956.
28. TIMOSHENKO, S. P. and GOODIER, J. N.: *Theory of Elasticity*. McGraw-Hill, New York, 3rd edn., 1970.
29. COWPER, G. R.: The shear coefficient in Timoshenko’s beam theory. *Journ. Appl. Mech.*, **33**(2), (1966), 335–340.

CALCULATION OF J -INTEGRAL FOR LARGE STRAINS USING THE FINITE ELEMENT METHOD

ÁGNES HORVÁTH

Institute of Applied Mechanics,
University of Miskolc, H-3515 Miskolc-Egyetemváros
mechva@uni-miskolc.hu

[Received: December 2, 2014, Accepted: January 16, 2015.]

Abstract. The present paper deals with the development of the two-dimensional J -integral for large strains. The line of thought is based on a continuum mechanical approach by using elastic or elastic-plastic bodies and presents some numerical examples.

1. INTRODUCTION

The phenomenon of failure caused by catastrophic crack propagation in structural materials poses problems of design and analysis in many fields of engineering. Cracks are present to some degree in all structures. They may exist as basic defects in the constituent materials or they may be induced in construction or during service life.

Using the finite element method, a lot of papers deal with the calculation of stress intensity factors for two- and three-dimensional models of solid bodies which contain cracks of different shapes and are subjected to various loading conditions. In order to increase the accuracy of the results, special singular and transition elements have been used. These are described together with the methods that are used to determine the stress intensity factors from the results computed. The methods mentioned include the displacement substitution method, J -integral and the virtual crack extension technique.

Over the past decades the finite element technique has become firmly established as a useful tool for numerical solution of engineering problems. In order to be able to apply the finite element method to the efficient solution of fracture problems, appropriate adaptations and/or further developments must be made.

At the vicinity of a crack tip the strains are not always small, sometimes they may be large ones, too. The J -integral can also be applied to characterize the cracks in elastic or elastic-plastic bodies under the assumption of finite strains.

In the literature there are only a few papers dealing with the J -integral for large strains. For example Lau et al. [1, 2] presented a revised J -estimation method under large plastic deformation. May and Kobayashi [3] investigated plane stress stable crack growth and J -integral using Moiré interferometry. Boothman et al. [4] developed the J - and Q -estimation schemes for homogeneous plates. Jackiewicz [5] applied a hybrid model of steel cracking. Bouchard et al. [6] demonstrated their

two-dimensional local approach finite element study compared with conventional J -estimation schemes and cracked body J -integral analysis. Sączuk et al. [7] presented a continuum model with inelastic material behaviour and a generalization of the J -integral.

The aim of the present paper is a further development of the two-dimensional J -integral based on continuum mechanics assuming large strains and elastic or elastic-plastic material behavior: computation of the J -integral is made by using the finite element method and the numerical results show the efficiency of the procedure we have developed.

2. FUNDAMENTAL CONCEPTS AND NOTATIONS

Continuum mechanics is the part of mechanics that deals with the mechanical motion of bodies using continuum models. The general theory of continuum mechanics applies to 3-dimensional models. It is, in general, supposed that the continuum (in the present case the solid body considered) has a deformation and stress-free initial state referred to as initial configuration for which $t = t_0 = 0$. At time t (when we perform our investigation) the state of continuum is referred to as present configuration.

The mechanical motion of a continuum is analyzed in a reference coordinate system which is usually the cartesian coordinate system (xyz) . An arbitrary point of the moving continuum is denoted by \hat{P} . The position of this point is P^o in the initial configuration and P in the present configuration. In the coordinate system (xyz) the coordinates of the point P^o are x^o, y^o, z^o , the corresponding base vectors are denoted by $\mathbf{e}_x^o, \mathbf{e}_y^o$ and \mathbf{e}_z^o . The coordinates of the point P are x, y, z . For the sake of making a difference the base vectors in the present configuration are denoted by $\mathbf{e}_x, \mathbf{e}_y$ and \mathbf{e}_z [$\mathbf{e}_m^o = \mathbf{e}_m$ ($m = x, y, z$)]. In accordance with what has been said above the quantities in the initial configuration are designated by the superscript o .

Scalar quantities are typeset in mathematical italic letters, e.g. U, s . Boldface letters stand for vector quantities: e.g. \mathbf{u}, \mathbf{E} . Tensors of order two are denoted by slanted boldface letters, e.g. \mathbf{T}, \mathbf{F} .

When using indicial notation in the cartesian coordinate system (a) 1, 2 and 3 correspond to x, y, z ; (b) all the indices are subscripts, (c) summation over repeated indices is implied. The other notational conventions are the same as before.

The inverse of a tensor is denoted by the superscript $^{-1}$, the notation for a transposed tensor is the superscript T . Scalar and double scalar multiplications are denoted by a dot, or a double-dot (energy product of two tensors of the second order).

We remark that the Lagrangian description will be used throughout the present paper.

3. DESCRIPTION OF THE J -INTEGRAL

Figure 1 shows a line integral path which encloses the crack tip and has initial and end points which lie on the two crack faces. It has been shown independently by Rice [8] and Cherepanov [9] that the following integral quantity is path independent when taken along any path, which satisfies the above conditions:

$$J = \int_{\Gamma} \left(U n_x - T_i \frac{\partial u_i}{\partial x} \right) ds . \quad (1)$$

In this formula U is the strain energy density, T_i is the traction vector on a plane defined by the outward normal, n_i , u_i is the displacement vector, ds is the arc element along the path, Γ . For a closed path not containing the crack tip, $J = 0$ [8].

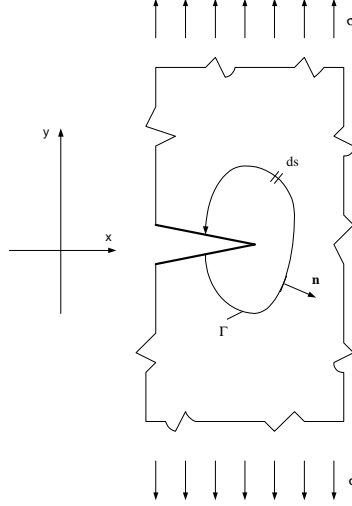


Figure 1. Contour path for J -integral evaluation

Knowles and Sternberg [10] noted that this expression could be considered as the first component of a vector:

$$J_k = \int_{\Gamma} \left(U n_k - T_i \frac{\partial u_i}{\partial x_k} \right) ds , \quad k = 1, 2. \quad (2)$$

This integral is also path independent provided that the contour touches each surface of the crack at the tip. As $x_1 = x$ and $x_2 = y$, applying formulae $n_x = dy/ds$ and $n_y = -dx/ds$, by means of (2) we can write the two components of the J -integral in the following form:

$$J_x = \int_{\Gamma} \left(U dy - T_i \frac{\partial u_i}{\partial x} ds \right) , \quad J_y = - \int_{\Gamma} \left(U dx + T_i \frac{\partial u_i}{\partial y} \right) . \quad (3)$$

For elastic-plastic bodies the strain energy density consists of two parts:

$$U = U_e + U_p . \quad (4)$$

U_e is given by

$$U_e = \frac{1}{2} \sigma_{ij} (\varepsilon_{ij})_e , \quad (5)$$

where σ_{ij} is the stress tensor and $(\varepsilon_{ij})_e$ denotes the elastic components of strains. The plastic work contribution is given by

$$U_p = \int_0^{\bar{\varepsilon}_p} \bar{\sigma} d\bar{\varepsilon}_p. \quad (6)$$

In this expression $\bar{\sigma}$ and $\bar{\varepsilon}_p$ are the effective stress and effective plastic strain, respectively:

$$\bar{\sigma} = \left[\frac{3}{2} (\sigma'_{ij} \sigma'_{ij}) \right]^{1/2}, \quad (7)$$

in which σ'_{ij} denotes the components of the deviatoric stress tensor and

$$d\bar{\varepsilon}_p = \left\{ \frac{2}{3} [(d\varepsilon_{ij})_p (d\varepsilon_{ij})_p] \right\}^{1/2}, \quad (8)$$

where $(d\varepsilon_{ij})_p$ denotes the plastic part of the strain tensor increment.

Figure 2 represents the motion of a continuum with the initial and the present configurations.

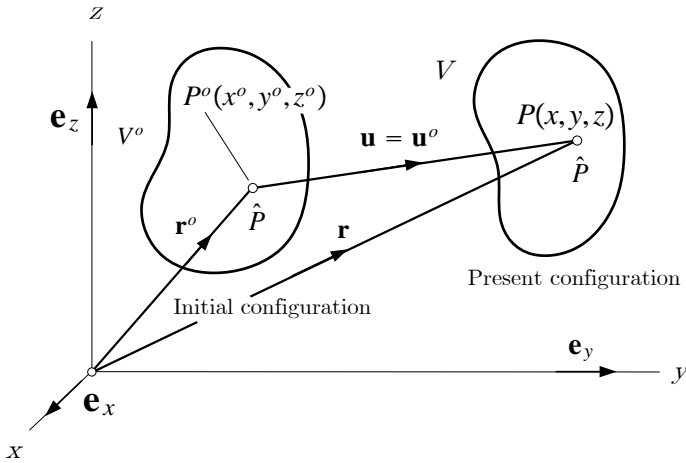


Figure 2. Motion of the continuum in the reference coordinate system (xyz)

Let us suppose that equation (2) is valid in the present configuration for large strains. As the initial configuration is known, it is necessary to express the quantities in the integrand in terms of the Green-Lagrange strain tensor (\mathbf{E}^0) and the second Piola-Kirchhoff stress tensor (\mathbf{T}^0). For elastic applications it can be proved that instead of the strain energy density U one can use the following formula:

$$U^o = \frac{1}{2} \mathbf{E}^o \cdot \mathbf{T}^o. \quad (9)$$

For two-dimensional problems equation (9) assumes the form:

$$U^o = \frac{1}{2} (E_{xx}^o T_{xx}^o + 2 E_{xy}^o T_{xy}^o + E_{yy}^o T_{yy}^o). \quad (10)$$

The arc element is

$$ds = ds^o \lambda_s = ds^o \sqrt{1 + 2 \mathbf{e}^o \cdot \mathbf{E}^o \cdot \mathbf{e}^o}, \quad (11)$$

where ds° and \mathbf{e}° are the arc element and the tangent vector to the curve Γ in the initial configuration and λ_s is the stretch.

For manipulating the traction vector $\mathbf{t} = \mathbf{T} \cdot \mathbf{n}$ into a suitable form we shall need the relations:

$$\mathbf{T} = \frac{1}{\mathfrak{J}} \mathbf{F} \cdot \mathbf{T}^\circ \cdot \mathbf{F}^T, \quad (12)$$

$$\mathfrak{J} = \det |\mathbf{F}|, \quad (13)$$

where $\mathbf{F} = \mathbf{r} \circ \nabla^\circ$ is the deformation gradient, \mathfrak{J} is the Jacobian and ∇° is the nabla operator in the initial configuration.

Applying the formula $d\mathbf{A} = \mathfrak{J} \mathbf{F}^{-T} \cdot d\mathbf{A}^\circ$ between the surface elements, the traction vector can be expressed as:

$$\mathbf{t} = \frac{1}{\lambda_A} \mathbf{F} \cdot \mathbf{T}^\circ \cdot \mathbf{n}^\circ = \frac{1}{\mathfrak{J} \sqrt{\mathbf{n}^\circ \cdot (2\mathbf{E}^\circ + \mathbf{I})^{-1} \cdot \mathbf{n}^\circ}} \mathbf{F} \cdot \mathbf{T}^\circ \cdot \mathbf{n}^\circ, \quad (14)$$

where \mathbf{I} is the unit tensor, \mathbf{n}° is the outward unit normal to Γ in the initial configuration, $d\mathbf{A}$ is the vectorial surface element in the present configuration, $d\mathbf{A}^\circ$ is the vectorial surface element in the initial configuration, $\lambda_A = dA/dA^\circ$ is the ratio of the scalar surface element [11].

It can be seen from Figure 2 that $\mathbf{r} = \mathbf{r}^\circ + \mathbf{u}^\circ$, therefore we can write

$$dy = \frac{\partial y}{\partial x^\circ} dx^\circ + \frac{\partial y}{\partial y^\circ} dy^\circ = dy^\circ + \frac{\partial u_y^\circ}{\partial x^\circ} dx^\circ + \frac{\partial u_y^\circ}{\partial y^\circ} dy^\circ, \quad (15)$$

$$dx = \frac{\partial x}{\partial x^\circ} dx^\circ + \frac{\partial x}{\partial y^\circ} dy^\circ = dx^\circ + \frac{\partial u_x^\circ}{\partial x^\circ} dx^\circ + \frac{\partial u_x^\circ}{\partial y^\circ} dy^\circ. \quad (16)$$

As $\mathbf{u} = \mathbf{u}^\circ$, the derivatives of the displacement vector are as follows:

$$\frac{\partial \mathbf{u}^\circ}{\partial x} = \frac{\partial u_x^\circ}{\partial x} \mathbf{e}_x^\circ + \frac{\partial u_y^\circ}{\partial x} \mathbf{e}_y^\circ = \left(\frac{\partial u_x^\circ}{\partial x^\circ} \frac{\partial x^\circ}{\partial x} + \frac{\partial u_x^\circ}{\partial y^\circ} \frac{\partial y^\circ}{\partial x} \right) \mathbf{e}_x^\circ + \left(\frac{\partial u_y^\circ}{\partial x^\circ} \frac{\partial x^\circ}{\partial x} + \frac{\partial u_y^\circ}{\partial y^\circ} \frac{\partial y^\circ}{\partial x} \right) \mathbf{e}_y^\circ, \quad (17)$$

$$\frac{\partial \mathbf{u}^\circ}{\partial y} = \frac{\partial u_x^\circ}{\partial y} \mathbf{e}_x^\circ + \frac{\partial u_y^\circ}{\partial y} \mathbf{e}_y^\circ = \left(\frac{\partial u_x^\circ}{\partial x^\circ} \frac{\partial x^\circ}{\partial y} + \frac{\partial u_x^\circ}{\partial y^\circ} \frac{\partial y^\circ}{\partial y} \right) \mathbf{e}_x^\circ + \left(\frac{\partial u_y^\circ}{\partial x^\circ} \frac{\partial x^\circ}{\partial y} + \frac{\partial u_y^\circ}{\partial y^\circ} \frac{\partial y^\circ}{\partial y} \right) \mathbf{e}_y^\circ. \quad (18)$$

Since $\mathbf{r} = \mathbf{r}^\circ + \mathbf{u}^\circ$, it follows that

$$x = x^\circ + u_x^\circ, \quad y = y^\circ + u_y^\circ. \quad (19)$$

Making use of (19) for the deformation gradient \mathbf{F} , the inverse deformation gradient \mathbf{F}^{-1} and the Jacobian determinant \mathfrak{J} we obtain

$$[\mathbf{F}] = \begin{bmatrix} \frac{\partial x}{\partial x^\circ} & \frac{\partial x}{\partial y^\circ} \\ \frac{\partial y}{\partial x^\circ} & \frac{\partial y}{\partial y^\circ} \end{bmatrix} = \begin{bmatrix} 1 + \frac{\partial u_x^\circ}{\partial x^\circ} & \frac{\partial u_x^\circ}{\partial y^\circ} \\ \frac{\partial u_y^\circ}{\partial x^\circ} & 1 + \frac{\partial u_y^\circ}{\partial y^\circ} \end{bmatrix}, \quad (20)$$

$$[\mathbf{F}^{-1}] = \begin{bmatrix} \frac{\partial x^\circ}{\partial x} & \frac{\partial x^\circ}{\partial y} \\ \frac{\partial y^\circ}{\partial x} & \frac{\partial y^\circ}{\partial y} \end{bmatrix} = \frac{1}{\mathfrak{J}} \begin{bmatrix} 1 + \frac{\partial u_y^\circ}{\partial y^\circ} & -\frac{\partial u_x^\circ}{\partial y^\circ} \\ -\frac{\partial u_y^\circ}{\partial x^\circ} & 1 + \frac{\partial u_x^\circ}{\partial x^\circ} \end{bmatrix}, \quad (21)$$

$$\mathfrak{J} = \det |\mathbf{F}| = \left(1 + \frac{\partial u_x^o}{\partial x^o}\right) \left(1 + \frac{\partial u_y^o}{\partial y^o}\right) - \frac{\partial u_x^o}{\partial y^o} \frac{\partial u_y^o}{\partial x^o}. \quad (22)$$

Utilizing equations (20), (21) and (22), we can rewrite equations (17) and (18) in other form:

$$\frac{\partial \mathbf{u}^o}{\partial x} = \frac{1}{\mathfrak{J}} \left[\left(1 + \frac{\partial u_y^o}{\partial y^o}\right) \frac{\partial u_x^o}{\partial x^o} - \frac{\partial u_x^o}{\partial y^o} \frac{\partial u_y^o}{\partial x^o} \right] \mathbf{e}_x^o + \frac{1}{\mathfrak{J}} \left[\left(1 + \frac{\partial u_y^o}{\partial y^o}\right) \frac{\partial u_y^o}{\partial x^o} - \frac{\partial u_y^o}{\partial y^o} \frac{\partial u_x^o}{\partial x^o} \right] \mathbf{e}_y^o, \quad (23)$$

$$\frac{\partial \mathbf{u}^o}{\partial y} = \frac{1}{\mathfrak{J}} \left[\left(1 + \frac{\partial u_x^o}{\partial x^o}\right) \frac{\partial u_x^o}{\partial y^o} - \frac{\partial u_x^o}{\partial x^o} \frac{\partial u_x^o}{\partial y^o} \right] \mathbf{e}_x^o + \frac{1}{\mathfrak{J}} \left[\left(1 + \frac{\partial u_x^o}{\partial x^o}\right) \frac{\partial u_y^o}{\partial y^o} - \frac{\partial u_y^o}{\partial x^o} \frac{\partial u_x^o}{\partial y^o} \right] \mathbf{e}_y^o. \quad (24)$$

Substituting (10) - (24) into (3) we obtain the components of J -integral for large strains in two dimensions:

$$J_x = \int_{(\Gamma)} \left[U^o \left(dy^o + \frac{\partial u_y^o}{\partial x^o} dx^o + \frac{\partial u_y^o}{\partial y^o} dy^o \right) - \mathbf{t} \frac{\partial \mathbf{u}^o}{\partial x} \lambda_s ds^o \right] \quad (25)$$

$$J_y = \int_{(\Gamma)} \left[-U^o \left(dx^o + \frac{\partial u_x^o}{\partial x^o} dx^o + \frac{\partial u_x^o}{\partial y^o} dy^o \right) - \mathbf{t} \frac{\partial \mathbf{u}^o}{\partial y} \lambda_s ds^o \right] \quad (26)$$

For elastic-plastic bodies the strain energy density also has two parts:

$$U^o = U_e^o + U_p^o, \quad (27)$$

where U_e^o is given in equation (9) and U_p^o is similar to (6):

$$U_p^o = \int_o^{\bar{E}_p^o} \bar{T}^o d\bar{E}_p^o. \quad (28)$$

In this expression \bar{T}^o and \bar{E}_p^o are the effective stress and effective plastic strain in the initial configuration.

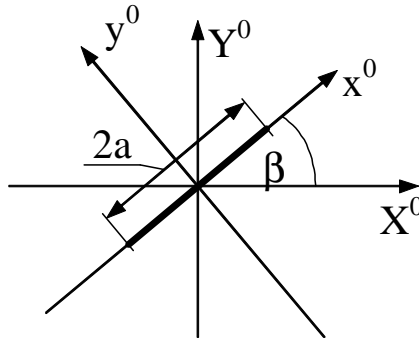


Figure 3. Coordinate systems in the initial configuration

For inclined cracks two coordinate systems and the corresponding transformation formulae are necessary – see Figure 3.

When one applies the finite element method the integration in equations (25) and (26) should be performed numerically.

4. PATH-INDEPENDENCE OF THE J -INTEGRAL

Rice has already investigated the problem of path-independence [8]. We remark that other researchers have also examined this question, e.g. Atluri [12], Brocks and Scheider [13] and Wang et al. [14].

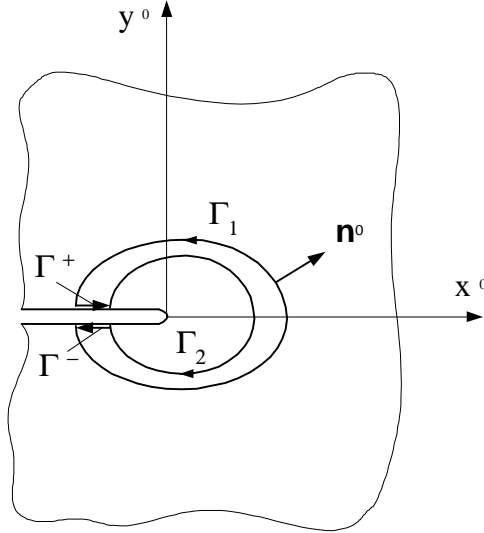


Figure 4. Closed contour for J -integral evaluation

Henceforth the path-independence of (25), (26) is proved for large strains and two dimensional problems. The following assumptions have been made:

- The material of the body is homogeneous.
- There are no body forces.
- The stress and strain fields depend on two coordinates (x^o, y^o) .
- The crack is straight.
- The stress-free crack borders are parallel to coordinate axis x^o .

Figure 4 shows a closed integral path which does not contain the crack tip.

The closed contour Γ does not include a singularity:

$$\Gamma = \Gamma_1 \cup \Gamma^+ \cup \Gamma_2 \cup \Gamma^-. \quad (29)$$

Then $J = 0$ along a closed contour Γ for large strains, too. Let us examine the component J_x along the path Γ .

$$J_x = 0 = \oint_{\Gamma_2} \left[U^o \left(dy^o + \frac{\partial u_y^o}{\partial x^o} dx^o + \frac{\partial u_x^o}{\partial y^o} dy^o \right) - \mathbf{t} \cdot \frac{\partial \mathbf{u}^o}{\partial x} \lambda_s ds^o \right] +$$

$$\begin{aligned}
& + \oint_{\Gamma_1} \left[U^o \left(dy^o + \frac{\partial u_y^o}{\partial x^o} dx^o + \frac{\partial u_y^o}{\partial y^o} dy^o \right) - \mathbf{t} \cdot \frac{\partial \mathbf{u}^o}{\partial x} \lambda_s ds^o \right] + \\
& + \int_{\Gamma^+} \left[U^o \left(dy^o + \frac{\partial u_y^o}{\partial x^o} dx^o + \frac{\partial u_y^o}{\partial y^o} dy^o \right) - \mathbf{t} \cdot \frac{\partial \mathbf{u}^o}{\partial x} \lambda_s ds^o \right] + \\
& + \int_{\Gamma^-} \left[U^o \left(dy^o + \frac{\partial u_y^o}{\partial x^o} dx^o + \frac{\partial u_y^o}{\partial y^o} dy^o \right) - \mathbf{t} \cdot \frac{\partial \mathbf{u}^o}{\partial x} \lambda_s ds^o \right]. \quad (30)
\end{aligned}$$

The integrals on Γ^+ and Γ^- differ from each other in sign only. Therefore they can be dropped. In this way we get

$$\begin{aligned}
J_x = 0 & = \oint_{\Gamma_2} \left[U^o \left(dy^o + \frac{\partial u_y^o}{\partial x^o} dx^o + \frac{\partial u_y^o}{\partial y^o} dy^o \right) - \mathbf{t} \cdot \frac{\partial \mathbf{u}^o}{\partial x} \lambda_s ds^o \right] + \\
& + \oint_{\Gamma_1} \left[U^o \left(dy^o + \frac{\partial u_y^o}{\partial x^o} dx^o + \frac{\partial u_y^o}{\partial y^o} dy^o \right) - \mathbf{t} \cdot \frac{\partial \mathbf{u}^o}{\partial x} \lambda_s ds^o \right]. \quad (31)
\end{aligned}$$

We get a useful expression if the integration on contour Γ_2 is performed counterclockwise:

$$\begin{aligned}
& \oint_{\Gamma_2} \left[U^o \left(dy^o + \frac{\partial u_y^o}{\partial x^o} dx^o + \frac{\partial u_y^o}{\partial y^o} dy^o \right) - \mathbf{t} \cdot \frac{\partial \mathbf{u}^o}{\partial x} \lambda_s ds^o \right] = \\
& = - \oint_{\Gamma_2} \left[U^o \left(dy^o + \frac{\partial u_y^o}{\partial x^o} dx^o + \frac{\partial u_y^o}{\partial y^o} dy^o \right) - \mathbf{t} \cdot \frac{\partial \mathbf{u}^o}{\partial x} \lambda_s ds^o \right]. \quad (32)
\end{aligned}$$

Substituting (32) into equation (31) we obtain the following formula:

$$\begin{aligned}
0 & = - \oint_{\Gamma_2} \left[U^o \left(dy^o + \frac{\partial u_y^o}{\partial x^o} dx^o + \frac{\partial u_y^o}{\partial y^o} dy^o \right) - \mathbf{t} \cdot \frac{\partial \mathbf{u}^o}{\partial x} \lambda_s ds^o \right] + \\
& + \oint_{\Gamma_1} \left[U^o \left(dy^o + \frac{\partial u_y^o}{\partial x^o} dx^o + \frac{\partial u_y^o}{\partial y^o} dy^o \right) - \mathbf{t} \cdot \frac{\partial \mathbf{u}^o}{\partial x} \lambda_s ds^o \right]. \quad (33)
\end{aligned}$$

Rearrangement of (34) results in

$$\begin{aligned}
& \oint_{\Gamma_2} \left[U^o \left(dy^o + \frac{\partial u_y^o}{\partial x^o} dx^o + \frac{\partial u_y^o}{\partial y^o} dy^o \right) - \mathbf{t} \cdot \frac{\partial \mathbf{u}^o}{\partial x} \lambda_s ds^o \right] = + \\
& = + \oint_{\Gamma_1} \left[U^o \left(dy^o + \frac{\partial u_y^o}{\partial x^o} dx^o + \frac{\partial u_y^o}{\partial y^o} dy^o \right) - \mathbf{t} \cdot \frac{\partial \mathbf{u}^o}{\partial x} \lambda_s ds^o \right]. \quad (34)
\end{aligned}$$

which shows the path independence of the first component of the vector J . This holds for the other component, too.

5. APPLICABILITY OF SPECIAL ISOPARAMETRIC ELEMENTS

Consider a one-dimensional element that may form a side of a 2D or 3D n th-order isoparametric element (see Figure 5).

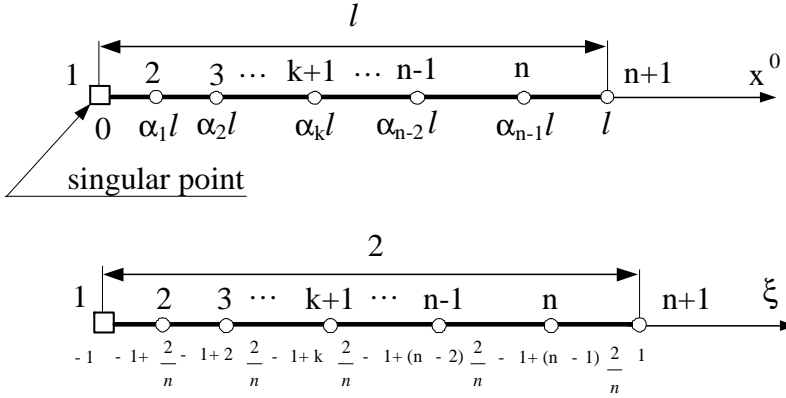


Figure 5. Element coordinate mapping

The above transformation is accomplished by means of the usual isoparametric mapping technique [15]. Without entering into details we obtain the following expressions:

$$x^o = \frac{\ell}{2^m} (1 + \xi)^m, \tag{35}$$

$$\xi = -1 + 2 \left(\frac{x^o}{\ell} \right)^{1/m}. \tag{36}$$

For an isoparametric element the displacement u_x^o takes the form

$$u_x^o = b_0 + b_1 \xi + b_2 \xi^2 + \dots + b_n \xi^n, \quad n \geq 2. \tag{37}$$

from where

$$\frac{\partial u_x^o}{\partial \xi} = b_1 + 2b_2 \xi + 3b_3 \xi^2 + \dots + nb_n \xi^{(n-1)}. \tag{38}$$

This expression can be manipulated further by inserting (36)

$$\begin{aligned} \frac{\partial u_x^o}{\partial \xi} &= b_1 + 2b_2 \left[-1 + 2 \left(\frac{x^o}{\ell} \right)^{1/m} \right] + 3b_3 \left[-1 + 2 \left(\frac{x^o}{\ell} \right)^{1/m} \right]^2 + \dots + \\ &+ nb_n \left[-1 + 2 \left(\frac{x^o}{\ell} \right)^{1/m} \right]^{(n-1)}. \end{aligned} \tag{39}$$

The strain in the x^o -direction is then

$$E_{xx}^o = \frac{du_x^o}{dx^o} + \frac{1}{2} \left(\frac{du_x^o}{dx^o} \right)^2. \tag{40}$$

Utilizing equation (37) the axial strain (40) can be rewritten

$$E_{xx}^o = \frac{du_x^o}{d\xi} \frac{d\xi}{dx^o} + \frac{1}{2} \left(\frac{du_x^o}{d\xi} \frac{d\xi}{dx^o} \right)^2. \tag{41}$$

Substituting (39) and the derivative of (36) into (41) we obtain

$$\begin{aligned}
 E_{xx}^o &= A_1 (x^o)^{\frac{1-m}{m}} + A_2 (x^o)^{\frac{2-m}{m}} + A_3 (x^o)^{\frac{3-m}{m}} + \dots + \\
 &+ A_n (x^o)^{\frac{n-m}{m}} + A_{n+1} (x^o)^{\frac{2(1-m)}{m}} + A_{n+2} (x^o)^{\frac{2(1-m)+1}{m}} + \dots + \\
 &+ A_{(3n-1)} (x^o)^{\frac{2(n-m)}{m}} ,
 \end{aligned} \tag{42}$$

where

$$\begin{aligned}
 A_1 &= C (b_1 - 2b_2 + 3b_3 - \dots \pm nb_n) , \\
 A_2 &= \frac{C}{\ell^{1/m}} 2 [2b_2 - 6b_3 + 12b_4 - \dots \pm (n-1)nb_n] , \\
 &\vdots \\
 A_n &= \frac{C}{\ell^{(n-1)/m}} 2^{(n-1)} nb_n , \\
 A_{(n+1)} &= \frac{C^2}{2} [b_1^2 + 4b_2^2 + \dots + n^2 b_n^2 - 4b_1 b_2 + 6b_1 b_3 - \dots \pm 2nb_1 b_n \pm \dots \pm \\
 &\pm 2(n-1)nb_{(n-1)}b_n] , \\
 A_{(n+2)} &= \frac{C^2}{2} \frac{2^2}{\ell^{1/m}} [2b_1 b_2 - 6b_1 b_3 + 18b_2 b_3 - 4b_2^2 - 18b_3^2 - \dots \pm \\
 &\pm n^2 (n-1)b_{(n-1)}b_n - (n-1)(nb_n)^2] , \\
 &\vdots \\
 A_{(3n-1)} &= \frac{C^2}{2} \frac{2^{2(n-1)}}{\ell^{2(n-1)/m}} (nb_n)^2 , \\
 C &= \frac{2}{m} \frac{1}{\ell^{1/m}} .
 \end{aligned}$$

Equation (42) clearly shows that the strain is singular at $x^o = 0$ ($\xi = -1$). The leading strain term is of order $(x^o)^{\frac{1-m}{m}}$. Therefore when $x^o \rightarrow 0$, the type of the strain singularity is $(x^o)^{(1-m)/m}$ ($m \geq 2$).

6. NUMERICAL EXAMPLE

The author has developed a Fortran program by means of Microsoft Developer Studio 97 to compute the J -integral numerically for small and large strains. For a real physical problem the strains can be either small or large depending on the loading of the body. As regards the present example both kind of strains are computed so that one can see what the difference is between the two kind of strains. When computing elastic-plastic problems the Von Mises yield criterion, the Newton-Raphson iteration technics and the Euler-Cauchy incremental method are applied.

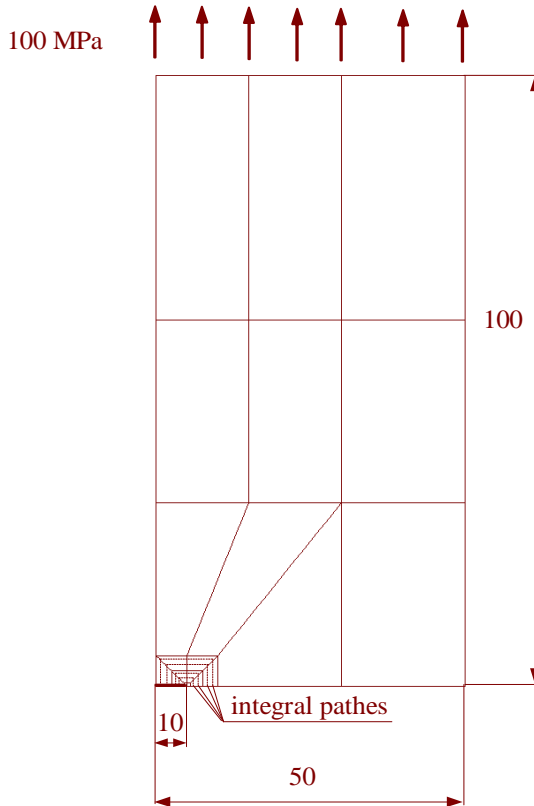


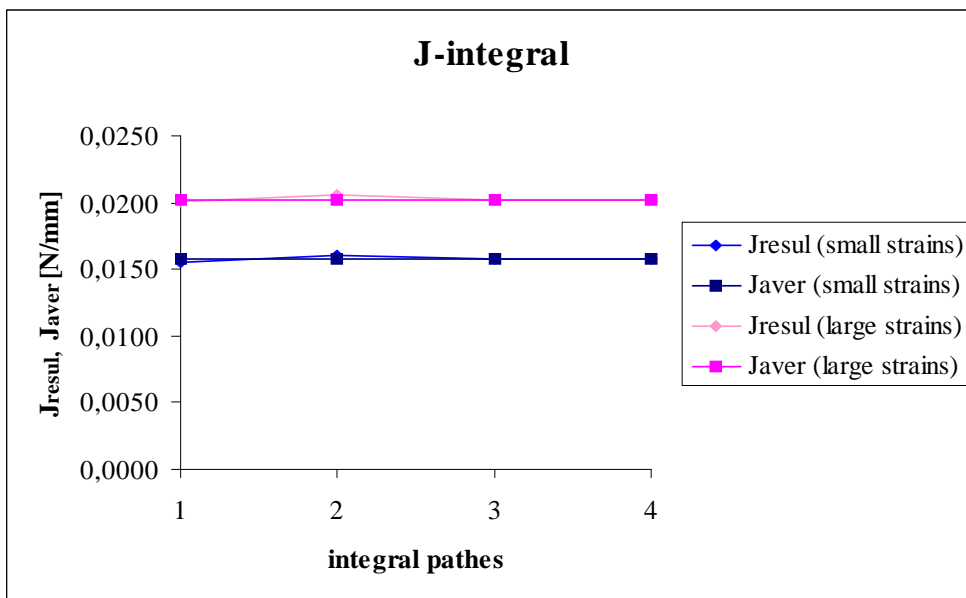
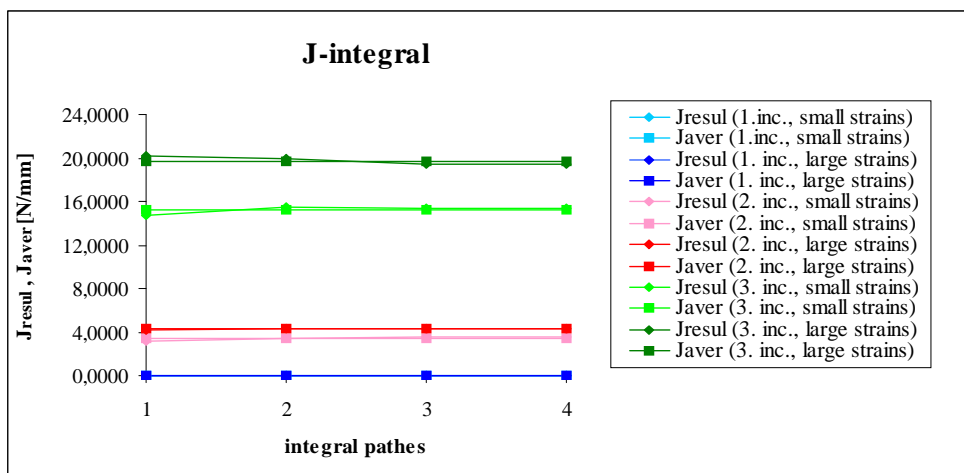
FIGURE 6. Finite element mesh

The example considered is that of a plate under tension which contains a crack of length 20 mm perpendicular to the direction of loading. The width of the plate is 100 mm and the thickness is assumed to be unity. The length of the plate is 200 mm. For the first computations the material is linear elastic with the properties $E = 2 \times 10^5$ MPa and $\nu = 0.3$. The applied tensile traction is $p = 100$ MPa. Because of the symmetrical properties of the problem the finite element mesh represents only a quarter of the body considered – see Figure 6. The finite element mesh contains singular and transition elements as well.

Theoretically J_y is zero for this problem. Figure 7 shows the values computed for the J -integral.

For the second series of computations the material of the plate is a linear elastic linear hardening material for which $H' = 0,1E$ and the yield stress is $\sigma_F = 100$ MPa. The loading is applied in incremental steps. The increments are $0.1p = 10$ MPa, $1.0p = 100$ MPa, $0.3p = 30$ MPa. Figure 8 shows the values computed for the J -integral both for small strains and for large strains.

Figure 9 depicts the plastic zones for the third load increment. Figure 10 shows the von Mises stresses for the third load increment.

Figure 7. J -integral for elastic deformationsFigure 8. J -integral for elastic-plastic deformations

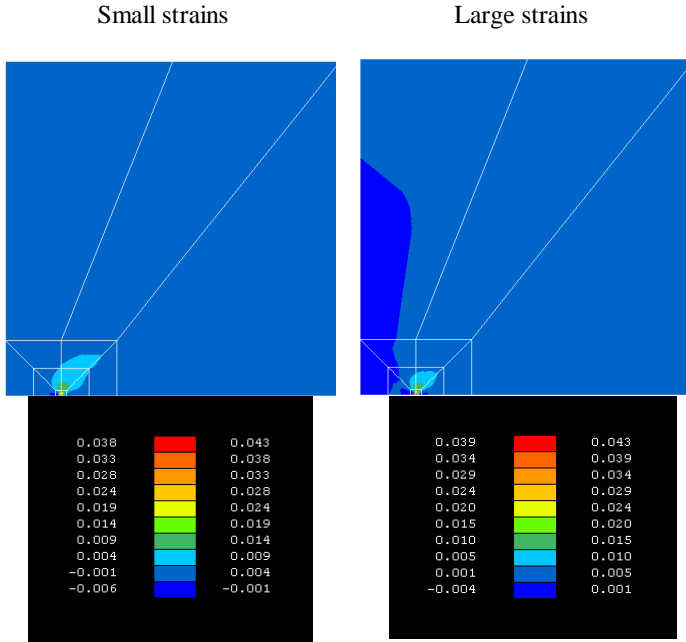


Figure 9. Plastic zones for the third load increment

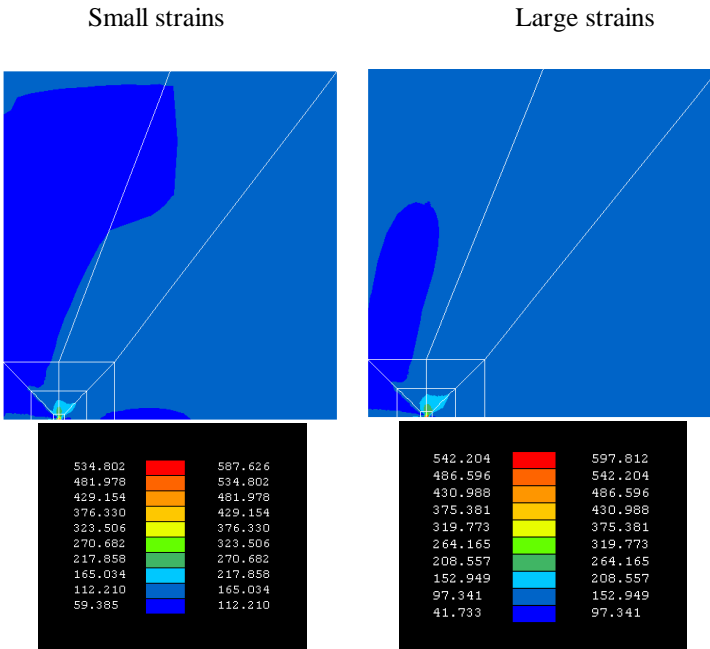


Figure 10. Von Mises stresses for the third load increment

7. CONCLUSIONS

This paper proves the formulations and applicability of the J -integral for large strains under the assumption of elastic and elastic-plastic material behaviour. The J -integral values are higher for large strains, as can be seen from the numerical examples we have solved. This fact means that the safety of the cracked body increases from the aspect of service life. The path independence of the two-dimensional J -integral is also proved for large strains – the numerical results confirm the validity of this statement. The paper presents the mapping and applicability of special isoparametric elements for the finite element meshes. Using these elements the type of the strain singularity is $(x^0)^{(1-m)/m}$ ($m \geq 2$) at the crack tip. The application of the special isoparametric elements gives good results for relatively coarse finite element meshes, too.

REFERENCES

1. LAU, C. L., LEE, M. M. K., and LUXMOORE, A. R.: Methodologies for Predicting J -integrals under Large Plastic Deformation-i. further Developments for Tension Loading. *Eng. Frac. Mech.*, **49**(3), (1994), 337–354.
2. LAU, C. L., LEE, M. M. K., and LUXMOORE, A. R.: Methodologies for Predicting J -integrals under Large Plastic Deformation-ii. single Edge Notch Specimens in Pure Bending. *Eng. Frac. Mech.*, **49**(3), (1994), 355–369.
3. MAY, G. B. and KOBAYASHI, A. S.: Plane Stress Stable Crack Growth and J -integral/hrr Field. *Int. J. of Solids and Structures*, **32**(6/7), (1995), 857–881.
4. BOOTHMAN, D. P., LEE, M. M. K., and LUXMOORE, A. R.: The Effects of Weld Mismatch on J -integrals and Q -values for Semi-elliptical Surface Flaws. *Eng. Frac. Mech.*, **64**, (1994), 433–458.
5. JACZKIEWICZ, J.: Numerical Aspects of Non-local Modelling of the Damage Evolution in Elastic-plastic Materials. *Comp. Mat. Science*, **19**, (2000), 235–251.
6. BOUCHARD, P. J., GOLDTHORPE, M. R., and PROTTEY, P.: J -integral and Local Damage Fracture Analyses for a Pump Casing Containing Large Weld Repairs. *Int. J. Pressure Vessels*, **78**, (2001), 295–305.
7. SACZUK, J., STUMPF, H., and VALLEE, C.: A Continuum Model Accounting for Defect and Mass Densities in Solids with Inelastic Material Behaviour. *Int. J. of Solids and Structures*, **38**(52), (2001), 9545–9568.
8. RICE, J. R.: A Path Independent Integral and the Approximate Analysis of Strain Concentration by Notches and Cracks. *J. App. Mech.*, **34**, (1968), 379–386.
9. CHEREPANOV, G. P.: Cracks in Solids. *Prikl. Mat. Mekh.*, **25**, (1967), 476–488.
10. KNOWLES, J. K. and STERNBERG, E.: On a Class of Conservation Laws in Linearized and Finite Elastostatics. *Arch. Rat. Mech. Anal.*, **44**, (1972), 187–211.
11. BÉDA, G., KOZÁK, I., and VERHÁS, J.: *Continuum Mechanics*. Akadémiai Kiadó, Budapest, 1995.
12. ATLURI, S. N.: Path-independent integrals in finite elasticity and inelasticity, with body forces, inertia, and arbitrary crack-face conditions. *Eng. Frac. Mech.*, **16**(3), (1982), 341–364.

13. BROCKS, W. and SCHEIDER, I.: Numerical Aspects of the Path-Dependence of the J-Integral in Incremental Plasticity. *GKSS Forschungszentrum, Geesthacht*, **1**, (2001), 1–33.
14. WANG, X.-M. and SHEN, Y.-P.: The conservation laws and path-independent integrals with an application for linear electro-magneto-elastic media. *Int. J. Solids Structures*, **33**(6), (1996), 865–878.
15. HORVÁTH, Á.: Higher-order Singular Isoparametric Elements for Crack Problems. *Comm. in Num. Meth. Eng.*, **10**, (1994), 73–80.

CONNECTION BETWEEN THE LEAKING AND THE VISCOELASTIC BEHAVIOR OF FLANGE GASKETS

GÁBOR L. SZEPESI - ZOLTÁN SIMÉNFALVI

Institute of Energy Engineering and Chemical Machinery, Dept. of Chemical Machinery
University of Miskolc
H-3515 Miskolc-Egyetemváros, Hungary
szepesi@uni-miskolc.hu

[Received: October 20, 2014, Accepted: February 12, 2015.]

Abstract. This paper presents a measurement and calculation method to determine the stress relaxation function parameters of a flange gasket which has a viscoelastic behavior. It is so important, because it has a strong connection to the vessels leakage.

Mathematical Subject Classification: 05C38, 15A15

Keywords: gasket, stress relaxation, Generalized Maxwell Model, penalty function.

1. INTRODUCTION

Operation of closed systems often cause isolation problems. In this case the air contaminant may leak into the working area or into the environment. The flange-gasket untightness is the source of the leaking most times. This paper points out the main cause of the leakage of soft PTFE (Polytetrafluoroethylene) covered textile gasket between flange joints. An investigation unit has been created to examine the PTFE covered gaskets. With the help of this investigation unit, the stress and deformation in the gasket can be measured.

2. GASKET INVESTIGATION UNIT

The investigation unit has been created for gasket measuring is shown in Figure 1. The main parts of the investigation unit are:

1. tension tester (load capacity: 25 kN),
2. load cell,
3. flange,
4. gasket,
5. displacement transmitter,
6. A/D converter,
7. computer.

During the measurements the flange gasket is pressed by the tension tester. The compression-stress and the gasket deformation (compressive strain) recorded by the A/D logger-converter. When the stress reaches the maximum, the increment of the stress is stopped. With this procedure we can simulate a flange-joint gasket deformation and stress relaxation.

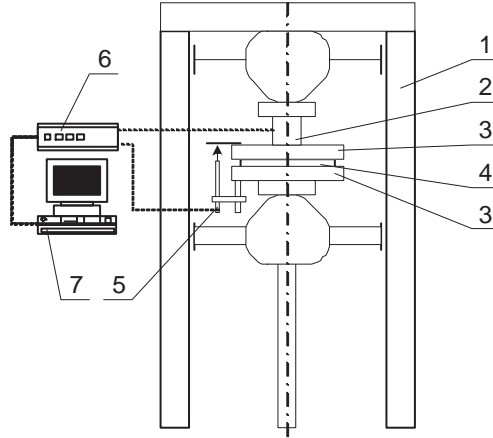


Figure 1. The investigation unit

If the gasket is not working properly leaking can occur. This happens if the gasket parameters are not correct or the gasket is damaged. If the gasket stress can not reach the required value or the stress is reduced below the required value a leaking process can start. Due to the leakage, the air contaminant mass flow spilling into the atmosphere is determinable[1].

3. MECHANICAL MODEL OF FLANGE CONNECTION

The simplified mechanical model of flange connection is showed on Figure 2. The base load of the flange is the bending momentum. This load arise from the bolt force, the inner pressure force and the gasket force. The flange and the gasket forces are different in case of operation state and assembling state. The inner pressure forces are zero in case of assembling state. In the present case the gasket force is higher then another state. The minimum bolt force in assembling state can calculate by:

$$W_A = \pi b G y, \quad (1)$$

where b is the effective gasket width, G is the diameter of the gasket center line, y is the minimal gasket stress.

If the applied bolt force is lower than W_A (calculated with (1)) the gasket is not working acceptably and it cause leaking.

In case of operational state the bolt force has to be higher then assembling state. This force can calculate with this equation:

$$W_{OP} = \frac{\pi}{4} G^2 P + 2\pi GmP, \quad (2)$$

where P is the pressure, m is the gasket parameter. This gasket parameter depends on the material of the gasket. The table shows the gasket parameter and the minimal gasket stress in case of different type of gaskets:

Table 1. Typical gasket parameters and minimal stresses

| Type of the gasket | Gasket parameter, m | Gasket minimal stress, y , MPa |
|---------------------|-----------------------|------------------------------------|
| Rubber | 0.5 - 1 | 0 - 1.4 |
| PVC | 1.5 | 1.2 |
| PTFE | 2 - 2.75 | 1.2 - 1.6 |
| Rubber with textile | 1.25 | 2.75 |
| IT sheet | 2.25 - 2.75 | 15 - 25 |
| Wawed seal | 2.5 - 3.5 | 25 - 52 |

The effective gasket stress is depends on the bolt force, the gasket parameter, the gasket minimal stress and of course the geometry of the flanged connection. If

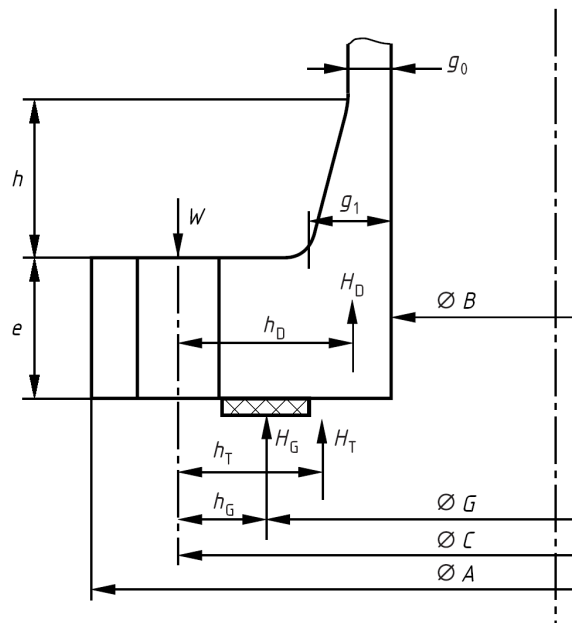


Figure 2. General mechanical model of flange connection

the gasket material shows viscoelastic or viscoplastic property, the gasket stress also depends on the time.

4. GENERALIZED MAXWELL MODEL

The material of the PTFE covered textile gasket shows viscoelastic property. The viscoelastic material-model is described by rheological elements. The Generalized Maxwell model[2], shown in Figure 3 is used for describing the material behavior of the gasket.

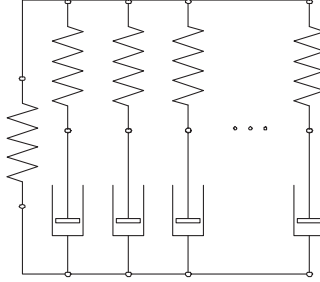


Figure 3. Generalized Maxwell Model

Assuming that gasket deformation is only in axial direction, there is no radial deformation. Consequently, only volumetric stresses occur in the gasket. This linear viscoelastic behavior is commonly using the Boltzmann superposition integral[4]:

$$\sigma(\tau) = \int_0^{\tau} K(\tau - \tau') \frac{\partial \epsilon}{\partial \tau'} \partial \tau', \quad (3)$$

where K is the relaxation function, τ is the time, ϵ is the deformation. The relaxation function is approximated with the following formula:

$$K(\tau) = K_{\infty} + K_0 \sum_{k=1}^m w_k e^{-\frac{\tau}{\tau_k}}. \quad (4)$$

The $\sigma(\tau)$ stress-function approximated with:

$$f_k(t) = A + B \sum_{j=1}^m w_j e^{-t/\tau_k}, \quad (5)$$

where A is the residual stress, B is the relaxation factor, w_j is the weighting coefficient, m is the number of the Maxwell elements, τ_k is the relaxation time of the one of the Maxwell element.

According to the investigation results, in case of $m = 3$, the approximation is suitable. The least squares method is used in the approximation process:

$$F = \sum_{i=1}^n (f_{ki} - f_{mi})^2 \rightarrow \min, \quad (6)$$

where n is the number of the measuring points, f_{ki} the approximated stress-function, f_{mi} is the measured stress values.

Derivative of function (6) with respect to the variable A :

$$\frac{\partial F}{\partial A} = 2 \sum_{i=1}^n (f_{mi} - f_{ki}). \quad (7)$$

Derivative of function (6) with respect to the variable B :

$$\frac{\partial F}{\partial B} = 2 \sum_{i=1}^n (f_{mi} - f_{ki}) \cdot \sum_{j=1}^m (w_j e^{-\frac{t_i}{\tau_j}}). \quad (8)$$

Derivative of function (6) with respect to the variable w_k , where $k=1,2,3$:

$$\frac{\partial F}{\partial w_k} = 2 \sum_{i=1}^n (f_{mi} - f_{ki}) \left[B e^{-t_i/\tau_k} \right]. \quad (9)$$

Derivative of function (6) with respect to the variable τ_k , where $k=1,2,3$:

$$\frac{\partial F}{\partial \tau_k} = 2 \sum_{i=1}^n (f_{mi} - f_{ki}) \left[B w_k \frac{t_i}{\tau_k^2} e^{-t_i/\tau_k} \right]. \quad (10)$$

The eight nonlinear equation involves eight unknown parameters. These parameters give to the approximation-function unknown values. The nonlinear equation systems in reduced form is the following:

$$\sum_{i=1}^n \left[A + B \left(w_1 e^{-\frac{t_i}{\tau_1}} + w_2 e^{-\frac{t_i}{\tau_2}} + w_3 e^{-\frac{t_i}{\tau_3}} \right) - f_{mi} \right] = 0. \quad (11)$$

$$\sum_{i=1}^n \left[A + B \left(w_1 e^{-\frac{t_i}{\tau_1}} + w_2 e^{-\frac{t_i}{\tau_2}} + w_3 e^{-\frac{t_i}{\tau_3}} \right) - f_{mi} \right] \left[w_1 e^{-\frac{t_i}{\tau_1}} + w_2 e^{-\frac{t_i}{\tau_2}} + w_3 e^{-\frac{t_i}{\tau_3}} \right] = 0. \quad (12)$$

$$\sum_{i=1}^n \left[A + B \left(w_1 e^{-\frac{t_i}{\tau_1}} + w_2 e^{-\frac{t_i}{\tau_2}} + w_3 e^{-\frac{t_i}{\tau_3}} \right) - f_{mi} \right] \left[B e^{-\frac{t_i}{\tau_1}} \right] = 0. \quad (13)$$

$$\sum_{i=1}^n \left[A + B \left(w_1 e^{-\frac{t_i}{\tau_1}} + w_2 e^{-\frac{t_i}{\tau_2}} + w_3 e^{-\frac{t_i}{\tau_3}} \right) - f_{mi} \right] \left[B e^{-\frac{t_i}{\tau_2}} \right] = 0. \quad (14)$$

$$\sum_{i=1}^n \left[A + B \left(w_1 e^{-\frac{t_i}{\tau_1}} + w_2 e^{-\frac{t_i}{\tau_2}} + w_3 e^{-\frac{t_i}{\tau_3}} \right) - f_{mi} \right] \left[B e^{-\frac{t_i}{\tau_3}} \right] = 0. \quad (15)$$

$$\sum_{i=1}^n \left[A + B \left(w_1 e^{-\frac{t_i}{\tau_1}} + w_2 e^{-\frac{t_i}{\tau_2}} + w_3 e^{-\frac{t_i}{\tau_3}} \right) - f_{mi} \right] \left[B w_1 \frac{t_i}{\tau_1^2} \right] = 0. \quad (16)$$

$$\sum_{i=1}^n \left[A + B \left(w_1 e^{-\frac{t_i}{\tau_1}} + w_2 e^{-\frac{t_i}{\tau_2}} + w_3 e^{-\frac{t_i}{\tau_3}} \right) - f_{mi} \right] \left[B w_2 \frac{t_i}{\tau_2^2} \right] = 0. \quad (17)$$

$$\sum_{i=1}^n \left[A + B \left(w_1 e^{-\frac{t_i}{\tau_1}} + w_2 e^{-\frac{t_i}{\tau_2}} + w_3 e^{-\frac{t_i}{\tau_3}} \right) - f_{mi} \right] \left[B w_3 \frac{t_i}{\tau_3^2} \right] = 0. \quad (18)$$

If this equation system is solved, we get the approximation-functions' parameters. During this minimization method, the following equations should be satisfied:

$$\sum_{j=1}^k w_k - 1 = 0 \rightarrow h(X) = 0, \quad (19)$$

$$\begin{bmatrix} -A \\ -B \\ -w_1 \\ -w_2 \\ -w_3 \\ \tau_1 \\ \tau_2 \\ \tau_3 \end{bmatrix} \leq 0 \rightarrow g(X) \leq 0. \quad (20)$$

The following constrained-extremum problem should be solved in order to simplify:

$$\begin{aligned} F(X) &\rightarrow \min, \\ h(X) &= 0, \\ g(X) &\leq 0. \end{aligned} \quad (21)$$

Relevant mathematical literature offers a lot of methods to solve (21). A penalty-function technique [3] is used to solve the problem. The following penalty function is used in the procedure:

$$\Theta(X, \sigma) = F(X) + \sigma \sum_{q=1}^r h_q^2(X) + \sigma \sum_{y=1}^c (\max(g_y(X), 0))^2. \quad (22)$$

The constrained-extremum problem (21) can be converted to an unconditional extremum problem with the help of the penalty function. The *Nelder-Mead* procedure, which is implemented in *MATLAB*, is used to solve the problem. For the σ sequence: $\sigma_k = 10^{k-1}$.

Figure 4 shows one of the approximated results.

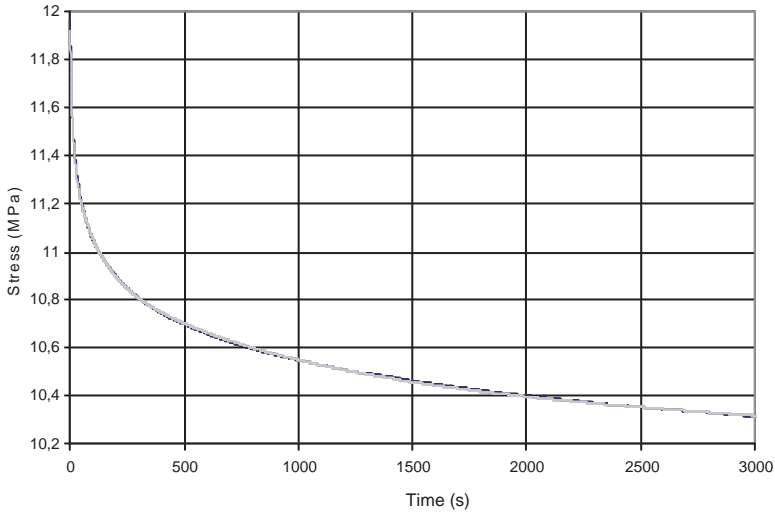


Figure 4. The measured and calculated stress

Measurements are made in different maximal gasket stress states. Summary of the approximation results are shown in the tables.

Results for 3 MPa gasket loading:

| No. | A | B | w_1 | w_1 | w_1 | τ_1 | τ_1 | τ_1 | A/σ_{max} |
|-----|------|------|-------|-------|-------|----------|----------|----------|------------------|
| 1 | 2.03 | 0.58 | 0.37 | 0.28 | 0.35 | 19.9 | 556 | 7454 | 0.77 |
| 2 | 1.94 | 0.49 | 0.35 | 0.27 | 0.38 | 40.1 | 634 | 7388 | 0.77 |
| 3 | 1.96 | 0.57 | 0.3 | 0.33 | 0.37 | 37 | 408 | 3765 | 0.74 |

Results for 6 MPa gasket loading:

| No. | A | B | w_1 | w_1 | w_1 | τ_1 | τ_1 | τ_1 | A/σ_{max} |
|-----|------|------|-------|-------|-------|----------|----------|----------|------------------|
| 1 | 4.96 | 1.62 | 0.35 | 0.27 | 0.38 | 72.4 | 918 | 11359 | 0.72 |
| 2 | 5.17 | 1.64 | 0.35 | 0.29 | 0.36 | 41.7 | 740 | 9902 | 0.72 |

Results for 13 MPa gasket loading:

| No. | A | B | w_1 | w_1 | w_1 | τ_1 | τ_1 | τ_1 | A/σ_{max} |
|-----|-------|------|-------|-------|-------|----------|----------|----------|------------------|
| 1 | 11.36 | 2.34 | 0.41 | 0.26 | 0.33 | 43.9 | 717.5 | 8571 | 0.79 |
| 2 | 11.62 | 2.49 | 0.42 | 0.25 | 0.32 | 45.3 | 907 | 11042 | 0.79 |
| 3 | 10.7 | 2.31 | 0.41 | 0.27 | 0.33 | 64.3 | 930.3 | 9836 | 0.79 |
| 4 | 11.12 | 2.47 | 0.38 | 0.26 | 0.36 | 47.5 | 736.5 | 9137.8 | 0.78 |

In the tables the last columns show that how many percent the maximal gasket stress decreased after the relaxation process. In the case of the worst (often in engineering) the residual stress is 70 % of the maximal gasket stress. If this value does not reach the minimal stress of the gasket, leaking may happen.

5. CONCLUSION

The presented calculation and measuring method is suitable to describe the viscoelastic type gasket time-stress function and determine the residual gasket stress on account of the stress relaxation process. In the future the effects of the re-loading for the relaxation properties will be investigated.

REFERENCES

1. G. SZEPESI and M. ORTUTAY: *Mathematical model of gas leaking*. GÉP, **10-11**, (2004), 126-131.
2. K.D. PAPOULIA, V.P. PANOSKALTSIS; and I. KOROVAJCHUK: A class of models of 3D finite viscoelasticity *School of Civil and Environmental Engineering, Cornell University, Ithaca, USA*.
3. A. GALÁNTAI and A. JENEY: *Numerical Methods Miskolc, University Press, Miskolc, 1998*. (in Hungarian)
4. M.A. DEL NOBILE, S.CHILLO, A. MENTANA and A. BAIANO: Use of the generalized Maxwell model for describing the stress relaxation behavior of solid-like foods. *Journal of Food Engineering*, **78**, (2007), 978-983. (1998)
5. J. A. GONZÁLEZ and R. ABASCAL: Linear viscoelastic boundary element formulation for steady state moving loads *Engineering Analysis with Boundary Elements*, **28**(7) (2004), 815-823.

BOUNDARY CONTOUR METHOD FOR MIXED BOUNDARY VALUE PROBLEMS IN THE DUAL SYSTEM OF PLANE ELASTICITY

SÁNDOR SZIRBIK

Institute of Engineering Mechanics, University of Miskolc
H-3515 Miskolc, Miskolc–Egyetemváros, Hungary
Sandor.Szirbik@uni-miskolc.hu

[Received: November 24, 2014, Accepted: January 30, 2015]

Abstract. In this paper the boundary contour method in the dual system of plane elasticity is developed further by clarifying the issue of how to apply the method to mixed boundary value problems on simply and multiply connected regions. In contrast to [1], [2] in which the contour is divided into two arcs on which tractions and displacements are imposed, respectively, here we shall allow the contour to be divided into an even number of arcs (the number of arcs should be at least four) assuming that tractions and displacements are prescribed on the subsequent arcs. This means that the equations of the boundary contour method set up in [2] are not sufficient to solve these mixed boundary value problems since they do not involve the supplementary conditions of single valuedness which should be kept in order for obtaining correct solutions. This paper presents the supplementary conditions of single valuedness and shows how to add them to the solution algorithm. Numerical examples prove the efficiency of this technique.

Mathematical Subject Classification: 74G05, 34B05

Keywords: Boundary contour method, the dual system of plane elasticity, supplementary conditions

1. INTRODUCTION

The paper presents a procedure which makes possible the application of the boundary contour method in the dual system of the plane elasticity to a class of the mixed boundary value problems.

The first paper devoted to the boundary contour method (BCM) in the primal system of two-dimensional linear elasticity was published in 1994 by A. Nagarjan et al. [3]. By observing that the integrand vector of the boundary element integrals without body forces is demonstrably divergence free in the primal system of the two and three-dimensional elasticity theory, the authors of [3] came to the conclusion that the numerical solution of three-dimensional problems requires the calculation of line integrals instead of surface integrals [4], while for planar problems evaluation

of functions should be performed instead of calculating line integrals. The stress calculation established by this method is probably more accurate in many cases than that applied by the conventional boundary element method (BEM). This technique was developed further both for more 2D and for some 3D problems [5]. With this technique one can compute stresses and can solve shape optimization problems in two dimensions [6]. By using a hypersingular formulation, the accuracy of the stress components can be further increased at points on the contour [7].

The boundary integral equations of the direct method in the dual system of plane elasticity was formulated in [8] and [9]. In the dual system the first-order stress function and the rigid body rotation are the unknown functions, in contrast to the primal system of plane elasticity in which the fundamental variable is the displacement. The choice of first-order stress functions provides advantages in the stress computation and if the tractions are not continuous on the region's boundary. For multiply-connected regions or if there are two (or more) arcs subjected to tractions, supplementary conditions of single valuedness should be prescribed and satisfied – in this respect details are given in [10].

The boundary contour method in the dual system of plane elasticity is published in [1,2]. The divergence freedom in the dual system is based on the fact that the stress functions of order one and the rigid body rotation (the unknowns of problem) satisfy the field equations of plane elasticity. As a consequence of this condition, potential functions exist. Papers [1] and [2] publish the proof of the divergence freedom, present the appropriate potential functions assuming linear and quadratic approximations for the shape functions, and set up the discretized equations to prepare an algorithm for the numerical computations. Consequently, the greatest advantage of BCM in the dual system is that the computation of stresses on the boundary elements requires derivations only, that is, unlike conventional BEM, one can avoid the computation of singular integrals.

The present paper is organized into six sections. Section 2 is devoted to some preliminaries in which the direct method in the dual system of plane elasticity and the corresponding boundary conditions are shown assuming simple connected regions. In addition we have determined the corresponding shape functions in Section 3, provided that the approximation is quadratic. Section 4 deals with the issue of how to extend the dual boundary contour method for the class of boundary value problems in which the boundary is divided into even number of arcs (the number of arcs should be at least four) provided that displacements or tractions are prescribed on the subsequent arcs. We shall clarify that the integrand in the conditions of single valuedness is also divergence free in the dual system of plane elasticity and shall determine the corresponding shape functions assuming quadratic approximation. In addition we present the conditions of single valuedness in a form discretized appropriately for the algorithm of computations. Section 5 contains some simple numerical examples. The last section is the conclusion. Some earlier results which are utilized in the paper are gathered in the Appendix.

2. PRELIMINARIES

Throughout this paper x_ρ are rectangular Cartesian coordinates referred to an origin O . Greek subscripts are assumed to have the range (1, 2). In accordance with the notations introduced $\delta_{\rho\lambda}$ is the Kronecker symbol, ∂_ρ stands for the derivatives with respect to x_ρ and $\epsilon_{\rho\pi 3}$ is the permutation symbol.

Consider a simply connected inner region \mathcal{A}_i and its supplementary exterior region \mathcal{A}_e . The common contour \mathcal{L}_o of the regions can be divided into two parts denoted by \mathcal{L}_t and \mathcal{L}_u . We shall assume that $[\mathcal{L}_t] \{\mathcal{L}_u\}$ is the union of those arcs on which [stress functions (arcs subjected to tractions)] {strain boundary conditions (derivatives of displacements with respect to the arc coordinate)} are imposed. If the number of arcs on the boundary is four they are denoted by \mathcal{L}_{t1} , \mathcal{L}_{t3} and \mathcal{L}_{u2} , \mathcal{L}_{u4} , respectively.

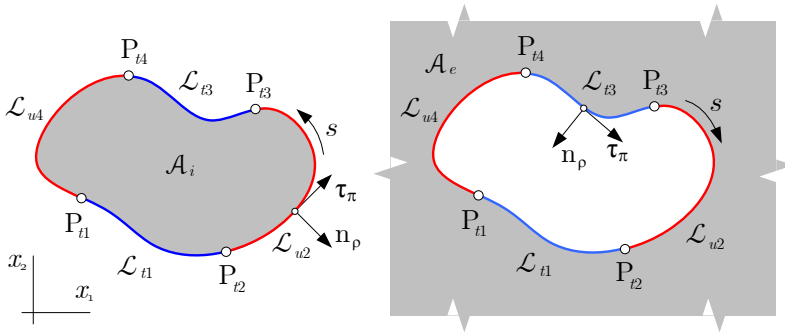


Figure 1. The inner region \mathcal{A}_i and the exterior region \mathcal{A}_e

Let Q and M be two points in the region \mathcal{A}_i or \mathcal{A}_e (the source point and the point of effect). We shall assume temporarily that the point Q is fixed.

The integral equation (the second dual Somigliana formula) to be solved is of the form:

$$c_{\kappa\lambda}(Q)u_\lambda(Q) = \tilde{u}_\kappa(Q) + \oint_{\mathcal{L}_o} \mathfrak{U}_{\kappa\lambda}(M, Q)t_\lambda(M) ds - \oint_{\mathcal{L}_o} \mathfrak{T}_{\kappa\lambda}(M, Q)u_\lambda(M) ds$$

$$Q, M \in \mathcal{L}_o, \quad (2.1)$$

where $u_\lambda(Q)$ is the stress function vector, $t_\lambda(M)$ stands for the derivative $-du_\lambda/ds$ (u_λ denotes the displacements, s is the arc coordinate on the contour \mathcal{L}_o), the points Q and M are taken on the contour \mathcal{L}_o , $\tilde{u}_\kappa(Q)$ is the stress function vector that gives a constant stress state at infinity, $\mathfrak{U}_{\kappa\lambda}(M, Q)$ and $\mathfrak{T}_{\kappa\lambda}(M, Q)$ are the fundamental solutions of order one and two – see Appendix A and [9] for details – and $c_{\kappa\lambda}(Q) = \delta_{\kappa\lambda}/2$ if the contour is smooth at Q , otherwise it depends on the angle formed by the tangents to the contour at Q . The above integral equation is that of the direct method in the dual system of elasticity with unknowns $u_\lambda(M)$ on \mathcal{L}_u and $t_\lambda(M)$ on \mathcal{L}_t . We remark that the two line integrals in (2.1) should be taken in principal value.

As the distance between the points Q and M tends to zero, weak (logarithmic) and strong singularity appear in the integrands of formula (2.1). We can avoid computation of strongly singular integrals if we assume that $\mathbf{u}_\lambda(Q) = \mathbf{u}_\lambda(M) = \text{constant}$ on the whole boundary. Under this condition $\mathbf{t}_\lambda(M) = 0$. In other words there are no stresses due to constant stress functions. On the basis of all that has been said equation (2.1) yields

$$c_{\kappa\lambda}(Q)\mathbf{u}_\lambda(Q) = \oint_{\mathcal{L}_o} \mathfrak{T}_{\kappa\lambda}(M, Q)\mathbf{u}_\lambda(Q)ds \quad Q, M \in \mathcal{L}_o. \quad (2.2)$$

Subtracting equation (2.2) from (2.1), we obtain the regularized form

$$0 = \tilde{\mathbf{u}}_\kappa(Q) + \underbrace{\oint_{\mathcal{L}_o} \{\mathfrak{U}_{\kappa\lambda}(M, Q)\mathbf{t}_\lambda(M) - \mathfrak{T}_{\kappa\lambda}(M, Q)[\mathbf{u}_\lambda(M) - \mathbf{u}_\lambda(Q)]\} ds}_{I_\kappa(Q)} \quad Q, M \in \mathcal{L}_o. \quad (2.3)$$

In this way we have eliminated the tensor $c_{\kappa\lambda}(Q)$ and the strong singularity from equation (2.1).

We have proved [1] that the integrand in formula (2.3) is divergence free. Consequently there exists a potential function $\phi_\kappa(M, Q)$. After factoring out the outward normal $n_\rho(M)$ from the integrand on the right-hand side in (2.3), the coefficient of $n_\rho(M)$ is denoted, for brevity, by $P_{\kappa\rho}(M, Q)$. Let M_1 and M_3 be two points on the contour for which $s_1 < s_3$. Taking now the line integral between the points M_1 and M_3 and making use of the above results we have

$$\int_{M_1}^{M_3} P_{\kappa\rho}(M, Q)n_\rho(M) ds = \phi_\kappa(M_3, Q) - \phi_\kappa(M_1, Q). \quad (2.4)$$

Assume that the contour \mathcal{L}_o is divided into n_{be} boundary elements. We regard the points M_1 and M_3 if they were the two extremities of an element on the boundary. Then integrating element by element we get

$$I_\kappa(Q) = \sum_{e=1}^{n_{be}} [\phi_\kappa^e(M_3, Q) - \phi_\kappa^e(M_1, Q)], \quad (2.5)$$

where the superscript e shows that ϕ_κ is taken on the e -th element.

If the region under consideration is the exterior one \mathcal{A}_e , the regularized integral equation (2.3) assumes the form

$$0 = \tilde{\mathbf{u}}_\kappa(Q) + I_\kappa(Q). \quad (2.6)$$

The results considered above make it possible to establish the boundary contour method in the dual system of plane elasticity by using linear and quadratic approximations [1, 2].

Equation (2.3) should be associated with appropriate boundary conditions. One can readily check that the stress function vector (the dual displacement vector) on

the arcs \mathcal{L}_{ti} is of the form

$$\hat{\mathbf{u}}_\rho(s) = \int_{P_{ti}}^s \hat{t}_\rho(\sigma) d\sigma \quad s \in \mathcal{L}_{ti} \quad i = 1, 3, \quad (2.7)$$

where a hat on the letters denotes the values prescribed. Consequently, equation

$$\mathbf{u}_\rho(s) = \hat{\mathbf{u}}_\rho(s) + C_\rho^{(ti)} \quad s \in \mathcal{L}_{ti} \quad i = 1, 3 \quad (2.8)$$

is equivalent to the traction boundary condition. Observe that the quantities $C_\rho^{(ti)}$ in this equation are undetermined constants of integration.

The strain boundary conditions on the arcs of \mathcal{L}_{ui} have the following form:

$$\frac{d\hat{u}_\lambda}{ds} = n_\rho[\epsilon_{\rho\pi 3}e_{\pi\lambda} - \delta_{\rho\lambda}\varphi_3] \quad s \in \mathcal{L}_{ui} \quad i = 2, 4, \quad (2.9)$$

where $\hat{u}_\lambda(s)$ is the displacement vector prescribed on \mathcal{L}_{ui} , the in-plane components of strain are denoted $e_{\kappa\lambda}$ and φ_3 stands for the rigid-body rotation.

If tractions (stress functions) are imposed on the whole contour \mathcal{L}_o ($\mathcal{L}_t \equiv \mathcal{L}_o$) the compatibility condition in the large

$$\int_{\mathcal{L}_o} n_\rho[\epsilon_{\rho\pi 3}e_{\pi\lambda} - \delta_{\rho\lambda}\varphi_3] ds = 0 \quad (2.10)$$

should also be satisfied. If tractions (stress functions) are imposed only on the arcs \mathcal{L}_{t1} , \mathcal{L}_{t3} of the contour \mathcal{L}_o , the supplementary conditions of single valuedness to be satisfied assume the form

$$\int_{\mathcal{L}_{ti}} n_\rho[\epsilon_{\rho\pi 3}e_{\pi\lambda} - \delta_{\rho\lambda}\varphi_3] ds - \hat{u}_\lambda|_{P_{ti}}^{P_{t,i+1}} = 0 \quad i = 1, 3, \quad (2.11)$$

where the extremities of the arc \mathcal{L}_{ti} are denoted by P_{ti} and $P_{t,i+1}$, respectively.

If the compatibility field equations

$$\epsilon_{\kappa\rho 3}e_{\lambda\kappa}\partial_\rho + \varphi_3\partial_\lambda = \epsilon_{\kappa\rho 3}(e_{\lambda\kappa} - \epsilon_{\lambda\kappa 3}\varphi_3)\partial_\rho = 0 \quad (2.12)$$

are fulfilled then the supplementary compatibility conditions (2.11) are not independent – one can be omitted [11].

In this way we have as many independent conditions of single valuedness (2.11) as there are undetermined integration constants $C_\rho^{(ti)}$ in the traction boundary condition (2.8). We can also set two constants (one vector $C_\rho^{(ti)}$) to zero since no stresses belong to constant stress functions – see [10, 11] for details. Papers [1, 2] deal with simply connected regions assuming that the contour is divided into two arcs: displacements are prescribed in one arc and tractions on the other. For this reason there is no need to imply the supplementary conditions of single valuedness into the model. If there are, however, more than two arcs subjected to tractions, we have no choice but to involve the supplementary conditions of single valuedness in the equations system to make it determined.

3. SHAPE AND POTENTIAL FUNCTIONS

Assume that the contour \mathcal{L}_o is divided into n_{be} boundary elements and a boundary element e has five nodal points. The first, third, and fifth nodal points are denoted by M_1 , M_2 and M_3 the second and fourth by K_1 and K_2 . Over the element and its neighborhood we shall approximate the fundamental variables \mathbf{u}_λ and φ_3 . Observe that, according to the strain boundary conditions (2.9), the displacement derivative $\mathbf{t}_\lambda(M)$ in equation (2.3) requires the knowledge of the rotation φ . In order to obtain appropriate approximations, the vector of the fundamental variables $[\mathbf{u}_i]^T = [\mathbf{u}_1 \mid \mathbf{u}_2 \mid \varphi_3]$ should satisfy the basic equation (see equation (3.3) in [9] for details). We have selected the approximation

$$\begin{bmatrix} \mathbf{u}_1 \\ \mathbf{u}_2 \\ -\varphi_3 \end{bmatrix}^e = \begin{bmatrix} a_1^e + a_2^e x_1 + a_3^e x_2 - 2a_7^e x_1 x_2 + a_8^e x_1^2 + a_9^e x_2^2 \\ a_4^e + a_5^e x_1 - a_2^e x_2 + a_7^e x_2^2 - 2a_8^e x_1 x_2 + a_{10}^e x_1^2 \\ a_6^e + K a_7^e x_2 + K a_8^e x_1 + K a_9^e x_1 + K a_{10}^e x_2 \end{bmatrix}, \quad (3.1)$$

where $K = (1 - \nu) / \mu$. This approximation satisfies the basic equation. The constants

$$[\mathbf{a}^e]^T = [a_1^e \quad a_2^e \quad a_3^e \quad a_4^e \quad a_5^e \quad a_6^e \quad a_7^e \quad a_8^e \quad a_9^e \quad a_{10}^e] \quad (3.2)$$

in (3.2) are related to the ten physical quantities

$$[\mathbf{p}^e]^T = [\mathbf{u}_1^{M_1} \mid \mathbf{u}_2^{M_1} \mid \mathbf{t}_1^{K_1} \mid \mathbf{t}_2^{K_1} \mid \mathbf{u}_1^{M_2} \mid \mathbf{u}_2^{M_2} \mid \mathbf{t}_1^{K_2} \mid \mathbf{t}_2^{K_2} \mid \mathbf{u}_1^{M_3} \mid \mathbf{u}_2^{M_3}] \quad (3.3)$$

taken on the element e via the equation

$$\underbrace{\mathbf{p}^e}_{(10 \times 1)} = \underbrace{\mathbf{T}^e}_{(10 \times 10)} \underbrace{\mathbf{a}^e}_{(10 \times 1)}, \quad (3.4)$$

where the transformation matrix \mathbf{T}^e – see Appendix B.2 in [12] for details – depends only on the nodal coordinates and the outward unit normals at K_1 and K_2 . It can be proved that transformation (3.4) is one to one if the nodal points are different.

A new local coordinate system (η_1, η_2) centered at the point M_1 is introduced and its axes (η_1, η_2) are parallel to the global ones. If we approximate the vector \mathbf{u}_k in equation (3.1) in the local coordinate system (η_1, η_2) by quadratic functions over the elements we get the following vector:

$$\begin{bmatrix} \mathbf{u}_1 \\ \mathbf{u}_2 \\ -\varphi_3 \end{bmatrix}^e = \begin{bmatrix} \hat{a}_1^e + \hat{a}_2^e \eta_1 + \hat{a}_3^e \eta_2 - 2a_7^e \eta_1 \eta_2 + a_8^e \eta_1^2 + a_9^e \eta_2^2 \\ \hat{a}_4^e + \hat{a}_5^e \eta_1 - \hat{a}_2^e \eta_2 + a_7^e \eta_2^2 - 2a_8^e \eta_1 \eta_2 + a_{10}^e \eta_1^2 \\ \hat{a}_6^e + K a_7^e \eta_2 + K a_8^e \eta_1 + K a_9^e \eta_1 + K a_{10}^e \eta_2 \end{bmatrix}, \quad (3.5)$$

in which

$$\hat{a}_1^e = a_1^e + a_2^e x_1 + a_3^e x_2 - 2a_7^e x_1 x_2 + a_8^e x_1^2 + a_9^e x_2^2, \quad \hat{a}_2^e = a_2^e - 2a_7^e x_2 + 2a_8^e x_1, \quad (3.6a)$$

$$\hat{a}_3^e = a_3^e - 2a_7^e x_1 + 2a_9^e x_2, \quad \hat{a}_4^e = a_4^e + a_5^e x_1 - a_2^e x_2 + a_7^e x_2^2 - 2a_8^e x_1 x_2 + a_{10}^e x_1^2, \quad (3.6b)$$

$$\hat{a}_5^e = a_5^e - 2a_8^e x_2 + 2a_{10}^e x_1, \quad \hat{a}_6^e = a_6^e + K a_7^e x_2 + K a_8^e x_1 + K a_9^e x_1 + K a_{10}^e x_2. \quad (3.6c)$$

By

$$[\hat{\mathbf{a}}^e]^T = [\hat{a}_1^e \quad \hat{a}_2^e \quad \hat{a}_3^e \quad \hat{a}_4^e \quad \hat{a}_5^e \quad \hat{a}_6^e \quad a_7^e \quad a_8^e \quad a_9^e \quad a_{10}^e] \quad (3.7)$$

we denote the vector of constants in the local system. For the relation between \mathbf{a} and $\hat{\mathbf{a}}$ one can write

$$\underbrace{\hat{\mathbf{a}}^e}_{(10 \times 1)} = \underbrace{\mathbf{B}^{M_1}}_{(10 \times 10)} \underbrace{\mathbf{a}^e}_{(10 \times 1)}, \quad (3.8)$$

where the transformation matrix \mathbf{B}^{M_1} depends only on the coordinates x_1 and x_2 of the point M_1 – see [1,2] for details. Consequently we obtain a relation of the form

$$\underbrace{\hat{\mathbf{a}}^e}_{(10 \times 1)} = \underbrace{\mathbf{B}^{M_1}}_{(10 \times 10)} \underbrace{(\mathbf{T}^e)^{-1}}_{(10 \times 10)} \underbrace{\mathbf{p}^e}_{(10 \times 1)} \quad (3.9)$$

which relates the physical quantities to the weight parameters.

After approximating vector \mathbf{u}_k in the local coordinate system (η_1, η_2) over an element we arrive at a linear combination of the linearly independent shape vectors

$$\begin{aligned} [{}^1\mathbf{u}_k]^T &= [1 \ 0 \ 0], & [{}^6\mathbf{u}_k]^T &= [0 \ 0 \ 1], \\ [{}^2\mathbf{u}_k]^T &= [\eta_1 \ -\eta_2 \ 0], & [{}^7\mathbf{u}_k]^T &= [-2\eta_1\eta_2 \ \eta_2^2 \ K\eta_2], \\ [{}^3\mathbf{u}_k]^T &= [\eta_2 \ 0 \ 0], & [{}^8\mathbf{u}_k]^T &= [\eta_1^2 \ -2\eta_1\eta_2 \ K\eta_1], \\ [{}^4\mathbf{u}_k]^T &= [0 \ 1 \ 0], & [{}^9\mathbf{u}_k]^T &= [\eta_2^2 \ 0 \ K\eta_1], \\ [{}^5\mathbf{u}_k]^T &= [0 \ \eta_1 \ 0], & [{}^{10}\mathbf{u}_k]^T &= [0 \ \eta_1^2 \ K\eta_2], \end{aligned} \quad (3.10)$$

which satisfies the basic equation in [9]. Later on, it will be advantageous to choose always the current source point Q for the center of the local coordinate system.

By substituting these shape vectors into

$${}^i\phi_\kappa(\eta_1, \eta_2) = \int \epsilon_{\rho\pi 3} \{ \mathfrak{U}_{\kappa\lambda}(\eta_1, \eta_2) {}^i\mathfrak{t}_{\lambda\rho}(\eta_1, \eta_2) - \mathfrak{T}_{\kappa\lambda\rho}(\eta_1, \eta_2) {}^i\mathbf{u}_\lambda(\eta_1, \eta_2) \} d\eta_\pi \quad i = 1, \dots, 10 \quad (3.11)$$

and performing the integrals for each shape function one can set up the corresponding potential functions ${}^i\phi_\kappa$ in a closed form. The matrix $\mathfrak{T}_{\kappa\lambda\rho}(\eta_1, \eta_2)$ in equation (3.11) is given in Appendix A. The potential functions ${}^i\phi_\kappa$ which belong to the regularized dual Somigliana formula (2.3) are also presented in Appendix B.

Fulfillment of the boundary element equations is enforced only at the points M_1 , M_2 and M_3 of the elements. Assume that the collocation point Q coincides with the first nodal point of the h -th element. Further for the stress functions at this point we introduce the notations $\mathbf{u}_1(Q) = \hat{a}_1^h$ and $\mathbf{u}_2(Q) = \hat{a}_4^h$ in the local coordinate system. With these notations, we can write

$$\underbrace{[\mathbf{u}^e(M)]}_{(2 \times 1)} - \underbrace{[\mathbf{u}^h(Q_j)]}_{(2 \times 10)} = \underbrace{\mathbf{U}^e(\eta_1, \eta_2)}_{(2 \times 10)} \underbrace{\tilde{\mathbf{a}}^e}_{(10 \times 1)}, \quad (3.12)$$

where $[\mathbf{u}^e(M)]^T = [\mathbf{u}_1^e(M) \mid \mathbf{u}_2^e(M)]$ is the vector of stress functions at the point M of the e -th element and the columns of the matrix $\mathbf{U}^e(\eta_1, \eta_2)$ are constituted by

the vectors ${}^i\mathbf{u}_\kappa$ ($i = 1, \dots, 10$). In this way the vector of constants $\tilde{\mathbf{a}}^e$ can now be rewritten as:

$$\begin{aligned} [\tilde{\mathbf{a}}^e]^T &= [\beta_1^e \quad \hat{a}_2^e \quad \hat{a}_3^e \quad \beta_4^e \quad \hat{a}_5^e \quad \hat{a}_6^e \quad a_7^e \quad a_8^e \quad a_9^e \quad a_{10}^e] , \\ \beta_1^e &= \hat{a}_1^e - \hat{a}_1^h, \quad \beta_4^e = \hat{a}_4^e - \hat{a}_4^h. \end{aligned} \quad (3.13)$$

The potential functions ϕ_{11} and ϕ_{24} have singularity if the point of effect M approaches the source point. In this case $\hat{a}_1^e = \hat{a}_1^j$ and $\hat{a}_4^e = \hat{a}_4^j$, therefore $\beta_1^e = \beta_4^e = 0$, and so the evaluation of these singular potential functions can be avoided. Fulfillment of the regularized form of the boundary element equation (2.3) is enforced only at the points M_1 , M_2 and M_3 of elements. Turning to global numbering we denote these points by Q_j where $j = 1, \dots, 2n_{be}$. Hereafter, the point Q_j is called nodal point. As is shown in [1, 2] the regularized dual Somigliana formula (2.3) can be rewritten into the discretized form

$$\sum_{e=1}^{n_{be}} \underbrace{\Phi^{je} \mathbf{B}^j (\mathbf{T}^e)^{-1}}_{\mathbf{N}^{je}} \mathbf{p}^e = \tilde{\mathbf{u}}(\infty) \quad j = 1, \dots, 2n_{be} , \quad (3.14)$$

where Φ^{je} is a matrix with size (2×10) that are formed by the differences of the potential functions ${}^i\phi_\kappa$ between the end points of the e -th boundary element, the transformation matrix \mathbf{T}^e – in accordance with all that has been said so far – depends only on the nodal coordinates and the outward unit normal at K_j and the transformation matrix \mathbf{B}^j depends only on the global coordinates Q_j . If the region under consideration is an exterior one, the right side is not zero but is equal to the stress function representation $\tilde{\mathbf{u}}(\infty)$ of the stresses at infinity. If the contour is divided into only two arcs on which tractions and displacements are imposed, then the equation system (3.14) is solvable, otherwise too many undetermined constants of integration remain in (2.8).

4. COMPATIBILITY CONDITIONS IN DISCRETIZED FORM

This means that the equations of the boundary contour method in the dual system [1, 2] are to be supplemented with further conditions of single valuedness which are needed for determining the integration constants $C_\rho^{(ti)}$. However, as has already been mentioned, one supplementary condition of single valuedness should not be fulfilled since two constants (one of the vectors $C_\rho^{(ti)}$) can be set to zero. In this section we shall show how to add the necessary supplementary conditions of single valuedness to the solution algorithm.

One can prove with ease that the integral in the compatibility conditions (2.10, 2.11) is divergence free if the stress function vector $\mathbf{u}_\lambda(M)$ and the corresponding rotation $\varphi_3(M)$ fulfill the field equations. This means that these quantities are derived from the fundamental solution. It is also clear that the tensor $e_{\kappa\pi\lambda}(M, Q)$ – which is in fact a strain tensor – is obtained from the fundamental solution of order one via the dual kinematic equation

$$t_{\kappa\lambda} = \epsilon_{\kappa\rho 3} \mathbf{u}_\lambda \partial_\rho + \overset{o}{t}_{\kappa\lambda} \quad (4.1)$$

(the particular solution, denoted by $t_{\kappa\lambda}^o$, is equal to zero if there are no body forces.) and Hooke's law

$$e_{\kappa\lambda} = \frac{1}{2\mu} (t_{\kappa\lambda} - \nu t_{\psi\psi} \delta_{\kappa\lambda}) \quad (4.2)$$

(μ is the shear modulus of elasticity, ν is the Poisson number), in a such way that we substitute the tensor $\mathfrak{U}_{\kappa\lambda}(M, Q)$ for the vector $\mathbf{u}_\lambda(M)$ and the corresponding rotation $\varphi_3(M)$ for $\mathfrak{U}_{\kappa 3}(M, Q)$ as follows:

$$e_{\kappa\pi\lambda}(M, Q) = \frac{1}{2\mu} (\epsilon_{\pi\rho 3} \mathfrak{U}_{\kappa\lambda} \partial_\rho - \nu \epsilon_{\psi\rho 3} \mathfrak{U}_{\kappa\psi} \partial_\rho \delta_{\pi\lambda}) . \quad (4.3)$$

After substitution of equation (4.3) in the compatibility condition in the large (2.10), we get the following line integral:

$$\int_{\mathcal{L}_o} n_\rho(M) [\epsilon_{\rho\pi 3} e_{\kappa\pi\lambda}(M, Q) - \delta_{\rho\lambda} \mathfrak{U}_{\kappa 3}(M, Q)] ds = 0 \quad Q, M \in \mathcal{L}_o . \quad (4.4)$$

If we apply Gauss's theorem, the integral on the left hand side can be transformed into an integral taken over \mathcal{A}_i :

$$\int_{\mathcal{A}_i}^M \partial_\rho [\epsilon_{\rho\pi 3} e_{\kappa\pi\lambda}(M, Q) - \delta_{\rho\lambda} \mathfrak{U}_{\kappa 3}(M, Q)] dA = 0 . \quad (4.5)$$

Observe that the term in square brackets in equation (4.5) is nothing but the dual balance equation since the quantities are derived from the fundamental solution $\mathfrak{U}_{\kappa\lambda}(M, Q)$. Consequently, the derivative of the expression with respect to η_ρ is identically equal to zero. By using this condition, we arrive at the potential functions

$${}^i\psi_\kappa(\eta_1, \eta_2) = \int \epsilon_{\rho\pi 3} [\epsilon_{\rho\lambda 3} {}^i e_{\lambda\kappa}(\eta_1, \eta_2) - \delta_{\rho\kappa} {}^i \varphi_3(\eta_1, \eta_2)] d\eta_\pi , \quad (4.6)$$

which belong again to the weight parameters a_i . The corresponding potential functions ${}^i\psi_\kappa$ have been calculated by making use of equation (4.6) for each ${}^i e_{\lambda\kappa}$ and ${}^i \varphi_3$ – the former two quantities can be calculated from the vectors ${}^i \mathbf{u}_k$ ($i = 1, \dots, 10$). Hence we have set up the corresponding potential functions ${}^i\psi_\kappa$ in a closed form. The potential functions ${}^i\psi_\kappa$ are given by:

$$\begin{aligned} {}^1\psi_1 &= 0, & {}^1\psi_2 &= 0, & {}^6\psi_1 &= \eta_2, & {}^6\psi_2 &= -\eta_1, \\ {}^2\psi_1 &= -\frac{1}{2\mu} \eta_2, & {}^2\psi_2 &= -\frac{1}{2\mu} \eta_1, & {}^7\psi_1 &= \frac{2-\nu}{2\mu} \eta_2^2, & {}^7\psi_2 &= \frac{\nu}{\mu} \eta_1 \eta_2, \\ {}^3\psi_1 &= \frac{1}{2\mu} (1-\nu) \eta_1, & {}^3\psi_2 &= -\frac{\nu}{2\mu} \eta_2, & {}^8\psi_1 &= -\frac{\nu}{\mu} \eta_1 \eta_2, & {}^8\psi_2 &= -\frac{2-\nu}{2\mu} \eta_1^2, \\ {}^4\psi_1 &= 0, & {}^4\psi_2 &= 0, & {}^9\psi_1 &= \frac{1-\nu}{\mu} \eta_1 \eta_2, & {}^9\psi_2 &= -\frac{1-\nu}{2\mu} \eta_1^2, \\ {}^5\psi_1 &= \frac{\nu}{2\mu} \eta_1, & {}^5\psi_2 &= -\frac{1-\nu}{2\mu} \eta_2, & {}^{10}\psi_1 &= \frac{1-\nu}{2\mu} \eta_2^2, & {}^{10}\psi_2 &= -\frac{1-\nu}{\mu} \eta_1 \eta_2. \end{aligned}$$

With the knowledge of the functions ${}^i\psi_\kappa$ one can handle the line integrals in the supplementary condition of single valuedness in the same way as the other line integrals in the integral equation (2.1), i.e. by using potential functions. Let M_1 and M_3

be two points on the contour for which $s_1 < s_3$. Considering now the line integral between the points M_1 and M_3 and making use of the above results we have

$$\int_{M_1}^{M_3} n_\rho(M) [\epsilon_{\rho\lambda 3} e_{\lambda\kappa}(M, Q) - \delta_{\rho\kappa} u_3(M)] ds = \psi_\kappa(M_3, Q) - \psi_\kappa(M_1, Q) \quad M \in \mathcal{L}_{ti}. \quad (4.7)$$

The actual position of Q has no influence on the result of integral (4.7), however, it is advised to choose the position of Q so that it should be out of the arc \mathcal{L}_{ti} .

The number of arcs on which tractions are prescribed is denoted by n_t . It is clear from Figure 1 that now we have two arcs (denoted by \mathcal{L}_{t1} , \mathcal{L}_{t3}) with prescribed tractions. Hence $n_t = 2$. Here and in the sequel the extremities of arcs \mathcal{L}_{t1} , \mathcal{L}_{t3} are assumed to coincide with some nodal points on \mathcal{L}_o . The regularized form of the boundary conditions can be written on one of these two arcs as

$$\sum_{e \in \mathcal{L}_{ti}} \underbrace{\Psi^{2n_{be}+j,e} \mathbf{B}^{2n_{be}+j} (\mathbf{T}^e)^{-1}}_{\mathbf{M}^{2n_{be}+j,e}} \mathbf{p}^e = \hat{\mathbf{u}}^{2n_{be}+j} \quad j = 1, \dots, 2(n_t - 1), \quad (4.8)$$

where Ψ^{je} is a matrix with size (2×10) . The elements of this matrix are the differences of the potential functions ${}^i\psi_\kappa$ between the end points of the e -th boundary element, while $\hat{\mathbf{u}}^{2n_{be}+j}$ ($j = 1, 2$) denotes the difference of displacements at the extremities of the arc \mathcal{L}_{ti} :

$$\hat{\mathbf{u}}^{2n_{be}+j} = \begin{bmatrix} \hat{u}_1(P_{t,2i}) \\ \hat{u}_2(P_{t,2i}) \end{bmatrix} - \begin{bmatrix} \hat{u}_1(P_{t,2i-1}) \\ \hat{u}_2(P_{t,2i-1}) \end{bmatrix} \quad i = 1 \text{ or } 2. \quad (4.9)$$

Making use of equations (3.14) and (4.8) and exploiting that the stress functions are continuous at the extremities of the elements, one can construct an equation system. However, we eliminate the continuity of the stress functions at those points which coincide with some extremities of the arcs \mathcal{L}_{t1} , \mathcal{L}_{t3} . Accordingly, the corresponding columns in matrices \mathbf{N}^{je} and \mathbf{M}^{je} can be added to each other. The continuity conditions that the elements of the matrices \mathbf{p}^e should meet are also to be taken into account. Under these conditions, we obtain the equations

$$\mathbf{K} \mathbf{f} = \begin{bmatrix} \mathbf{0} \\ \hat{\mathbf{u}} \end{bmatrix} \quad \text{for the inner region and} \quad \mathbf{K} \mathbf{f} = \begin{bmatrix} \tilde{\mathbf{u}} \\ \hat{\mathbf{u}} \end{bmatrix} \quad \text{for the outer region.} \quad (4.10)$$

Here \mathbf{K} is a matrix with size $(4n_{be} + 2(n_t - 1)) \times (8n_{be} + 2(n_t - 1))$ and \mathbf{f} denotes the vector of physical quantities. The columns of the matrix \mathbf{K} that are multiplied by the prescribed quantities should be grouped on the right side of the equation in order to obtain the equation system to be solved. As the approximation we have chosen satisfies the basic equation in [9], the given displacement derivatives already determine the integration constants $C_\rho^{(ti)}$ in the traction boundary condition on each curve separately.

After solving the equations system (4.10), we have the nodal values of the unknown stress functions and the unknown displacement derivatives on the boundary curve, that is, every element of the vector \mathbf{p}^e is known. The first dual Somigliana formula

for the outer region to be solved is of the form:

$$\mathbf{u}_\kappa(Q) = \tilde{\mathbf{u}}_\kappa(Q) + \oint_{\mathcal{L}_o} \mathfrak{u}_{\kappa\lambda}(M, Q) \mathfrak{t}_\lambda(M) ds - \oint_{\mathcal{L}_o} \mathfrak{T}_{\kappa\lambda}(M, Q) \mathbf{u}_\lambda(M) ds \quad Q \in \mathcal{A}_e. \quad (4.11)$$

For an inner region, $\tilde{\mathbf{u}}_\kappa(Q)$ is zero in the previous equation. The formula (4.11) can be rewritten – in accordance with that has been seen earlier – into a discretized form with the notations introduced. In this way, one can compute the stress functions $\mathbf{u}_\lambda(Q)$ at an arbitrary point from the following equation:

$$\mathbf{u}(Q) = \tilde{\mathbf{u}}(\infty) + \sum_{e=1}^{n_{be}} \Phi^{Qe} \mathbf{B}^Q (\mathbf{T}^e)^{-1} \mathbf{p}^e, \quad (4.12)$$

where the transformation matrix \mathbf{B}^Q (see Appendix C for details) and Φ^{Qe} depend on the coordinates of the source point position. Derivatives of the stress functions follow from equation (4.12) taken at the source point Q . Hence

$$\frac{\partial}{\partial x_\kappa} \mathbf{u}(Q) = \frac{\partial}{\partial x_\kappa} \tilde{\mathbf{u}}(\infty) + \sum_{e=1}^{n_{be}} \left[\Phi^{Qe} \left(\frac{\partial}{\partial x_\kappa} \mathbf{B}^Q \right) - \left(\frac{\partial}{\partial \eta_\kappa} \Phi^{Qe} \right) \mathbf{B}^Q \right] (\mathbf{T}^e)^{-1} \mathbf{p}^e. \quad (4.13)$$

According to the dual kinematic equations (4.1) we can determine the stresses by using the following equations:

$$\begin{aligned} \sigma_{11}(Q) &= \sigma_{11}(\infty) + \left. \frac{\partial \mathbf{u}_1}{\partial x_2} \right|_Q, & \sigma_{22}(Q) &= \sigma_{22}(\infty) - \left. \frac{\partial \mathbf{u}_2}{\partial x_1} \right|_Q, \\ \tau_{12}(Q) &= \tau_{12}(\infty) - \left. \frac{\partial \mathbf{u}_2}{\partial x_2} \right|_Q = \tau_{21}(Q) = \tau_{21}(\infty) + \left. \frac{\partial \mathbf{u}_1}{\partial x_1} \right|_Q. \end{aligned} \quad (4.14)$$

5. NUMERICAL EXAMPLES

Problem 1. The first problem is a benchmark to test the discretized form of the supplementary conditions of single valuedness in the calculation algorithm. We consider a circular region with radius $R = 10$ mm. The material properties are $\mu = 8 \cdot 10^4$ MPa, $\nu = 0.3$. On the arcs AB ($\varphi \in [0, \pi/2]$) and CD ($\varphi \in [\pi, 1.5\pi]$) of the contour the normal stress is $\sigma_o = 100$ MPa and there is no shear stress. On the arcs BC ($\varphi \in [\pi/2, \pi]$) and DA ($\varphi \in [1.5\pi, 2\pi]$) of the contour

$$u_o = \frac{(1 - 2\nu)\sigma_o R}{2\mu}$$

is the radial displacement and there is no displacement in the circumferential direction – see Figure 2. The supplementary conditions of single valuedness are imposed on the

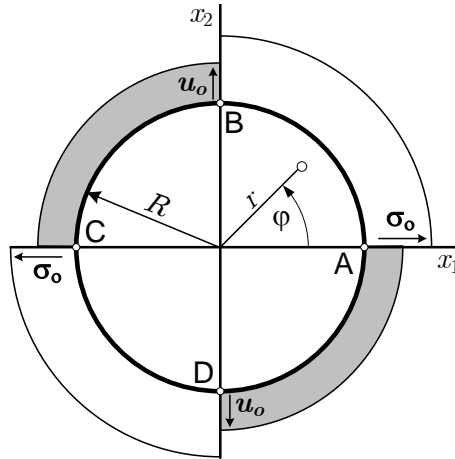


Figure 2. Circular region with two arcs subjected to tractions

arc CD and the difference between the displacements at the extremities of this arc is determined by the formula for the radial displacement. The exact solutions for this problem are given by the equations

$$\begin{aligned} u_1 &= \sigma_o r \sin \varphi, & u_2 &= -\sigma_o r \cos \varphi, \\ t_1 &= \frac{1-2\nu}{2\mu} \sigma_o \sin \varphi, & t_2 &= -\frac{1-2\nu}{2\mu} \sigma_o \cos \varphi, \end{aligned}$$

where r and φ are polar coordinates. One can check with ease that these solutions determine a homogeneous state of stress. At the internal points the exact solutions for the stresses are as follows: $\sigma_{11} = \sigma_{22} = \sigma_o = 100$ [MPa], $\tau_{12} = 0$. Table 1 below represents the numerical results obtained at various internal points.

Table 1: Solutions for stress components

| x_1 [mm] | x_2 [mm] | σ_{11} [MPa] | τ_{12} [MPa] | σ_{22} [MPa] |
|------------|------------|---------------------|-------------------|---------------------|
| -7.50 | 0.00 | 100.00 | 0.0000 | 100.00 |
| -2.50 | 0.00 | 100.00 | 0.0000 | 100.00 |
| 0.00 | 0.00 | 100.00 | 0.0000 | 100.00 |
| 5.00 | 7.50 | 99.999 | 0.0000 | 100.00 |
| 9.00 | 1.00 | 100.00 | 0.0000 | 100.00 |

Problem 2. We consider an outer region which includes two circular holes with radius $R = 10$ mm and a constant stress state $\sigma_{11}(\infty) = 100$ [MPa], $\tau_{12}(\infty) = \tau_{21}(\infty) = \sigma_{22}(\infty) = 0$ is prescribed at infinity. The material parameters are the same as those for the first problem.

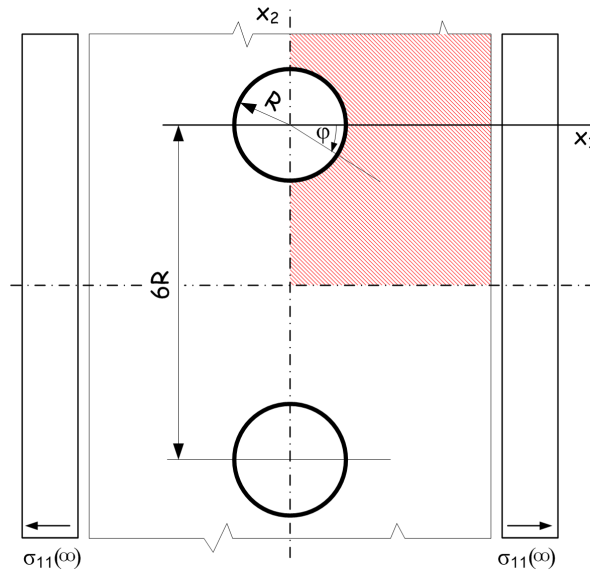


Figure 3. An outer region with two circular holes

In order to validate our numerical solutions for the stress distribution around the two circular holes, we have set up a finite element (FE) model utilizing the symmetry of the problem. The cross-hatched area in Figure 3 indicates the investigated area.

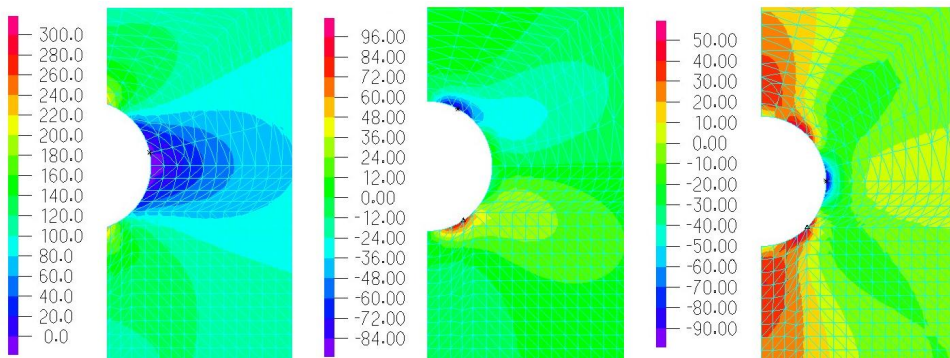


Figure 4. Normal stress σ_{11} , shear stress τ_{12} and normal stress σ_{22} distributions around the upper hole

The finite element analysis results of ADINA can be seen in Figure 4, where only the stress distributions around the upper circle are presented.

Table 2: Solutions for stress components along the axes x_1, x_2

| x_1 [mm] | x_2 [mm] | σ_{11} [MPa] | τ_{12} [MPa] | σ_{22} [MPa] |
|------------|------------|---------------------|-------------------|---------------------|
| 0.00 | 20.00 | 121.26 (122.87) | 0.00 (0.47) | 27.97 (30.03) |
| 0.00 | 15.00 | 150.31 (153.27) | 0.00 (0.16) | 36.53 (37.21) |
| 0.00 | 10.00 | 298.60 (303.20) | 0.00 (-1.57) | 0.63 (1.75) |
| 0.00 | -10.00 | 301.02 (302.43) | 0.00 (1.42) | 0.57 (-0,19) |
| 0.00 | -15.00 | 157.68 (154.15) | 0.00 (0.28) | 42.26 (39.06) |
| 0.00 | -20.00 | 127.17 (126.91) | 0.00 (0.10) | 36.76 (35.66) |
| 0.00 | -25.00 | 117.85 (117.46) | 0.00 (0.11) | 31.85 (29.36) |
| 0.00 | -30.00 | 115.55 (115.25) | 0.00 (0.15) | 30.23 (27.74) |
| 0.00 | -35.00 | 117.84 (117.46) | 0.00 (0.11) | 31.85 (29.36) |
| 0.00 | -40.00 | 127.16 (126.91) | 0.00 (0.10) | 36.76 (35.66) |
| 0.00 | -45.00 | 157.68 (154.15) | 0.00 (0.28) | 42.26 (39.06) |
| 0.00 | -50.00 | 300.91 (302.43) | 0.00 (1.42) | 0.55 (-0,19) |
| 10.00 | 0.00 | 0.58 (0.65) | 0.028 (-1.27) | -96.85 (-93.14) |
| 20.00 | 0.00 | 49.88 (48.04) | 3.32 (1.7) | 5.46 (5.16) |
| 50.00 | 0.00 | 92.92 (94.62) | 0.58 (0.73) | -0.099 (-0. 025) |
| 100.00 | 0.00 | 97.85 (97.77) | -0.66 (-0.84) | -0.87 (-0.84) |

The numerical results in Table 2 are in good agreement with those of the finite element analysis results which appear in round brackets.

6. CONCLUDING REMARKS

In contrast to the conventional boundary element method, there is a possibility for considering plane problems in a dual formulation. Then the equation system to be solved involves the representation of stresses in terms of stress functions of order one, Hooke's law and the compatibility equations. If the region is multiply connected and/or there is more than one arc on the contour with traction boundary conditions then the compatibility conditions are to be supplemented with further conditions of single valuedness. These are referred to as supplementary compatibility conditions (for single arcs) or compatibility conditions at large (for a whole contour). If the region under consideration is a simply connected one then the boundary element method as well as the boundary contour method have already been worked out in [1,2,9,13]. The present paper is concerned with the generalization of the boundary contour method for multiply-connected regions. For these regions the traction boundary conditions in terms of stress functions of order one contain undetermined constants of integration which can be determined if and only if the field equations are associated with the compatibility conditions at large and/or the supplementary compatibility conditions. In this way one can ensure that the boundary value is determinate. To achieve this goal, we also had to apply those mathematical parameters which are used in the derivation of the BCM equations when giving the compatibility conditions in a discretized form. Accordingly, the corresponding potential functions, which belong to the supplementary conditions of single valueness or the compatibility conditions

at large have been determined, provided that the approximation is quadratic. From these potential functions, we have established the discretized forms of the supplementary conditions of single valuedness on the arcs, which are subjected to tractions and the discretized forms of the compatibility condition at large. A program has been developed in Fortran 90 for the numerical investigations. We have found that the displacement derivatives could be replaced by the corresponding compatibility conditions on closed boundary curves. The examples shown represent the applicability of the algorithm to a simple and a bit more difficult problem.

Acknowledgements. The described work was carried out as part of the TÁMOP-4.2.1.B-10/2/KONV-2010-0001 project in the framework of the New Hungarian Development Plan. The realization of this project is supported by the European Union, co-financed by the European Social Fund.

REFERENCES

1. SZIRBIK, S.: Boundary contour method for plane problems in a dual formulation with linear elements. *Journal of Computational and Applied Mechanics*, **1**(2), (2000), 205–222.
2. SZEIDL, G. and SZIRBIK, S.: Boundary Contour Method for Plane Problems in a Dual Formulation with Quadratic Shape Functions, In: V. Kompis (ed) *Selected Topics in Boundary Integral Formulations for Solids and Fluids*, Internatiponal Centre for Mechanical Sciences, Volume 433, Springer, 2002, 209-232.
3. NAGARJAN, A., LUTZ, E. D., and MUKHERJEE, S.: A novel boundary element method for linear elasticity with no numerical integration for two dimensional and line integrals for three-dimensional problems. *Journal of Applied Mechanics*, **61**, (1994), 264–269.
4. NAGARJAN, A., LUTZ, E. D., and MUKHERJEE, S.: The boundary contour method for three-dimensional linear elasticity. *Journal of Applied Mechanics*, **63**, (1996), 278–286.
5. PHAN, A. V., MUKHERJEE, S., and MAYER, J. R. R.: The boundary contour method for two-dimensional linear elasticity with quadratic boundary elements. *Computational Mechanics*, **20**, (1997), 310–319.
6. PHAN, A. V., MUKHERJEE, S., and MAYER, J. R. R.: Stresses, stress sensitivities and shape optimization in two dimensional linear elasticity by the boundary contour method. *International Journal for Numerical Methods in Engineering*, **42**, (1998), 1391–1407.
7. PHAN, A. V., MUKHERJEE, S., and MAYER, J. R. R.: The hypersingular boundary contour method for two-dimensional linear elasticity. *Acta Mechanica*, **130**.
8. SZEIDL, G.: *Dual problems of continuum mechanics (derivation of defining equations, single valuedness of mixed boundary value problems, boundary element method for plane problems)*. Habilitation Booklets of the Miskolc University (in Hungarian), Faculty of Mechanical Engineering, University of Miskolc, Department of Mechanics, 1997.
9. SZEIDL, G.: Boundary integral equations for plane problems in terms of stress functions of order one. *Journal of Computational and Applied Mechanics*, **2**(2), (2001), 237–261.
10. SZEIDL, G.: On compatibility conditions for mixed boundary value problems. *Technische Mechanik*, **17**, (1997), 245–262.
11. SZEIDL, G.: *Problems of Continuum Mechanics in a Dual Formulation (Derivation of the defining equations, Single valudness of mixed boundary value problems, Boundary element*

- method for plane problems*). Thesis for the degree Doctor of Science awarded by the Hungarian Academy of Sciences (in Hungarian), 2004.
12. SZIRBIK, S.: *Boundary contour method for plane problems in the dual system of elasticity*. PhD dissertation (in Hungarian), Faculty of Mechanical Engineering, University of Miskolc, Department of Mechanics, 2003.
13. SZIRBIK, S.: Boundary contour method for plane problems with linear elements in dual system. In *microCAD-SYSTEM '2000 International Computer Science Conference, ME Miskolc*, 2000, pp. 157–162.

APPENDIX A.

A.1. The fundamental solutions of order one and two.

$$[\mathfrak{U}_{kl}(M, Q)] = \frac{\mu}{4\pi(1-\nu)} \begin{bmatrix} -2 \ln R - 3 - 2 \frac{r_2 r_2}{R^2} & 2 \frac{r_1 r_2}{R^2} & \frac{2}{\mu} (1-\nu) \frac{r_1}{R^2} \\ 2 \frac{r_2 r_1}{R^2} & -2 \ln R - 3 - 2 \frac{r_1 r_1}{R^2} & \frac{2}{\mu} (1-\nu) \frac{r_2}{R^2} \\ \frac{2}{\mu} (1-\nu) \frac{r_1}{R^2} & \frac{2}{\mu} (1-\nu) \frac{r_2}{R^2} & 0 \end{bmatrix} \quad (\text{A.1a})$$

$$[\mathfrak{T}_{1\lambda}(M, Q)] = \mathfrak{D}(R) \begin{bmatrix} n_1 r_1 [4 \frac{r_2^2}{R^2} - 2(3-2\nu)] + & -n_2 r_1 [4 \frac{r_2^2}{R^2} + 2(1-2\nu)] - \\ +n_2 r_2 [4 \frac{r_2^2}{R^2} - 2(3-2\nu)] & -n_1 r_2 [4 \frac{r_1^2}{R^2} - 2(1-2\nu)] \\ -n_1 r_2 [4 \frac{r_1^2}{R^2} + 2(1-2\nu)] - & n_2 r_2 [4 \frac{r_1^2}{R^2} - 2(3-2\nu)] + \\ -n_2 r_1 [4 \frac{r_2^2}{R^2} - 2(1-2\nu)] & +n_1 r_1 [4 \frac{r_1^2}{R^2} - 2(3-2\nu)] \\ -n_1 \frac{2}{\mu} (1-\nu) \frac{r_1^2 - r_2^2}{R^2} - & -n_1 \frac{4}{\mu} (1-\nu) \frac{r_1 r_2}{R^2} + \\ -n_2 \frac{4}{\mu} (1-\nu) \frac{r_1 r_2}{R^2} & +n_2 \frac{2}{\mu} (1-\nu) \frac{r_1^2 - r_2^2}{R^2} \end{bmatrix}, \quad (\text{A.1b})$$

where $\mathfrak{D}(R) = 1/8\pi(1-\nu)R^2$ and the normal n_ρ is taken at the point M . The distance between the points M and Q is R , which is defined as absolute value of the vector $r_\rho = x_\rho(M) - x_\rho(Q)$.

The matrix $\mathfrak{T}_{1\lambda\rho}$ is derived by factoring out the outward normal $n_1(M)$ from A.1b as follows:

$$[\mathfrak{T}_{1\lambda\rho}] = \mathfrak{D}(R) \begin{bmatrix} -2(3-2\nu)\eta_1 + \frac{4\eta_2^2\eta_1}{\eta_1^2 + \eta_2^2} & -2(3-2\nu)\eta_2 + \frac{4\eta_2^3}{\eta_1^2 + \eta_2^2} \\ 2(1-2\nu)\eta_2 - \frac{4\eta_1^2\eta_2}{\eta_1^2 + \eta_2^2} & -2(1-2\nu)\eta_1 - \frac{4\eta_2^2\eta_1}{\eta_1^2 + \eta_2^2} \end{bmatrix}$$

The matrix $\mathfrak{T}_{2\lambda\rho}$ is also derived by factoring out the outward normal $n_2(M)$ from A.1b as follows:

$$[\mathfrak{T}_{2\lambda\rho}] = \mathfrak{D}(R) \begin{bmatrix} -2(1-2\nu)\eta_2 - \frac{4\eta_1^2\eta_2}{\eta_1^2 + \eta_2^2} & 2(1-2\nu)\eta_1 - \frac{4\eta_1\eta_2^2}{\eta_1^2 + \eta_2^2} \\ -2(3-2\nu)\eta_1 + \frac{4\eta_1^3}{\eta_1^2 + \eta_2^2} & -2(3-2\nu)\eta_2 + \frac{4\eta_1^2\eta_2}{\eta_1^2 + \eta_2^2} \end{bmatrix}$$

APPENDIX B.

B.1. Quadratic shape functions. If the approximation is quadratic, the shape functions are as follows:

$$\begin{aligned}
{}^1\phi_1 &= \frac{1}{2\pi} \arctan \frac{\eta_2}{\eta_1} + \frac{1}{4\pi(1-\nu)} \frac{\eta_1\eta_2}{\eta_1^2 + \eta_2^2}, \\
{}^2\phi_1 &= -\frac{\eta_2}{4\pi(1-\nu)} \left\{ \ln \sqrt{\eta_1^2 + \eta_2^2} + \frac{4\nu-3}{2} + \frac{2\eta_2^2}{\eta_1^2 + \eta_2^2} \right\}, \\
{}^3\phi_1 &= \frac{\eta_1}{4\pi(1-\nu)} \left\{ (1-\nu) \ln \sqrt{\eta_1^2 + \eta_2^2} + \frac{3-\nu}{2} - \frac{\eta_1^2}{\eta_1^2 + \eta_2^2} \right\}, \\
{}^4\phi_1 &= -\frac{1}{4\pi(1-\nu)} \left\{ (1-2\nu) \ln \sqrt{\eta_1^2 + \eta_2^2} + \frac{\eta_1^2}{\eta_1^2 + \eta_2^2} \right\}, \\
{}^5\phi_1 &= \frac{\eta_1}{4\pi(1-\nu)} \left\{ \nu \ln \sqrt{\eta_1^2 + \eta_2^2} + \frac{5\nu}{2} - \frac{\eta_1^2}{\eta_1^2 + \eta_2^2} \right\}, \\
{}^6\phi_1 &= -\frac{\mu\eta_2}{4\pi(1-\nu)} \left\{ 2 \ln \sqrt{\eta_1^2 + \eta_2^2} + 3 \right\}, \\
{}^7\phi_1 &= \frac{1}{8\pi(1-\nu)} \left\{ 2(\nu-1)\eta_1^2 + (1-2\nu)\eta_2^2 + \right. \\
&\quad \left. + [(\nu-1)\eta_1^2 + (2-\nu)\eta_2^2] \ln(\eta_1^2 + \eta_2^2) + \frac{6\eta_2^4}{\eta_1^2 + \eta_2^2} \right\}, \\
{}^8\phi_1 &= \frac{1}{4\pi(1-\nu)} \left\{ [3-5\nu-\nu \ln(\eta_1^2 + \eta_2^2)] \eta_1\eta_2 - \frac{3\eta_1\eta_2^3}{\eta_1^2 + \eta_2^2} \right\}, \\
{}^9\phi_1 &= \frac{1}{4\pi(1-\nu)} \left\{ [4-3\nu+(1-\nu) \ln(\eta_1^2 + \eta_2^2)] \eta_1\eta_2 - \frac{\eta_1^3\eta_2}{\eta_1^2 + \eta_2^2} \right\}, \\
{}^{10}\phi_1 &= \frac{1}{8\pi(1-\nu)} \left\{ (1+4\nu)\eta_1^2 + (4-4\nu)\eta_2^2 + [(1-\nu)\eta_2^2 + \nu\eta_1^2] \ln(\eta_1^2 + \eta_2^2) - \frac{2\eta_1^4}{\eta_1^2 + \eta_2^2} \right\}, \\
{}^1\phi_2 &= \frac{1}{4\pi(1-\nu)} \left\{ (1-2\nu) \ln \sqrt{\eta_1^2 + \eta_2^2} + \frac{\eta_2^2}{\eta_1^2 + \eta_2^2} \right\}, \\
{}^2\phi_2 &= -\frac{\eta_1}{4\pi(1-\nu)} \left\{ \ln \sqrt{\eta_1^2 + \eta_2^2} + \frac{4\nu-3}{2} + \frac{2\eta_1^2}{\eta_1^2 + \eta_2^2} \right\}, \\
{}^3\phi_2 &= -\frac{\eta_2}{4\pi(1-\nu)} \left\{ \nu \ln \sqrt{\eta_1^2 + \eta_2^2} + \frac{5\nu}{2} - \frac{\eta_2^2}{\eta_1^2 + \eta_2^2} \right\}, \\
{}^4\phi_2 &= -\frac{1}{2\pi} \arctan \frac{\eta_1}{\eta_2} - \frac{1}{4\pi(1-\nu)} \frac{\eta_1\eta_2}{\eta_1^2 + \eta_2^2}, \\
{}^5\phi_2 &= -\frac{\eta_2}{4\pi(1-\nu)} \left\{ (1-\nu) \ln \sqrt{\eta_1^2 + \eta_2^2} + \frac{3-\nu}{2} - \frac{\eta_2^2}{\eta_1^2 + \eta_2^2} \right\}, \\
{}^6\phi_2 &= \frac{\mu\eta_1}{4\pi(1-\nu)} \left\{ 2 \ln \sqrt{\eta_1^2 + \eta_2^2} + 3 \right\}, \\
{}^7\phi_2 &= \frac{1}{4\pi(1-\nu)} \left\{ [5\nu-3+\nu \ln(\eta_1^2 + \eta_2^2)] \eta_1\eta_2 + \frac{3\eta_1^3\eta_2}{\eta_1^2 + \eta_2^2} \right\}, \\
{}^8\phi_2 &= \frac{1}{8\pi(1-\nu)} \left\{ (2\nu-1)\eta_1^2 + 2(1-\nu)\eta_2^2 + \right.
\end{aligned}$$

$$\begin{aligned}
& + [(1 - \nu) \eta_2^2 + (\nu - 2) \eta_1^2] \ln (\eta_1^2 + \eta_2^2) - \frac{6\eta_1^4}{\eta_1^2 + \eta_2^2} \Big\}, \\
{}^9\phi_2 &= \frac{1}{8\pi(1 - \nu)} \left\{ (4\nu - 4) \eta_1^2 - (1 + 4\nu) \eta_2^2 + [(\nu - 1) \eta_1^2 - \nu \eta_2^2] \ln (\eta_1^2 + \eta_2^2) + \frac{2\eta_2^4}{\eta_1^2 + \eta_2^2} \right\}, \\
{}^{10}\phi_2 &= \frac{1}{4\pi(1 - \nu)} \left\{ [3\nu - 4 - (1 - \nu) \ln (\eta_1^2 + \eta_2^2)] \eta_1 \eta_2 + \frac{\eta_1 \eta_2^3}{\eta_1^2 + \eta_2^2} \right\}.
\end{aligned}$$

APPENDIX C.

C.1. **The transformation matrix \mathbf{B}^Q .** If the approximation is quadratic, the matrix \mathbf{B}^Q is as follows:

$$\begin{aligned}
[\mathbf{B}^Q] &= \begin{bmatrix} 1 & x_1(Q) & x_2(Q) & 0 & 0 & 0 \\ 0 & 1 & 0 & 0 & 0 & 0 \\ 0 & 0 & 1 & 0 & 0 & 0 \\ 0 & -x_2(Q) & 0 & 1 & x_1(Q) & 0 \\ 0 & 0 & 0 & 0 & 1 & 0 \\ 0 & 0 & 0 & 0 & 0 & 1 \\ 0 & 0 & 0 & 0 & 0 & 0 \\ 0 & 0 & 0 & 0 & 0 & 0 \\ 0 & 0 & 0 & 0 & 0 & 0 \\ 0 & 0 & 0 & 0 & 0 & 0 \end{bmatrix}, \\
& \begin{bmatrix} -2x_1(Q)x_2(Q) & x_1^2(Q) & x_2^2(Q) & 0 \\ -2x_2(Q) & 2x_1(Q) & 0 & 0 \\ -2x_1(Q) & 0 & 2x_2(Q) & 0 \\ x_2^2(Q) & -2x_1(Q)x_2(Q) & 0 & x_1^2(Q) \\ 0 & -2x_2(Q) & 0 & 2x_1(Q) \\ Kx_2(Q) & Kx_1(Q) & Kx_1(Q) & Kx_2(Q) \\ 1 & 0 & 0 & 0 \\ 0 & 1 & 0 & 0 \\ 0 & 0 & 1 & 0 \\ 0 & 0 & 0 & 1 \end{bmatrix}
\end{aligned}$$

MATHEMATICAL MODELS FOR FLAW AND DAMAGE TOLERANCE ANALYSES

BARNA SZABÓ
Washington University
St. Louis, MO 63130 USA
szabo@wustl.edu

[Received: August 11, 2014, Accepted: September 4, 2014]

Dedicated to István Páczelt on the occasion of his 75th birthday.

Abstract. This paper is concerned with the conceptual development of mathematical models suitable for reliable prediction of fatigue life in metallic mechanical and structural components. Of particular interest is the prediction of the number of loading cycles to failure in parts that contain irregularities in material properties, inclusions and surface features caused by corrosion or other damage and are subjected to periodic loading.

Mathematical Subject Classification: 65N30, 65Z05

Keywords: Validation, metal fatigue, fracture mechanics, mathematical model

1. INTRODUCTION

Conceptual development of mathematical models is an inductive process that involves expert opinion, virtual experimentation and calibration. The end product of conceptualization is a mathematical model. This paper is concerned with aspects of conceptual development of mathematical models designed to support condition-based maintenance (CBM) and reliability-centered maintenance (RCM) decisions. The intended use of such models are: (a) identification of maintenance problems early, when they can be corrected at a relatively low cost and (b) scheduling maintenance only when needed, thereby realizing increased asset utilization, extension of equipment life, and reduction in operating costs.

Both CBM and RCM require mathematical models capable of predicting the remaining useful life of parts with a reasonably high degree of confidence. There are two seemingly competing approaches to fatigue life management: Flaw tolerance and damage tolerance. The purpose of flaw tolerance analysis is to evaluate the likelihood of crack initiation from flaws, given some cyclic loading. The purpose of damage tolerance analysis is to estimate crack growth caused by cyclic loading. A comprehensive overview of maintenance practices relating to military aircraft is presented in [1].

The conceptual development outlined in this paper is based on the idea that models formulated for the prediction of crack nucleation, i.e., for the purpose of supporting

flaw tolerance analysis, and models formulated for the prediction of crack growth, i.e., for the purpose of supporting damage tolerance analysis, are similar in the following sense: In both cases the physical events of interest; crack nucleation and crack growth, are highly nonlinear processes that occur on length scales that are typically less than about 0.5 mm for aluminum alloys, titanium and steel. The sites of crack nucleation and crack tip regions are called process zones (see, for example [2] and references cited therein). Within the process zone the usual assumptions of infinitesimal strain and small deformation do not hold. Nevertheless, as long as a process zone is completely surrounded by material for which those assumptions hold, crack nucleation and crack extension events occurring within the process zone should be predictable from the solutions of mathematical models that incorporate the assumptions of infinitesimal strain and small deformation only.

The paper is organized as follows: The classical approaches used for the prediction of the effects of notches on the endurance limit and their relationship to linear elastic fracture mechanics are summarized in Section 2. Procedures for the formulation and testing of mathematical models for the prediction of fatigue damage accumulation are outlined in Section 3. Experimental data obtained for twelve micro-machined test specimens made of AF1410 steel are presented in Section 4. Recommendations for a new family of models that account for size effects and removes difficulties associated with the application of linear elastic fracture mechanics in three dimensions are presented in Section 5. A brief summary is presented in Section 6.

2. CLASSICAL MODELS FOR DAMAGE ACCUMULATION

Failure initiation and crack propagation are inherently nonlinear processes that occur on length scales over which the assumptions of infinitesimal strain and small deformation do not hold. Nevertheless, computations based on mathematical models that incorporate the usual infinitesimal strain and small deformation assumptions, coupled with experimentation, have been proven to be useful for predicting crack initiation events and crack propagation rates.

Mathematical models constructed for the prediction of damage accumulation caused by cyclic loading are based on the following assumptions:

1. There exist one or more functionals, computable from the solution of mathematical models based on infinitesimal strain, small deformation theory, that can be correlated with crack initiation events and crack propagation rates with sufficient accuracy to suit the purposes of engineering decision-making.
2. There exist one or more procedures suitable for the generalization of the results of fatigue experiments performed under a particular cyclic loading, characterized by a mean value and constant amplitude, to cyclic loading characterized by arbitrary mean value and constant amplitude.
3. There exist one or more procedures suitable for correlating damage accumulation with variable amplitude cyclic loading, such as loading that represents flight spectra.

This paper is concerned with the formulation of functionals pertaining to assumption 1. The functionals are called driving forces for damage accumulation or simply driving forces.

2.1. Notch sensitivity. Several approaches have been proposed for the quantification of the effect of notches on the fatigue limit of machine components made of various metallic alloys. Essentially these approaches distinguish between the geometric stress concentration factor K_t and the effective stress concentration factor K_e where $0 < K_e \leq K_t$.

Definition 1. Nominal stress, defined for notched machine elements subjected to tension, bending and torsion, is understood in machine design to be the maximum normal or shearing stress at a notch computed by formulas based on the assumption that the strain distribution over the cross section is a linear function. Because this definition cannot be generalized to arbitrary domains, unless stated otherwise, we will understand nominal stress to mean the stress that would exist at the location of a notch if the notch were not present. \square

Definition 2. The geometric stress concentration factor, denoted by K_t , is the ratio of maximum stress to the nominal stress. \square

Definition 3. The notch sensitivity index (q) is defined as follows:

$$q = \frac{K_e - 1}{K_t - 1}. \quad (2.1)$$

It is dependent on the notch radius ϱ and a material property. Peterson [3], [4] defined the notch sensitivity index as:

$$q = \frac{1}{1 + \alpha/\varrho} \quad (2.2)$$

where α is an experimentally determined material constant. Peterson gave approximate values for α for steels as a function of their ultimate tensile strength (UTS). For UTS ranging between 345 and 1725 MPa the estimated range of α is 380 to 33 μm respectively. Although not stated explicitly, there has to be a lower bound on ϱ . The experimentally determined values of q for aluminum and steel published in [3] indicate that ϱ is greater than approximately $\alpha/4$.

An alternative definition of q , based on Neuber's work [5] is:

$$\bar{q} = \frac{1}{1 + \sqrt{\varrho'/\varrho}} \quad (2.3)$$

where ϱ' is an experimentally determined material constant (in length units). It is correlated with UTS in [6]: For UTS ranging between 345 and 1725 MPa the estimated range of ϱ' is 430 to 0.9 μm respectively. \square

Investigating notched machine elements subjected to tension, bending and torsion, Neuber formulated the following hypothesis: The driving force for the accumulation of fatigue damage is the elastic stress (shearing and tensile) at a notch tip averaged over a

material-dependent small distance that has to be determined through experimentation [5].

Neuber's hypothesis and variants of his hypothesis proposed by other investigators form the basis for flaw tolerance analysis. See, for example [8], a reference that makes comparisons among the Neuber-Kuhn, Peterson, Heywood, Stieler-Siebel and the Buch-Switek formulas, all proposed for the prediction of the effects of fillets, characterized by a radius, and notches, characterized by a depth, a notch angle and radius, on the fatigue limit.

Remark 1. Neuber's work was concerned with the fatigue strength of notched machine elements. Averaging stresses over a material-dependent distance for notched bars, shafts and beams can be understood also as averaging over an area or volume. Therefore Neuber's conceptualization admits alternative interpretations on general domains. \square

2.2. Linear elastic fracture mechanics. Linear elastic fracture mechanics (LEFM) is based on the hypothesis that the driving force for crack propagation under cyclic loading is the amplitude of the stress intensity factor.

Neuber's hypothesis and LEFM may appear to be fundamentally different models of damage accumulation. In reality LEFM can be viewed as a special case of Neuber's model in the following sense: Let us assume that a material-dependent critical distance d exists which is independent of the geometric features or the magnitude of stress or strain. Considering a two-dimensional domain with a crack, assuming that the crack is along the x -axis, periodic loading of amplitude ΔT_y is applied in the direction of the y -axis and the origin of the coordinate system is the crack tip, the driving force is the average stress $\Delta\sigma_d$ induced by ΔT_y . By definition;

$$\Delta\sigma_d = \frac{1}{d} \int_0^d \Delta\sigma_y(x, 0) dx. \quad (2.4)$$

The periodic loading ΔT_y induces variations in the stress intensity factor ranging between a minimum value $(K_I)_{\min}$ and a maximum value $(K_I)_{\max}$ where $(K_I)_{\min} \geq 0$. Let $\Delta K_I \equiv (K_I)_{\max} - (K_I)_{\min}$ and denote by $(\Delta K_I)_{\text{th}}$ the threshold value of ΔK_I below which the crack will not grow. Therefore a crack will not propagate when the amplitude of the average stress is

$$\Delta\sigma_d \leq \frac{1}{d} \int_0^d \frac{\Delta K_I}{\sqrt{2\pi x}} dx = \Delta K_I \sqrt{\frac{2}{\pi d}}. \quad (2.5)$$

Equating $\Delta\sigma_d$ to the endurance limit $\Delta\sigma_0$, we have the following estimate for the critical distance:

$$d = \frac{2}{\pi} \left(\frac{(\Delta K_I)_{\text{th}}}{\Delta\sigma_0} \right)^2. \quad (2.6)$$

If $(\Delta K_I)_{\text{th}}$ and $\Delta\sigma_0$ are material properties then d is a material property also. One has to bear in mind however that the endurance limit varies with the size of specimens: When the size increases, the endurance limit decreases. Therefore d is a material

property only if $(\Delta K_I)_{\text{th}}$ varies with size in the same way as $\Delta\sigma_0$. However, for reasons discussed in the following, it is not possible to determine $(\Delta K_I)_{\text{th}}$ accurately.

Example 1. The threshold stress intensity factor for conventionally processed AF1410 steel is approximately $16.0 \text{ MPa m}^{1/2}$ and its endurance limit is approximately 950 MPa. Therefore from eq. (2.6) we have ($d = 180 \text{ }\mu\text{m}$). This is an ultra high strength steel; its UTS is approximately 1670 MPa. This estimate of d is much larger than the estimate given in [3] and [6]. Note: The ASTM grain size number¹ of conventionally heat treated AF1410 steel is approximately 10.8 [7]. This corresponds to an average grain size of approximately $8.5 \text{ }\mu\text{m}$. \square

It is not difficult to show that the stress intensity factor is proportional to $\sigma_d\sqrt{d}$:

$$\sigma_y(x, 0) = \frac{K_I}{\sqrt{2\pi x}} \rightarrow K_I = \sigma_d\sqrt{\frac{\pi d}{2}}. \quad (2.7)$$

There are two important advantages of using eq. (2.4) instead of eq. (2.7):

1. Equation (2.4) is defined for both cracks and notches whereas eq. (2.7) is defined for cracks only.
2. Problems arise when attempting to interpret the results of physical experiments. Calibration involves correlation of crack growth with load cycles using the assumption that the stress distribution in the test articles very nearly satisfy the conditions of planar elasticity. However the asymptotic expansion of stresses in the neighborhood of a crack tip in two-dimensions is not applicable in three dimensions. This is because asymptotic expansion has a different character in the vicinity of the points where the crack front intersects a free surface. When the specimen is thin then these points are in close proximity and therefore tend to dominate the stress field ahead of the crack tip. When the specimen is thick then the stress fields in the vicinity of these points are usually ignored and the assumption is made that plane strain conditions exist. In reality generalized plane strain conditions exist [9].

In practical situations, such as shown in Fig. 1 where a crack represented by arc AB is originating at a countersunk fastener hole, there is substantial epistemic uncertainty as to how crack growth is influenced by the stress field in the vicinity of points A and B. Therefore it is not possible to justify application of conventional LFM methodology in such cases.

2.3. The theory of critical distances. The classical approaches proposed by Neuber, Peterson and others were precursors to what is called today the theory critical distances (TCD), see [10] - [13]. The line method of theory of critical distances states that for notched components in tension or bending the driving force is:

$$G_{\text{TCD}} = \frac{1}{2L} \int_0^{2L} \sigma_1(s) ds \quad (2.8)$$

¹ASTM Standard E 112 - 96 (2004).

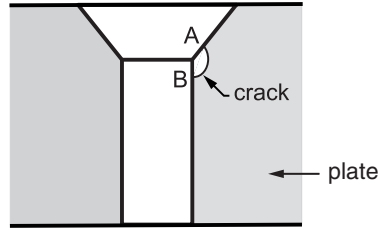


Figure 1. Crack originating at a countersunk hole.

where L is the critical distance, assumed to be a material property, $\sigma_1 > 0$ is the first principal stress, and the domain of integration is chosen such that G_{TCD} is maximal.

Remark 2. The relationship between the critical distance d defined in eq. (2.6) and the critical distance L defined in eq. (2.8) is $L = d/2$. See for example [10]. \square

In the following example it is shown that Peterson's definition of K_e can be understood as an approximation to the ratio of the average normal stress, in the direction of loading, over the distance a , to the nominal stress.

Example 2. We refer to the problem of a circular hole in an infinite plate subjected to unidirectional tension. The notation is shown in Fig. 2. The classical solution for σ_x is:

$$\sigma_x = \sigma_\infty \left[1 - \frac{a^2}{r^2} \left(\frac{3}{2} \cos 2\theta + \cos 4\theta \right) + \frac{3}{2} \frac{a^4}{r^4} \cos 4\theta \right] \quad (2.9)$$

where σ_∞ is the nominal stress. The geometric stress concentration factor is $K_t = \sigma_{\text{max}}/\sigma_\infty = 3$ where $\sigma_{\text{max}} = \sigma_x(a, \pm\pi/2)$. See, for example, [14].

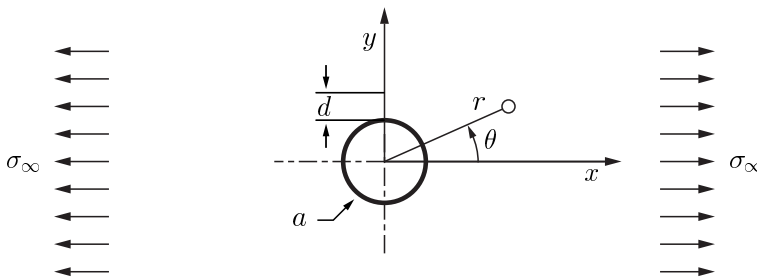


Figure 2. Circular hole in an infinite plate subjected to unidirectional tension (σ_∞). Notation.

We will be interested in the value of σ_x averaged over the interval $a \leq y \leq d$. The average value will be denoted by $\sigma_x^{(d)}$. Referring to eq. (2.9), we have

$$\begin{aligned}\sigma_x^{(d)} &= \frac{1}{d} \int_a^{a+d} \sigma_x(r, \pi/2) dr = \frac{\sigma_\infty}{d} \int_a^{a+d} \left(1 + \frac{1}{2} \frac{a^2}{r^2} + \frac{3}{2} \frac{a^4}{r^4} \right) dr \\ &= \sigma_\infty \left(1 + \frac{1}{2} \frac{1}{1+d/a} + \frac{3}{2} \frac{1+d/a+d^2/(3a^2)}{(1+d/a)^3} \right) \\ &= \sigma_\infty \left(1 + 2 \frac{1}{1+d/a} - \frac{3}{2} \frac{d/a+2d^2/(3a^2)}{(1+d/a)^3} \right) \\ &= \sigma_\infty \left(1 + 2 \frac{1}{1+d/a} + O(d/a) \right).\end{aligned}\tag{2.10}$$

Letting $\alpha = d$, $\varrho = a$ in eq. (2.2) and using eq. (2.1) we have:

$$K_e = \frac{\sigma_x^{(d)}}{\sigma_\infty} = q(K_t - 1) + 1\tag{2.11}$$

which is the same as eq. (2.10) if we neglect the term of $O(d/a)$ because $(K_t - 1) = 2$ for the infinite plate. Therefore K_e can be understood as an approximation of the ratio of the average stress over length α and the nominal stress. The error of approximation is explicitly given for the problem of the circular hole in an infinite plate. The relative error The percent relative error defined by

$$e_r = 100 \frac{\sigma_x^{(d)} - (q(K_t - 1) + 1)\sigma_\infty}{\sigma_x^{(d)}} \quad \text{where} \quad q = \frac{1}{1+d/a}$$

is shown in Fig. 3. The maximum relative error is 19.08 % which occurs at $d/a = 1.39$. In other words, if the fatigue limit depends on the average normal stress over the length d and Peterson's formula would be used to estimate this average stress then the error could be as large as 19.08 percent for the circular hole in the infinite plate.

3. VALIDATION

The formulation and testing of mathematical models for the prediction of damage accumulation due to fatigue under standard conditions, i.e., periodic loading characterized by fixed amplitude and mean value, involves the following processes:

1. Conceptualization: (a) formulation of a mathematical model that establishes a relationship between certain functionals of the stress or strain field and failure initiation or crack propagation events, (b) virtual experimentation and (c) calibration. The end product of conceptualization is a mathematical model.
2. Validation: Experiments performed to test the predictive capabilities of a mathematical model. The quality of predictions is evaluated with reference metrics and criteria formulated prior to the validation experiments. In the case of models formulated for the prediction of damage accumulation caused by metal fatigue, the metric is the number of cycles to failure. The formulation

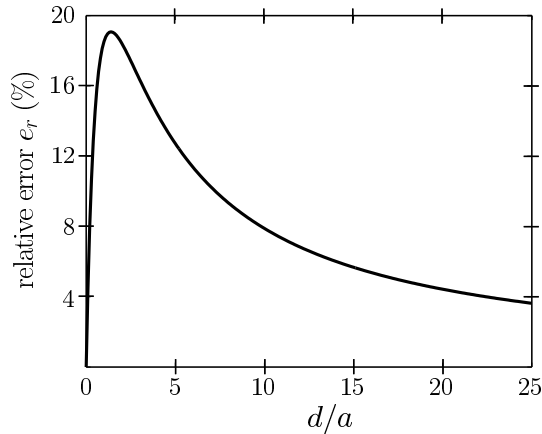


Figure 3. The relative error in Peterson’s formula applied to the circular hole in an infinite plate.

of criteria is complicated by the fact that accumulation of fatigue damage is inherently stochastic.

Examples of conceptualization were given in Section 2 and a general framework for conceptualization is proposed in Section 5. It is now becoming standard practice to perform validation experiments. Many papers and case studies have been published on this subject see, for example, [15] - [20] and the references cited therein.

In principle, a model is rejected if it fails to meet established criteria. In practice it is generally not possible to assign pass/fail scores to mathematical models on the basis of the outcome of a limited number of experiments because statistical variability in material properties, loading, constraints and geometric attributes complicates comparisons of predicted and observed data. Nevertheless, it is possible to formulate a framework for quantifying a “degree of belief” in a mathematical model and rank alternative models on the basis of accumulated experience with the accuracy of predictions based on the models.

Two types of uncertainty are associated with damage accumulation models: Epistemic (cognitive) uncertainty and aleatory (statistical) uncertainty. The goal is of validation is to minimize epistemic uncertainties through objective evaluation and ranking of alternative models of damage accumulation.

4. FATIGUE TESTS OF MICRO-MACHINED AF1410 STEEL SPECIMENS

In the course of investigation of the effects of small surface defects on the fatigue life of aircraft components made of AF1410 steel one group of investigators recommended fitting truncated ellipsoids to the surface features and using eq. (2.11):

$$K_e = q(K_t - 1) + 1 \quad (4.1)$$

with q defined by eq. (2.2) and the notch radius ϱ determined from the truncated ellipsoid. The truncated ellipsoid is characterized by three parameters; length, width and depth. It was called “pit metric” to convey the assumption that all surface features can be replaced for the purpose of fatigue life prediction with truncated ellipsoids. No limit was placed on the size of the pit metric, even though the notch radius in Peterson’s model has an implied lower bound, as noted in Section 2. The implied assumption is that Peterson’s model is capable of predicting crack nucleation events.

In order to test this assumption, twelve dog-bone specimens were machined from AF1410 steel. For each specimen the thickness of the test section was 3.05 mm (0.120 in), the width was 25.4 mm (1.0 in). The test sections were hand-polished and six features were micro-machined into the test section of nine specimens: Two ellipsoidal features, two conical features, and two pill-shaped features. The features were located at 60-degree intervals on the perimeter of a 12.7 mm (0.5 in) diameter circle, as shown in Fig. 4(a). One of the ellipsoidal and one of the pill-shaped features were oriented parallel with the direction of loading, the others were oriented perpendicular to it. The features were sufficiently far apart so that interaction among the features can be neglected. The remaining three specimens were tested without surface features.

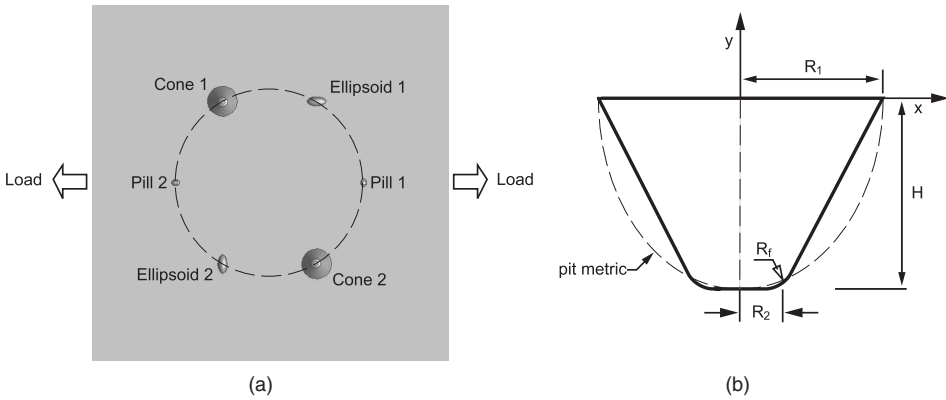


Figure 4. (a) Micro-machined features. The features lie on the perimeter of a 12.7 mm (0.5 in) diameter circle. (b) Conical feature. Relationship between the ellipsoidal pit metric and the micro-machined cone.

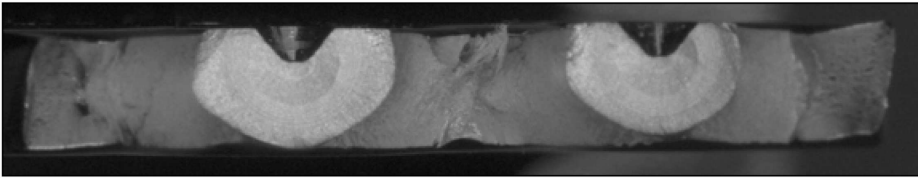
An example of replacement of a conical feature, characterized by four parameters ($R_1 = 1.02$ mm, $R_2 = 0.33$ mm, $H = 0.89$ mm, $R_f = 0.39$ mm), with a pit metric which in this case is characterized by only two parameters (R_1 , H) is shown in Fig. 4(b). The radius of curvature of the pit metric in the point $(0, -H, 0)$ is $\varrho_{\text{pm}} = R_1^2/H = 1.17$ mm. The ellipsoids are characterized by two radii $R_1 = 0.64$ mm, $R_2 = 0.32$ mm and the depth $H = 0.32$ mm. The pill-shaped features are comprised of a cylinder and two spherical caps of radius $R = 0.18$ mm, depth $H = 0.18$ mm and combined length $L = 0.57$ mm.

The maximum applied stress was 1380 MPa (200 ksi) the minimum stress was 138 MPa (20 ksi). Therefore the ratio of minimum to maximum stress was $R = 0.1$. The constant amplitude cyclic load was maintained at $R = 0.1$ for 1000 cycles then in each marker band block groups of 400 cycles at $R = 0.7$ stress was followed by 8 cycles at $R = 0.1$ stress.

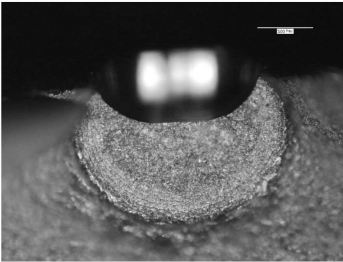
The computed values of K_e , based on the nominal dimensions of the micro-machined features, are shown in Table 1. According to Peterson's model the first occurrence of crack nucleation is expected at Ellipsoid 2, the long axis of which is oriented perpendicular to the load direction.

Table 1. The values of K_e for the three micro-machined features computed from Peterson's formula using $\alpha = 0.064$ mm.

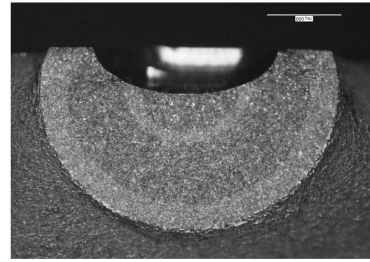
| Feature | ϱ (mm) | α/ϱ | q | K_t | K_e |
|-------------|----------------|------------------|--------|-------|-------|
| Cone | 0.391 | 0.164 | 0.8593 | 2.477 | 2.269 |
| Ellipsoid 2 | 0.635 | 0.101 | 0.9084 | 2.476 | 2.341 |
| Pill 1 | 0.178 | 0.360 | 0.7355 | 2.492 | 2.097 |



(a)



(b)



(c)

Figure 5. (a) Typical failure across conical features. (b) Secondary fatigue crack at a pill feature (specimen 598-2). (c) Secondary fatigue crack at an ellipsoidal feature (specimen 598-2).

Fractographic examination found that for all micro-machined specimens failure initiated at the conical features and the failure surface intersected the two conical

features, as shown in Fig. 5(a). Secondary fatigue cracks developed at the ellipsoidal and pill-shaped features that did not grow to critical size prior to failure. Typical secondary cracks are shown in Fig. 5(b) and Fig. 5(c). The number of cycles to initiation, which is defined as the first occurrence of a 0.254 mm (0.01 in) crack, is shown in Table 2.

Table 2. Results of fractographic examination of micromachined AF1410 dog-bone specimens. Number of $R = 0.1$ cycles to crack initiation and total number of cycles. Maximum applied stress: 1379 MPa (200 ksi).

| Specimen | Surface | primary conic | | secondary conic | |
|--------------------|---------|---------------|--------|-----------------|-------|
| | | $R = 0.1$ | Total | $R = 0.1$ | Total |
| 598-4 | smooth | 25,467 | 83,467 | - | - |
| 598-11 | smooth | 24,212 | 80,212 | - | - |
| 598-14 | smooth | 14,974 | 49,374 | - | - |
| 598-1 | notched | 1,767 | 6,567 | 1,800 | 6,600 |
| 598-2 | notched | 1,700 | 3,300 | 1,822 | 5,822 |
| 598-3 | notched | 1,968 | 4,368 | 1,971 | 4,371 |
| 598-5 | notched | 1,521 | 5,760 | 1,934 | 6,173 |
| 598-8 | notched | 1,418 | 4,209 | 1,869 | 4,660 |
| 598-9 | notched | 1,828 | 5,700 | 1,936 | 5,808 |
| 598-10 | notched | 1,500 | 3,100 | 1,833 | 3,433 |
| 598-12 | notched | 1,483 | 4,633 | 1,550 | 4,700 |
| 598-13 | notched | 1,790 | 6,502 | 1,970 | 6,682 |
| Average | | 1,664 | 4,904 | 1,854 | 5,361 |
| Standard deviation | | 179 | 1,218 | 124 | 1,053 |

We note that the predictions were based on the nominal dimensions of the surface features. The actual dimensions were measured for only one of the specimens by means of white light interferometry (WLI). The largest deviations were found in $R_f = 0.33$ mm (-15 %) for Cone 2 and $L = 0.69$ mm (+17 %) for Pill 1. Such deviations notwithstanding, the results indicate a strong probability that Peterson's model is not capable of predicting crack initiation events for the conical feature. The reason for this is that the stress distribution in the vicinity of the cones is qualitatively different from the stress distribution in the vicinity of notches considered by Peterson and Neuber. Arguably this was not a fair test of Peterson's model because the assumptions incorporated in that model were not satisfied by the test article. This could have been determined through virtual experimentation prior to performing the physical experiments.

We have seen in Section 2 that Peterson's effective stress concentration factor K_e can be understood as an approximation to the average stress over a material-dependent distance α , which in two dimensions is equivalent to an area. The original intent in the development of K_e was to estimate the fatigue life of machine elements

with notches that are characterized by a dominant curvature, the radius of curvature being larger than approximately $\alpha/4$. In those cases K_e gives a reasonably good approximation to the average stress. The underlying idea of using average stress over a line, area or volume has no such restrictions however and can be implemented into finite element analysis programs without difficulty.

The stress distribution in the vicinity of (a) the conical feature and (b) representation of the conical feature by the pit metric is shown in Fig. 6. It is seen that the stress distribution at the conical feature is not related to a clearly defined curvature but the stress distribution at the pit metric is. The same holds for the other surface features as well. This indicates that the idea of replacing surface features with a pit metric has to be rejected.

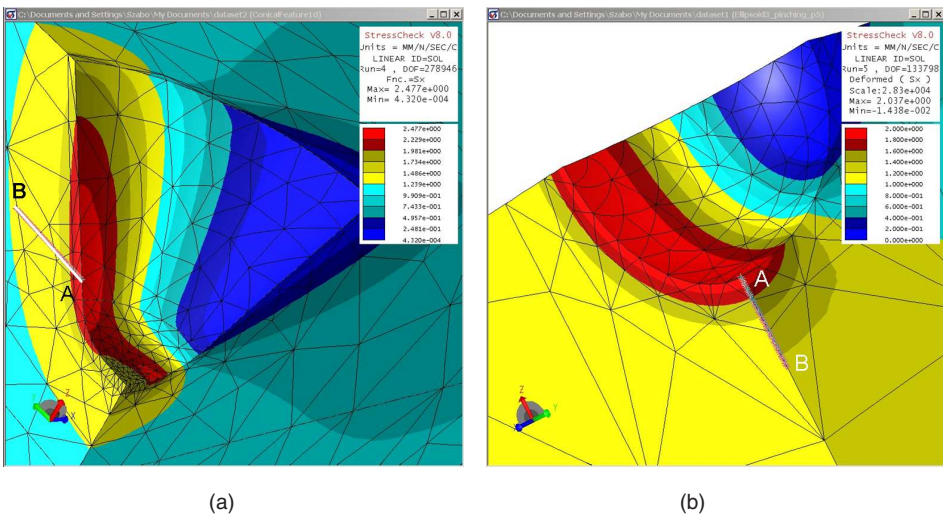


Figure 6. Stress distribution in the vicinity of (a) the conical feature and (b) representation of the conical feature by the pit metric. The nominal stress is 1 MPa applied in the x - direction.

The values of $\sigma_x^{(d)}/\sigma_\infty$ for the three micro-machined features for various values of the averaging interval d are shown in Table 3. The averaging intervals were chosen by inspection so as to approximately maximize the average values. Examples of averaging intervals are shown by the lines labeled AB in Fig. 6.

It is seen that for the averaging interval ranging between 0.05 mm and 0.5 mm $\sigma_x^{(d)}/\sigma_\infty$ is largest for the conical features. Therefore a failure initiation model based on $\sigma_x^{(d)}$ would have correctly predicted that failure would begin at the conical features. Furthermore it would have predicted that the ellipsoid would be the next site of failure initiation, and the pill-shaped features would be last for any choice of d . This sequence of events was confirmed by fractographic examination. It is therefore possible to

Table 3. The values of $\sigma_x^{(d)}/\sigma_\infty$ for the three micro-machined features.

| Feature | 0.5 mm | 0.25 mm | 0.10 mm | 0.05 mm |
|-------------|--------|---------|---------|---------|
| Cone | 1.640 | 1.894 | 2.165 | 2.296 |
| Ellipsoid 2 | 1.334 | 1.565 | 1.913 | 2.128 |
| Pill 1 | 1.189 | 1.352 | 1.683 | 1.953 |

conclude that predictions based on $\sigma_x^{(d)}$ are consistent with the results of experiments. The model based on the theory of critical distances passed the validation test.

5. GENERALIZATION OF CLASSICAL MODELS FOR DAMAGE ACCUMULATION

Examples of conceptualization were given in Sections 2. The conceptualization attributed to Neuber and the theory of critical distances are based on the assumption that a material constant, which has the dimension of length, exists and accumulation of fatigue damage can be correlated with the average stress over a line, area or volume characterized by that constant. This is contradicted by the experimental observation that the endurance limit depends on the size of the specimens, therefore the distance d cannot be a material constant. Consequently there appear to be fundamental problems with the classical models described in Section 2.

The classical models of driving force for damage accumulation exemplified by the work of Neuber, Peterson, Buch and others were developed for the estimation of the endurance limit of notched machine elements in tension, bending and shear. The computational tools available at that time were limited. The geometric stress concentration factors were determined mainly from classical solutions of the Navier-Lamé equations and photoelastic studies. The nominal stress was computed from simple formulae for bars, beams and shafts. Those limitations on computational tools no longer exist and there is a need for generalization of the classical models of damage accumulation to complicated parts, such as rotorcraft components, and small defects, such as those caused by manufacturing processes, corrosion, impact and wear. In this section the conceptual formulation of driving forces for damage accumulation is outlined. For the sake of simplicity in presentation the domain is assumed to be two-dimensional, unless otherwise noted, but the concept is not restricted to two dimensions.

Consider the neighborhood of a sharp or blunt notch, called stress riser. It is assumed in the following that the principles of continuum mechanics remain valid everywhere within the body up to the failure initiation event. At the site of damage accumulation the continuum model is likely to indicate strongly nonlinear behavior, such as the formation of shear bands, large strain and large rotation. This is the process zone, schematically indicated by the hatched area bounded by Γ_{PZ} and Γ in Fig. 7.

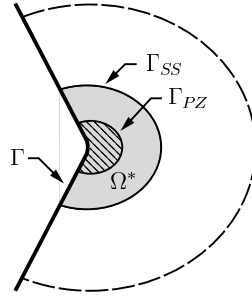


Figure 7. Notation.

Let $\mathbf{u}_{PZ}(\mathbf{x}, t) = \{u_x(\mathbf{x}, t) \ u_y(\mathbf{x}, t)\}_{PZ}$ be the solution of the general nonlinear continuum mechanics problem that accounts for strongly nonlinear behavior as well as heterogeneous material properties and let $\mathbf{u}_{SS}(\mathbf{x}, t) = \{u_x(\mathbf{x}, t) \ u_y(\mathbf{x}, t)\}_{SS}$ be the solution of the continuum mechanics problem that accounts only for infinitesimal strain, small deformation and homogeneous material properties. Both \mathbf{u}_{PZ} and \mathbf{u}_{SS} are defined on the entire domain Ω and may be functions of time t . It is assumed that there is a subdomain Ω^* , bounded by Γ_{SS} and Γ , such that outside of Ω^* $\mathbf{u}_{PZ} \approx \mathbf{u}_{SS}$. Specifically:

$$\|\mathbf{u}_{PZ}(\mathbf{x}, t) - \mathbf{u}_{SS}(\mathbf{x}, t)\|_{\max} \leq \tau \|\mathbf{u}_{PZ}(\mathbf{x}, t)\|_{\max} \quad \mathbf{x} \in (\Omega - \Omega^*) \quad (5.1)$$

where τ is some small tolerance. On the domain outside of Ω^* the usual infinitesimal strain and small deformation assumptions of continuum mechanics are reasonable representations of physical reality.

Implied in this assumption is that failure initiation, which depends on the solution of the highly nonlinear problem inside the process zone, is related to the solution of a linear or nonlinear problem of continuum mechanics for which the assumptions of infinitesimal strain, small deformation hold, even though these assumptions are violated inside the process zone. Consequently it should be possible to predict failure initiation events on the basis of \mathbf{u}_{SS} . An important special case is when \mathbf{u}_{SS} can be well approximated by models based on linear elasticity. In such cases $\mathbf{u}_{SS}(\mathbf{x}, t)$ can be written as the product of a function of \mathbf{x} and a function of t .

The key problem is identification of the driving force for damage accumulation, given $\mathbf{u}_{SS}(\mathbf{x}, t)$. Infinitely many conceptualizations are possible. For example, the following defines a family of possible definitions of driving force in terms of some functional $F(\mathbf{u}_{SS}) > 0$ and a parameter α :

$$G(F, \alpha, t, T) = \int_{\Omega_\alpha} F(\mathbf{u}_{SS}(\mathbf{x}, t), T) dV, \quad \mathbf{x} \in \mathbb{R}^3 \quad (5.2)$$

where T represents temperature. The domain of integration Ω_α depends on the magnitude of F :

$$\Omega_\alpha = \{\mathbf{x} \mid \alpha \leq F/F_{\text{lim}}, \ 0 < \alpha < 1\}. \quad (5.3)$$

Various definitions of $F_{\text{lim}} > 0$ are possible. The value of F_{lim} may depend on the yield stress, yield strain, the ultimate tensile stress or some other value. The choice Ω_α as a function of F is related to the experimentally observed fact that the larger the volume subjected to elevated stress or strain, the greater the likelihood of failure.

Remark 3. In general, the solution \mathbf{u}_{SS} is not known, only an approximation to \mathbf{u}_{SS} , which will be denoted by \mathbf{u}_{FE} , is known. Replacement of \mathbf{u}_{SS} by \mathbf{u}_{FE} is permissible only when $\|\mathbf{u}_{SS} - \mathbf{u}_{FE}\|_{\max}$ is sufficiently small on $\Omega - \Omega^*$. This follows from the inequality:

$$\|\mathbf{u}_{PZ} - \mathbf{u}_{SS}\|_{\max} \leq \|\mathbf{u}_{PZ} - \mathbf{u}_{FE}\|_{\max} + \|\mathbf{u}_{SS} - \mathbf{u}_{FE}\|_{\max}. \quad (5.4)$$

Numerical accuracy is essential because unless the accuracy of the computed data is known it is not meaningful to compare experimental observations with predictions based on a mathematical model. This is because it would not be possible to tell whether the mathematical model is wrong or the numerical errors are too large, or both. In some cases a large error in the mathematical model is nearly canceled by a similarly large numerical error, leading to false conclusions [21].

Example 3. The region of integration Ω_α is illustrated for the conical feature when $F = \sigma_1$, is defined as the first principal stress, $F_{\text{lim}} = \sigma_{\text{yld}} = 1517 \text{ MPa}$ is defined as the yield stress of AF1410 steel and $\alpha = 0.95$ in Fig. 8.

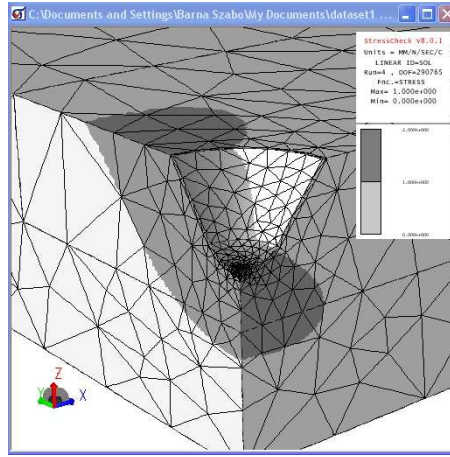


Figure 8. Example 3. The region of integration Ω_α is highlighted for $\alpha = 0.95$. Specifically, $\sigma_1 \geq 0.95\sigma_{\text{yld}}$ over the dark grey region.

6. CLOSING REMARKS

Damage tolerance and flaw tolerance methods employed in the management of mechanical and structural systems have a common conceptual basis: The highly nonlinear processes of crack nucleation and crack propagation are typically controlled by stress and strain fields that can be determined to a high degree of accuracy from

the solutions of mathematical models based on small displacement and infinitesimal strain theory.

Development of a predictive capability for crack nucleation and crack propagation based on small displacement and infinitesimal strain theory involves the definition of a driving force $G(F, \alpha, t, T)$, see eq. (5.2), and interpretation of the outcome of calibration experiments designed for determination of the parameters in G . The definition of G involves expert opinion, i.e., subjective judgment. Nevertheless it is possible to rank alternative definitions objectively through the application of verification and validation procedures. For example, the results of fatigue tests of the micro-machined AF1410 steel specimens presented in Section 4 clearly indicate that G defined as average stress over lengths ranging between 50 to 200 μm is preferable to Peterson's definition of the driving force.

Neuber's seminal work on the investigation of the fatigue limit of notched machine elements should be understood as an attempt to define a particular driving force G . Specifically, Neuber's driving force was the average tensile or shear stress over a length which he assumed to be a material property. This length was calibrated for various metals and was shown to provide useful predictions for typical notch configurations in machine elements. The notch radii in the calibration experiments were greater than about 0.5 mm. Scatter in the measured data tend to increase with decreasing notch radius. Furthermore, as seen in Section 4, not all surface features can be characterized by a single notch radius. For example, the stress distribution in the vicinity of the conical feature is not associated with a notch radius (see Fig. 6). Therefore Neuber's and Peterson's estimate of K_e is not applicable to the conical feature. Another difficulty is that the classical models do not account for the influence of size on fatigue limit.

There are conceptual problems also with mathematical models based on linear elastic fracture mechanics for the estimation of crack propagation rates. These problems arise because coupon tests designed for the determination of material parameters that characterize crack propagation are performed on test articles which do not meet the conditions of planar elasticity: The stress field at the intersection of the crack front with the surface of the test article is not the stress field assumed in LEFM and, furthermore, the crack front is typically curved. These conditions are typically ignored in the interpretation of calibration experiments, resulting in systematic errors when the results of calibration are applied to general crack configurations.

The class of driving forces defined in equations (5.2) and (5.3) do not have such limitations. Given the framework of verification and validation, it is possible to re-interpret the results of fatigue and fracture experiments with the objective to identify specific driving forces that have the best predictive capabilities, independent of notch configuration and size. This will minimize systematic errors in the prediction of crack nucleation and crack propagation events.

ACKNOWLEDGMENT

This paper is an elaboration on the author's presentation at the MITACS Workshop entitled "Methodology of Validation and Verification" held in Banff, Alberta, Canada between April 28 and May 1, 2008. The author is indebted to the participants for lively discussions on V&V issues. Special thanks are due to Professor Ivo Babuška, Dr. Paul Hoffman, Mr. David Rusk and Dr. Ricardo Actis.

REFERENCES

1. APPLIED VEHICLE TECHNOLOGY PANEL, TASK GROUP AVT-125, RESEARCH AND TECHNOLOGY ORGANISATION (NATO): Future Airframe Structural Lifting: Methods, Applications and Management. Report No. RTO-TR-AVT-125, Neuilly-sur-Seine Cedex, France, 2008.
2. MARIANO, P. M.: Multifield Theories in Mechanics of Solids. In *Advances in Applied Mechanics* 38, Edited by E. van der Giessen and T. Y. Wu, Academic Press, 2001, 2–95.
3. PETERSON, R. E.: *Stress Concentration Factors*. John Wiley & Sons, New York, 1974.
4. PILKEY, W. D.: *Peterson's Stress Concentration Factors*. 2nd ed. John Wiley & Sons, New York, 1997.
5. NEUBER, H.: *Kerbspannungslehre*. Springer-Verlag, Berlin, 1937.
6. KUHN, P. and HARDRATH, H. F., An Engineering Method for Estimating Notch-Size Effect in Fatigue Tests of Steel. NACA Technical Note 2805, 1952.
7. VIGILANTE, J. N., UNDERWOOD, J. H. and CRAYON, D.: Use of instrumented bolt and constant displacement bolt-loaded specimen to measure in-situ hydrogen crack growth in high-strength steels. *Fatigue and Fracture Mechanics: 30th Volume, ASTM STP 1360*. P. C. Paris and K. L. Jerina, Eds. American Society for Testing and Materials. West Conshohocken, PA, 2000, 377–387.
8. BUCH, A.: Notch-Size Effect of Steel Specimens - Verification of Some Calculation Methods. *Z. Werkstofftech*, **15**, 1984, 338–348.
9. BABUŠKA, I. and SZABÓ, B.: On the generalized plane strain problem in thermoelasticity. *Comput. Methods Appl. Mech. Engng.* **195**, 2006, 5390–5402.
10. TAYLOR, D.: *The Theory of Critical Distances. A New Perspective in Fracture Mechanics*. Elsevier, Oxford (2007).
11. TAYLOR, D.: The theory of critical distances. *Engineering Fracture Mechanics.* **7**, 2008, 1696–1705.
12. SUSMEL, L. and TAYLOR, D.: A novel formulation of the Theory of Critical Distances to estimate lifetime of notched components in the medium-cycle fatigue regime. *Fatigue Fract. Engng. Mater. Struct.* **30**, 2007, 567–581.
13. SUSMEL, L.: The theory of critical distances: a review of its applications to fatigue. *Engineering Fracture Mechanics.* **7** 2008, 1706–1724.
14. MUSKHELISHVILI, N. I.: *Some Basic Problems of the Mathematical Theory of Elasticity*, published in Russian in 1933, English translation of the 3rd edition: Groningen, Holland, 1953.
15. SZABÓ, B. A. and ACTIS, R. L.: On the role of hierarchic spaces and models in verification and validation. *Comput. Methods Appl. Mech. Engng.* **198**, 2009, 1273–1280.

16. ROACHE, P. J.: *Verification and Validation in Computational Science and Engineering* Hermosa Publishers, Albuquerque, New Mexico, 1998.
17. ROACHE P. J.: Verification of Codes and Calculations. *AIAA Journal* **36**, 1998, 696–702.
18. OBERKAMPF, W. L.: What are validation experiments? *Experimental Techniques* May/June, 2001, 35–40.
19. ASME V&V 10-2006: Guide for Verification and Validation in Computational Solid Mechanics. The American Society of Mechanical Engineers, ISBN No. 0-7918-3042-X, 2006.
20. BABUŠKA, I., NOBILE, F. and TEMPONE, R.: A systematic approach to model validation based on Bayesian updates and prediction related rejection criteria. *Comput. Methods Appl. Mech. Engrg.* **197**, 2008, 2517–2539.
21. SZABÓ, B. and BABUŠKA, I.: *Finite Element Analysis*. John Wiley & Sons. Inc. New York, 1991.

Notes for Contributors

to the Journal of Computational and Applied Mechanics

Aims and scope. The aim of the journal is to publish research papers on theoretical and applied mechanics. Special emphasis is given to articles on computational mechanics, continuum mechanics (mechanics of solid bodies, fluid mechanics, heat and mass transfer) and dynamics. Review papers on a research field and materials effective for teaching can also be accepted and are published as review papers or classroom notes. Papers devoted to mathematical problems relevant to mechanics will also be considered.

Frequency of the journal. Two issues a year (approximately 80 pages per issue).

Submission of Manuscripts. Submission of a manuscript implies that the paper has not been published, nor is being considered for publication elsewhere. Papers should be written in standard grammatical English. The manuscript is to be submitted in electronic, preferably in pdf, format. The text is to be 130 mm wide and 190 mm long and the main text should be typeset in 10pt CMR fonts. Though the length of a paper is not prescribed, authors are encouraged to write concisely. However, short communications or discussions on papers published in the journal must not be longer than 2 pages. Each manuscript should be provided with an English Abstract of about 50–70 words, reporting concisely on the objective and results of the paper. The Abstract is followed by the Mathematical Subject Classification – in case the author (or authors) give the classification codes – then the keywords (no more than five). References should be grouped at the end of the paper in numerical order of appearance. Author’s name(s) and initials, paper titles, journal name, volume, issue, year and page numbers should be given for all journals referenced.

The journal prefers the submission of manuscripts in L^AT_EX. Authors should prefer the $\mathcal{A}\mathcal{M}\mathcal{S}$ -L^AT_EX article class and are not recommended to define their own L^AT_EX commands. Visit our home page for further details concerning the issue of how to edit your paper.

For the purpose of refereeing the manuscripts should be sent either to Balázs Tóth (Balazs.TOTH@uni-miskolc.hu) or György SZEIDL (Gyorgy.SZEIDL@uni-miskolc.hu).

The eventual supply of an accepted-for-publication paper in its final camera-ready form will ensure more rapid publication. Format requirements are provided by the home page of the journal from which sample L^AT_EX files can be downloaded:

<http://www.mech.uni-miskolc.hu/jcam>

These sample files can also be obtained directly (via e-mail) from Balázs TÓTH (Balazs.TOTH@uni-miskolc.hu), upon request.

One issue of the journal and ten offprints will be provided free of charge and mailed to the correspondent author. Since JCAM is an open access journal each paper can be downloaded freely from the homepage of the journal.

The Journal of Computational and Applied Mechanics is abstracted in *Zentralblatt für Mathematik* and in the Russian *Referativnij Zhurnal*.

Secretariat of the Vice-Rector for Research and International Relations, University of Miskolc
Responsible for publication: Prof. Dr. Tamás Kékesi
Published by the Miskolc University Press under the leadership of Attila Szendi
Responsible for duplication: Works manager Erzsébet Pásztor
Number of copies printed: 75
Put to the Press on June 15, 2015
Number of permission: TNRT.2015-200.ME.

HU ISSN 1586–2070

A Short History of the Publications of the University of Miskolc

The University of Miskolc (Hungary) is an important center of research in Central Europe. Its parent university was founded by the Empress Maria Teresia in Selmecebánya (today Banská Štiavnica, Slovakia) in 1735. After the first World War the legal predecessor of the University of Miskolc moved to Sopron (Hungary) where, in 1929, it started the series of university publications with the title *Publications of the Mining and Metallurgical Division of the Hungarian Academy of Mining and Forestry Engineering* (Volumes I-VI). From 1934 to 1947 the Institution had the name Faculty of Mining, Metallurgical and Forestry Engineering of the József Nádor University of Technology and Economic Sciences at Sopron. Accordingly, the publications were given the title *Publications of the Mining and Metallurgical Engineering Division* (Volumes VII-XVI). For the last volume before 1950 – due to a further change in the name of the Institution – *Technical University, Faculties of Mining, Metallurgical and Forestry Engineering, Publications of the Mining and Metallurgical Divisions* was the title.

For some years after 1950 the Publications were temporarily suspended.

After the foundation of the Mechanical Engineering Faculty in Miskolc in 1949 and the movement of the Sopron Mining and Metallurgical Faculties to Miskolc, the Publications restarted with the general title *Publications of the Technical University of Heavy Industry* in 1955. Four new series - Series A (Mining), Series B (Metallurgy), Series C (Machinery) and Series D (Natural Sciences) - were founded in 1976. These came out both in foreign languages (English, German and Russian) and in Hungarian.

In 1990, right after the foundation of some new faculties, the university was renamed the University of Miskolc. At the same time the structure of the Publications was reorganized so that it could follow the faculty structure. Accordingly three new series were established: Series E (Legal Sciences), Series F (Economic Sciences) and Series G (Humanities and Social Sciences). The latest series, i.e., series H (European Integration Studies), was founded in 2001. The eight series are formed by some periodicals and such publications which are issued at various frequencies.

Papers on computational and applied mechanics were published in the

Publications of the University of Miskolc, Series D, Natural Sciences.

This series was given the name Natural Sciences, Mathematics in 1995. The name change reflects the fact that most of the papers published in the journal are of a mathematical nature though papers on mechanics also come out.

The series

Publications of the University of Miskolc, Series C, Fundamental Engineering Sciences

founded in 1995, also published papers on mechanical issues. The present journal, which is published with the support of the Faculty of Mechanical Engineering and Informatics as a member of Series C (Machinery), is the legal successor of the above journal.



Contents

Contributed Papers

| | |
|--|--------|
| Dániel BURMEISTER: Buckling of circular plates with shell-stiffening on the boundary | 3–23 |
| Ákos József LENGYEL and István ECSEDI: Static and dynamic analyses of composite beams with interlayer slip | 25–40 |
| Ágnes HORVÁTH: Calculation of J -integral for large strains using the finite element method | 41–55 |
| Gábor L. SZEPESI and Zoltán SIMÉNFALVI: Connection between the leaking and the viscoelastic behavior of flange gaskets | 57–64 |
| Sándor SZIRBIK: Boundary contour method for mixed boundary value problems in the dual system of plane elasticity | 65–82 |
| Barna SZABÓ: Mathematical models for flaw and damage tolerance analyses | 83–100 |